

MANITOBA

INVEST. BUILD. GROW



OPEN FILE OF2018-4
GEOLOGY OF THE TOWER
Cu-Zn-Ag-Au DEPOSIT,
SUB-PHANEROZOIC
SUPERIOR BOUNDARY ZONE,
CENTRAL MANITOBA
(PART OF NTS 63G14)

Manitoba Geological Survey





Open File OF2018-4

**Geology of the Tower Cu-Zn-Ag-Au deposit,
sub-Phanerozoic Superior boundary zone,
central Manitoba (part of NTS 63G14)**

by C.G. Couëslan
Manitoba Geological Survey
Winnipeg, 2018

©Queen's Printer for Manitoba, 2018

Every possible effort is made to ensure the accuracy of the information contained in this report, but Manitoba Growth, Enterprise and Trade does not assume any liability for errors that may occur. Source references are included in the report and users should verify critical information.

Any third party digital data and software accompanying this publication are supplied on the understanding that they are for the sole use of the licensee, and will not be redistributed in any form, in whole or in part. Any references to proprietary software in the documentation and/or any use of proprietary data formats in this release do not constitute endorsement by Manitoba Growth, Enterprise and Trade of any manufacturer's product.

When using information from this publication in other publications or presentations, due acknowledgment should be given to the Manitoba Geological Survey. The following reference format is recommended:

Couëslan C.G. 2018: Geology of the Tower Cu-Zn-Ag-Au deposit, sub-Phanerozoic Superior boundary zone, central Manitoba (part of NTS 63G14); Manitoba Growth, Enterprise and Trade, Manitoba Geological Survey, Open File OF2018-4, 38 p.

NTS grid: 63G14

Keywords: juvenile volcanic arc; klippe; Manitoba; Superior boundary zone; Superior margin; Thompson nickel belt; Tower deposit; Trans-Hudson orogen; volcanogenic massive-sulphide

Published by:

Manitoba Growth, Enterprise and Trade
Manitoba Geological Survey
360–1395 Ellice Avenue
Winnipeg, Manitoba
R3G 3P2 Canada

Telephone: 1-800-223-5215 (General Enquiry)
204-945-6569 (Publication Sales)

Fax: 204-945-8427

E-mail: minesinfo@gov.mb.ca

Website: manitoba.ca/minerals

ISBN No.: 978-0-7711-1592-9

This publication is available to download free of charge at manitoba.ca/minerals

Cover illustrations:

Left: The author logging Tower deposit drillcore at Rockcliff Metals Corporation's storage facility.

Right: Chlorite schist representing intense hydrothermal alteration associated with the T2 zone of the Tower deposit.

Abstract

The Tower Cu-Zn-Ag-Au deposit is a bimodal, likely mafic-dominated volcanogenic massive-sulphide (VMS) system located along the sub-Phanerozoic Superior craton margin. The deposit is hosted in a sequence of variably altered metavolcanic rocks now represented by hornblende, biotite-garnet, and grunerite-magnetite gneisses, and biotite-muscovite, garnet-biotite, cummingtonite, and heterogeneous chlorite schists. The various hornblende gneisses represent the least altered mafic volcanic rocks, whereas the biotite-garnet and grunerite-magnetite gneisses represent the least altered felsic to intermediate volcanic rocks. The schists represent zones of more intensely altered volcanic rocks. The biotite-muscovite, and garnet-biotite and cummingtonite schists correspond to zones of intense sericite-paragonite alteration of felsic and mafic rocks, whereas the chlorite schist represents zones of intense chlorite alteration of dominantly mafic rocks. The Tower stratigraphy is intruded by gabbroic and ultramafic intrusions now represented by plagioclase amphibolite and ultramafic schist, respectively. A granodiorite intrusion is present in the structural hangingwall to the deposit. The rocks of the Tower deposit are characterized by middle amphibolite-facies mineral assemblages.

The T1 zone mineralization is discordant to stratigraphy and is hosted within biotite-muscovite schist in the north and hornblende gneiss in the south. The T1 zone varies from a sulphidic schist to a sulphide breccia, the latter consisting of fragments of wall-rock hosted in solid sulphide, interpreted to result

from mobilization along a late (D_3 - D_4) structure. The biotite-muscovite schist may represent an intense sericitic footwall alteration zone to the T1 mineralization. The T2 zone mineralization is hosted near the structural base of the chlorite schist unit, which likely represents a zone of intense chloritic alteration in the stratigraphic footwall of the deposit. The geometry of the T2 zone and host footwall alteration suggests the Tower stratigraphy may be overturned.

Lithochemistry and Sm-Nd isotope geochemistry suggest the Tower stratigraphy consists of juvenile volcanic arc rocks. The arc rocks are distinct from those in the adjacent East Kiseynew domain based on trace-element profiles and ϵ_{Nd} values of +0.1 to +3.2, compared to +3.0 to +3.7 for the East Kiseynew domain. The presence of felsic volcanic rocks with FII-FIIIa rhyolite geochemistry, local mafic rocks with boninitic affinity, and ultramafic intrusions are suggestive of a rifted arc environment. Extensional arc environments are characterized by high heat-flow and localized structural permeability, features conducive to the formation of VMS mineralization. The rocks hosting the Tower deposit likely formed in an island-arc environment, within the Manikewan ocean basin, at an unknown distance from the Superior craton margin. These juvenile arc rocks were likely thrust onto the Superior craton margin during the Trans-Hudson orogeny and preserved as a klippe, or erosional remnant. Additional thrust slices with similar VMS potential could exist elsewhere along the sub-Phanerozoic portion of the Superior craton margin.

TABLE OF CONTENTS

Page

Abstract.....	iii
Introduction.....	1
Regional setting	2
Ospwagan group stratigraphy	3
Winnipegosis komatiite belt.....	4
East Kiseynew domain	5
Geology of the Tower deposit.....	5
Stratigraphy of the Tower deposit.....	5
Methodology	5
Footwall to the T1 zone mineralization	8
The T1 zone mineralization	9
Stratigraphy between the T1 and T2 zones.....	9
The T2 zone mineralization	12
Hangingwall to the Tower deposit	12
Comments on the Tower stratigraphy.....	12
Intrusions.....	13
Litho geochemistry and Sm-Nd isotope geochemistry.....	13
Sampling and analytical methods	14
Tower chemostratigraphy.....	14
Intrusions.....	16
Metamorphism	16
Methods.....	16
Mineral assemblages.....	18
Phase equilibrium modelling	20
Discussion.....	20
Comparison with rocks of the Pikwitonei granulite domain	20
Stratigraphic comparison with the Ospwagan group rocks	22
Geochemical comparisons	22
Comparison with East Kiseynew deposits	26
Interpretation of the Tower stratigraphy	30
Economic considerations	34
Acknowledgments.....	34
References.....	34

TABLES

Table 1: Litho geochemical data for representative rock samples from the Tower deposit.....	15
Table 2: Sm-Nd isotopic data for select samples from the Tower deposit.....	16
Table 3: Normative mineral alteration indices calculated for Tower deposit rocks using the NORMAT method	24

FIGURES

Figure 1: Geological domains along the Superior boundary zone, central Manitoba	1
Figure 2: Simplified geology of the exposed Thompson nickel belt and adjacent portions of the Kiseynew domain and Superior craton	2

Figure 3: Schematic lithostratigraphic section of the Ospwagan Group	4
Figure 4: Simplified geology of the William Lake area.....	6
Figure 5: Schematic petrostratigraphic section of the Tower deposit from structural footwall to hangingwall.....	7
Figure 6: Drillcore and thin section images of units in the footwall to the Tower deposit.....	8
Figure 7: Drillcore images from the T1 mineralized zone of the Tower deposit.....	9
Figure 8: Drillcore images of units between the T1 and T2 mineralized zones	10
Figure 9: Drillcore images from the T2 mineralized zone and its footwall.....	11
Figure 10: Drillcore images from the hangingwall of the Tower deposit.....	12
Figure 11: Drillcore images of intrusive phases at the Tower deposit.....	13
Figure 12: SiO ₂ -Al ₂ O ₃ diagrams for estimating the siliciclastic component of metasedimentary rocks.....	17
Figure 13: P2 member-normalized multi-element profiles for rocks from the Tower stratigraphy and Ospwagan group.....	18
Figure 14: Geochemical diagrams for the plagioclase amphibolite.....	19
Figure 15: Geochemical diagrams for the granodiorite	19
Figure 16: Photomicrographs in plane-polarized light of Tower stratigraphy rocks	20
Figure 17: Phase diagram sections in MnNCKFMASHT	21
Figure 18: Zr/TiO ₂ -Ni diagram for discriminating metasedimentary and meta-igneous rocks	23
Figure 19: Discrimination diagrams showing the compositions of Tower stratigraphy rocks	26
Figure 20: Chondrite-normalized REE profiles and primitive mantle-normalized multi-element profiles for Tower stratigraphy rocks.....	27
Figure 21: Chondrite-normalized REE profiles and primitive mantle-normalized multi-element profiles of mafic rocks associated with East Kisseynew domain VMS deposits, and least-altered hornblende gneiss of the Tower stratigraphy	28
Figure 22: Primitive mantle-normalized multi-element profiles of intermediate and felsic rocks associated with East Kisseynew domain VMS deposits, and the grunerite-magnetite and biotite-garnet gneisses of the Tower stratigraphy	29
Figure 23: Schematic protolithostratigraphic section of the Tower stratigraphy from the structural footwall to the structural hangingwall	31
Figure 24: Discrimination diagrams for the least altered mafic rocks of the Tower deposit.....	32
Figure 25: Discrimination diagrams for the hangingwall granodiorite and biotite-muscovite schist samples 108-17-T06, 108-17-T07, and 108-17-T22.....	33

Introduction

The Tower Cu-Zn-Ag-Au deposit is located along the eastern margin of the sub-Phanerozoic Thompson nickel belt (TNB; Figure 1). It was discovered by Falconbridge Ltd. (now Glencore plc) in September of 2000 during exploration for Ni-sulphide deposits in the William Lake area (Assessment Files 73953, 73950, Manitoba Growth, Enterprise and Trade, Winnipeg). Follow-up drilling in the autumn of 2000 and winter of 2001 intersected significant Cu-Zn-Au mineralization in what has become known as the T1 zone of the Tower deposit (Assessment File 63G13256). The property was then acquired by Pure Nickel Inc. in August of 2007 (Beaudry, 2007). Rockcliff Resources Inc. (now Rockcliff Metals Corp.) entered an option and joint-venture agreement with Pure Nickel to explore the Tower deposit in February of 2008. Rockcliff Resources completed drill programs from 2010 to 2014 to further delineate the deposit, and the T2 zone was discovered during the 2012 drill program (Assessment Files 63G13256, 63G14375). An indicated-resource estimate released in 2013 included 1 Mt at 3.7% Cu, 1.0% Zn, 17 g/t Ag and 0.5 g/t Au (Caracle Creek

International Consulting Inc., 2013). In April of 2015, Rockcliff Resources agreed to sell its interest in the Tower property to Akuna Minerals Inc., and Pure Nickel sold its remaining interest to Akuna Minerals in June of the same year. Akuna Minerals is working toward developing the Tower deposit, and hopes to bring the deposit into production in the near future.

The significance of volcanogenic massive-sulphide (VMS) mineralization within a metalotect known for its magmatic Ni deposits is uncertain and brings into question the affinity of the hostrocks. Initial work by Falconbridge suggested that the mineralization is hosted by metasedimentary rocks of the Ospwagan group intruded by altered ultramafic rocks (Beaudry, 2007; Assessment Files 73953, 73950), implying that the Precambrian rocks in the area are part of the TNB; however, later work by Rockcliff Resources suggested that the metasedimentary rocks are subordinate to metavolcanic rocks and metamorphosed ultramafic intrusions (Assessment File 63G13256), possibly more in keeping with greenstone belts in the adjacent Superior province or Trans-Hudson orogen (THO). Garnet, amphibole and biotite are described as common constituents in the

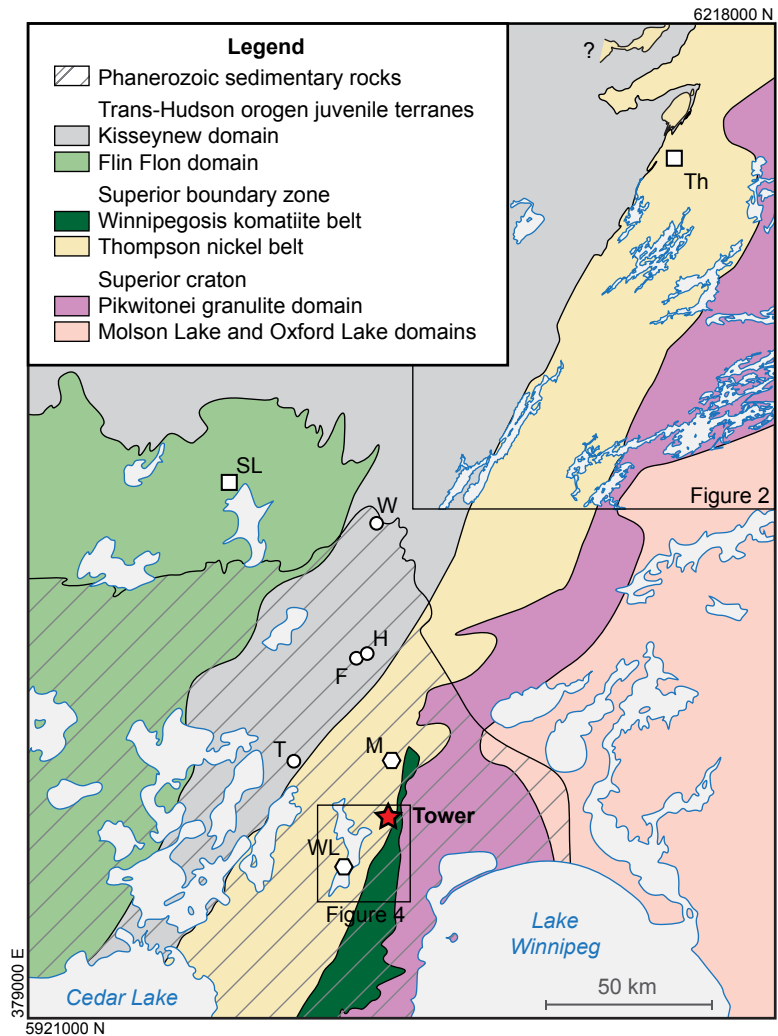


Figure 1: Geological domains along the Superior boundary zone, central Manitoba (modified from NATMAP Shield Margin Project Working Group, 1998; Macek et al., 2006; Waterton et al., 2017). Symbols: circles, Cu-Zn deposits in the sub-Phanerozoic East Kiseynew domain; hexagons, Ni-Cu deposits/occurrences in the sub-Phanerozoic Thompson nickel belt; squares, towns/cities; star, Tower deposit. Abbreviations: F, Fenton deposit; H, Harmin deposit; M, Minago deposit; SL, Snow Lake; T, Talbot deposit; Th, Thompson; W, Watts River deposit; WL, William Lake occurrence.

ultramafic rocks. Garnet-bearing ultramafic rocks are unknown in the Paleoproterozoic of the TNB but are described in the adjacent Pikwitonei granulite domain (PGD) of the Superior province (Böhm, 2005a, b; Couëslan, 2014). In contrast, VMS deposits have not been documented in the TNB or PGD but are widespread in the Flin Flon and East Kiseynew domains of the THO: several deposits have been discovered to date in the sub-Phanerozoic East Kiseynew domain, including the Talbot deposit, located roughly 32 km northwest of the Tower deposit (Simard et al., 2010a). In this regard, it is possible that the rocks hosting the Tower deposit could represent a klippe of juvenile THO rocks lying unconformably on TNB rocks.

The aim of this project is to evaluate the rocks hosting the Cu-Zn-Ag-Au mineralization at Akuna Minerals' Tower

property, establish any genetic affiliation to the East Kiseynew domain, TNB or PGD, and identify possible VMS-related hydrothermal alteration. Identifying the provenance of the host rocks could expand the mineral potential of the TNB or PGD, or expand the known area of the sub-Paleozoic FFD. Identifying VMS-related hydrothermal alteration could provide exploration vectors to additional mineralization.

Regional setting

The TNB forms a segment of the Superior boundary zone, flanked to the northwest by the Kiseynew domain of the Trans-Hudson orogen and to the southeast by the PGD of the Superior craton (Figure 1). The exposed TNB is underlain largely by reworked Archean gneiss of the Superior craton (Figure 2),

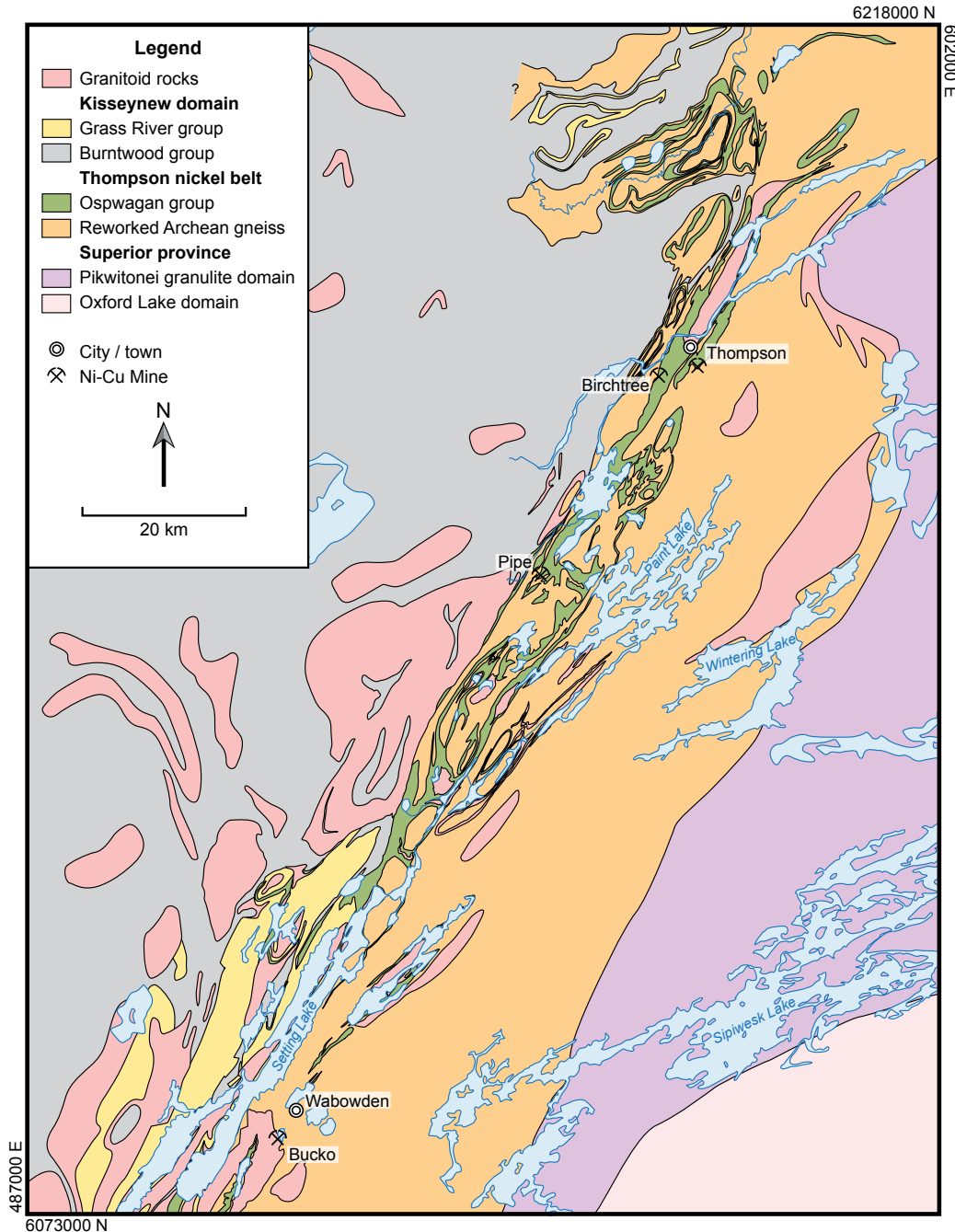


Figure 2: Simplified geology of the exposed Thompson nickel belt and adjacent portions of the Kiseynew domain and Superior craton (modified from Macek et al., 2006).

which is typically quartzofeldspathic with enclaves of mafic to ultramafic rock. It is commonly migmatitic and characterized by complex internal structures that are the result of multiple generations of Archean and Paleoproterozoic deformation and metamorphism; clearly recognizable paragneiss is rare. The gneiss is interpreted to be derived from the adjacent PGD, which was subjected to amphibolite- to granulite-facies metamorphic conditions from ca. 2720 to 2640 Ma (Hubregtse, 1980; Mezger et al., 1990; Heaman et al., 2011; Guevara et al., 2016a, b; Guevara et al., 2018). The granulites of the PGD were exhumed and unconformably overlain by the Paleoproterozoic supracrustal rocks of the Ospwagan group (TNB) prior to intrusion of the Molson dike swarm and associated ultramafic intrusions at ca. 1883 Ma (Bleeker, 1990; Zwanzig et al., 2007; Heaman et al., 2009; Scoates et al., 2017). The Archean basement gneiss and Ospwagan group were subjected to multiple generations of deformation and metamorphic conditions ranging from middle-amphibolite facies to lower-granulite facies during the Trans-Hudson orogeny (Bleeker, 1990; Burnham et al., 2009; Couëslan and Pattison, 2012).

The dominant phase of penetrative deformation is D_2 , which affected the Ospwagan group and ca. 1883 Ma magmatic rocks. This deformation phase resulted in the formation of F_2 nappe structures, which incorporated the underlying Archean gneiss. The nappe structures have been interpreted as either east verging (Bleeker, 1990; White et al., 2002) or southwest verging (Zwanzig et al., 2007; Burnham et al., 2009). The recumbent folds are associated with regionally penetrative S_2 fabrics. The D_2 phase of deformation is interpreted to be the result of convergence between the Superior craton margin and the Reindeer zone of the Trans-Hudson orogen from ca. 1830 to 1800 Ma, and was accompanied, and outlasted, by prograde to peak regional metamorphism. The D_3 phase of deformation resulted in isoclinal folds with vertical to steeply southeast-dipping axial planes (Bleeker, 1990; Burnham et al., 2009). Mylonite zones with subvertical stretching lineations parallel many of the regional F_3 folds. Tightening of D_3 structures continued during D_4 , marked by localized retrograde greenschist metamorphism along northeast-striking, mylonitic and cataclastic shear zones that commonly record southeast-side-up sinistral movement (Bleeker, 1990; Burnham et al., 2009).

Ospwagan group stratigraphy

The following summary of the Ospwagan group is sourced largely from Bleeker (1990) and Zwanzig et al. (2007). The Paleoproterozoic Ospwagan group unconformably overlies Archean basement gneiss in the TNB (Figure 3). The lowermost unit of the Ospwagan group is the Manasan formation, which consists of two members: the lower M1 member, consisting of layered to laminated sandstone with local conglomerate layers near the base; and the overlying M2 member, consisting of semipelitic rock. The Manasan formation is interpreted as a transgressive, fining-upward sequence deposited along a passive margin. This siliciclastic system grades into the overlying calcareous sedimentary rocks of the Thompson formation.

The Thompson formation consists of three members: the T1 member comprises a variety of calcareous–siliceous rocks including chert, calcsilicate and impure marble; the T2 member

is a semipelitic calcareous gneiss that is rarely present; and the T3 member consists of impure dolomitic marble with local horizons of calcsilicate (Figure 3). The Thompson formation represents a transition from a siliciclastic-dominated to a carbonate-dominated system.

The Pipe formation is subdivided into three members (Figure 3). The P1 member consists of a graphite-rich, sulphide-facies iron formation at the base (the locus of the Pipe II and Birchtree Ni sulphide orebodies), overlain by a silicate-facies iron formation. The top of the P1 member consists of a reddish, laminated, siliceous rock. The P1 member grades into the overlying pelitic rocks of the P2 member, the top of which is marked by a sulphide-facies iron formation (the locus of the Thompson Ni sulphide orebody). The overlying P3 member consists of a wide variety of rock types, including laminated, siliceous sedimentary rocks; silicate-, carbonate- and local oxide-facies iron formations; and semipelitic rocks, calcsilicate and a local horizon of relatively pure dolomitic marble. The Pipe formation represents a mix of chemical sediments and fine to very fine siliciclastic sediments that were deposited in either an open-marine environment (Zwanzig et al., 2007) or during the development of a foredeep basin (Bleeker, 1990).

The Setting formation is divided into two members and is defined to include all siliciclastic rocks above the uppermost iron formation of the P3 member (Figure 3). The S1 member consists of rhythmically interbedded quartzite and pelitic schist with local calcareous concretions, which are very characteristic of the S1 member. The S2 member consists of thickly layered greywacke, with local horizons grading from conglomeratic at the base to pelitic at the top. No contact has been observed between the S1 and S2 members. It is possible that they represent a lateral facies change as opposed to a vertical succession. The S2 member appears to be missing altogether in the area of the Pipe mine, where contacts between the S1 member and the overlying Bah Lake assemblage are exposed. The Setting formation is interpreted to have been deposited by turbidity currents in a relatively deep-marine environment, possibly a foredeep basin (Bleeker, 1990). The coarse clastic material and thick turbidite bedding of the S2 member may record the shallowing of the basin, the onset of active tectonism, or a lateral sedimentary facies change possibly to a submarine-channel or upper-fan environment (Zwanzig et al., 2007).

At the top of the Ospwagan group is the Bah Lake assemblage, which consists of mafic to ultramafic volcanic rocks dominated by massive to pillowed basalt flows with local picrite and minor synvolcanic intrusions (Figure 3). The Bah Lake assemblage is dominated by a high-Mg suite (similar to normal mid-ocean ridge basalt; N-MORB) that occurs throughout much of the main TNB, and an incompatible-element-enriched suite (similar to enriched mid-ocean ridge basalt; E-MORB) that occurs in the northwestern Setting Lake area and along the margin of the Kisseynew domain (Zwanzig, 2005). The enriched suite is interpreted to overlie the high-Mg suite; however, it is uncertain if this represents a stratigraphic or tectonic relationship. The Bah Lake assemblage may suggest the onset of active rifting in the TNB (Zwanzig, 2005; Zwanzig et al., 2007), or that the foredeep was magmatically active (Bleeker, 1990).

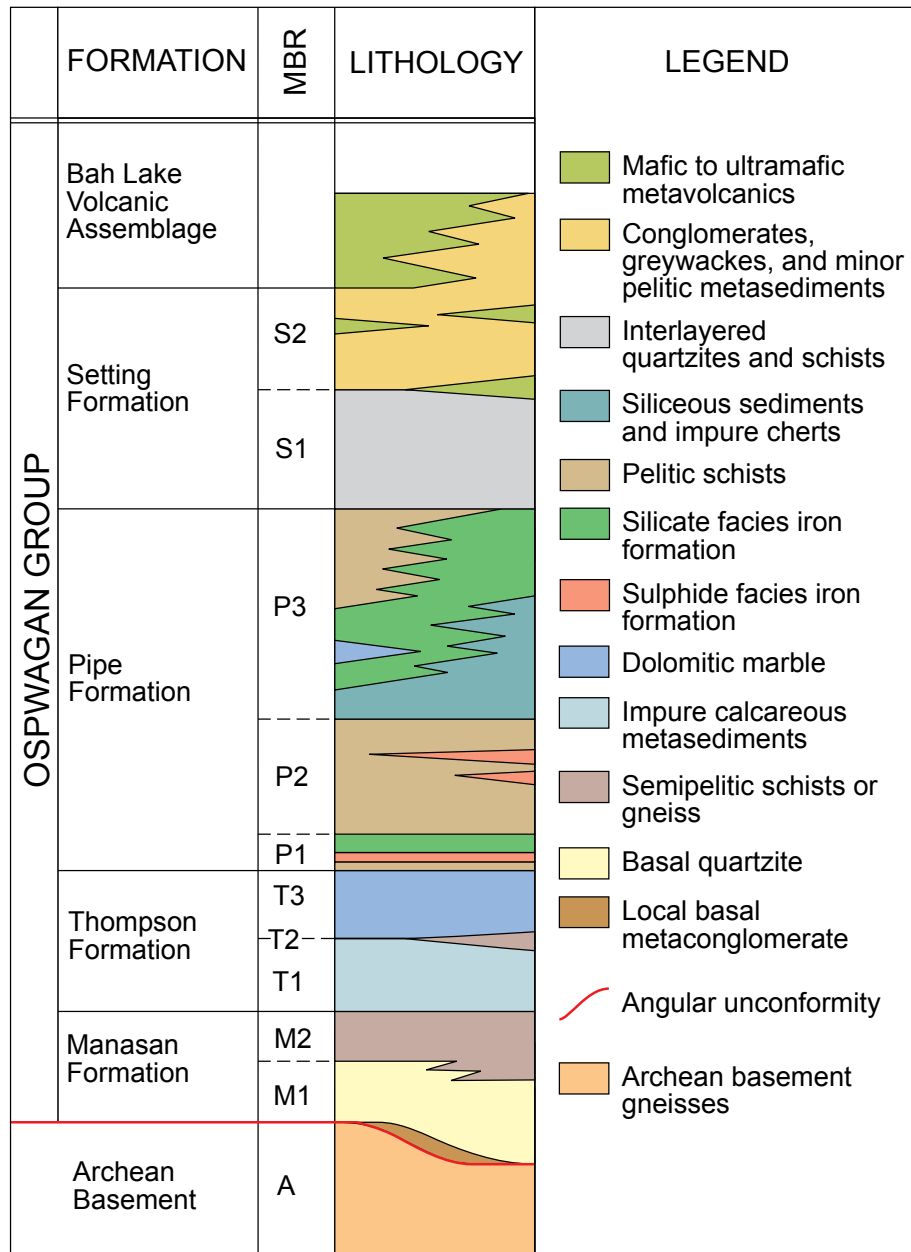


Figure 3: Schematic lithostratigraphic section of the Oswagan Group (adapted from Bleeker, 1990). Abbreviation: MBR, member.

A maximum age for the Oswagan group is provided by a ca. 1974 Ma zircon recovered from Setting formation greywacke (Bleeker and Hamilton, 2001). A minimum age for the Oswagan group is provided by crosscutting amphibolitized dikes interpreted to be part of the Molson dike swarm, and the possibly comagmatic Ni-ore-bearing ultramafic sills, which intruded the Oswagan group at all stratigraphic levels at ca. 1883 Ma (Bleeker, 1990; Zwanzig et al., 2007; Heaman et al., 2009; Scoates et al., 2017), and a ca. 1878–1890 Ma intrusive complex that intrudes the Bah Lake assemblage on Setting Lake (Zwanzig et al., 2003; Percival et al., 2004).

Winnipegosis komatiite belt

The Winnipegosis komatiite belt (WKB) occurs along the eastern side of the sub-Phanerozoic Superior boundary zone in

the Lake Winnipegosis–Cedar Lake area (Figure 1). It forms a 150 km by 30 km greenstone belt adjacent to the TNB and occurs under 150–500 m of Phanerozoic cover (Hulbert et al., 1994; Pearson, 1996). Initially misidentified as Oswagan group rocks, the mafic to ultramafic volcanic rocks of the WKB are distinctly younger (ca. 1870 Ma), than the volcanic rocks of the Oswagan group (ca. >1890 Ma, Zwanzig, 2005; McGregor, 2012; Waterton et al., 2017). The WKB is subdivided into three mafic to ultramafic volcanic packages: the western Upper tholeiite suite, central Winnipegosis komatiite suite, and the eastern Grand Island tholeiite suite (Lin et al., 1998; McGregor, 2012). Little is known about the two tholeiite suites which are characterized by MORB-like trace-element profiles; however, they have marginally different geochemistry, the Upper tholeiite suite being slightly more evolved in terms of Mg:Fe ratios (Lin et al., 1998).

The Winnipegosis komatiite suite forms a west-facing homoclinal sequence that rests unconformably on weathered Superior craton tonalite to granodiorite (Lin et al., 1998). The sequence consists of a thin, discontinuous interval of tonalite-derived basal conglomerate and sandstone (Waterton et al., 2017). This is overlain by <1 km thick package of Fe-tholeiite flows with thick sulphidic argillite interflow horizons. The tholeiites are overlain by a <500 m thick sequence of clastic and chemical sedimentary rocks which are dominantly carbonate at the base and become increasingly shale-rich at the top, indicating a subsiding basin. The sedimentary rocks are overlain by a thick succession (<1 km) of komatiite which vary from thin sheet flows to ponded cumulate horizons. Gabbro and peridotite–dunite bodies intrude all of the above units (Pearson, 1996; McGregor, 2012). Rocks of the WKB are characterized by sub-greenschist to greenschist facies metamorphic assemblages (Waterton et al., 2017), and appear to extend northward to where komatiites of similar low metamorphic grade are recognized east of the William Lake area (Lin et al., 1998). Recent studies suggest the komatiitic magmas were generated by a mantle plume deflected towards the margins of the Superior craton by a thick lithospheric keel, and were emplaced within an evolving rift environment (Waterton et al., 2017; Ciborowski et al., 2017). The Upper and Grand Island tholeiite suites have yielded initial ϵ_{Nd} values ranging from +3.24 to +4.5, while the Winnipegosis komatiite suite has yielded ϵ_{Nd} values ranging from +1.03 to +7.8 (Hulbert et al., 1994; Burnham et al., 2009; Ciborowski et al., 2017). The nature of the contact between the TNB and WKB remains uncertain.

East Kiseynew domain

The East Kiseynew domain is the southern extension of the Kiseynew domain below the Phanerozoic cover. Situated between the Superior craton margin and the Flin Flon domain it was interpreted to consist of migmatitic metasedimentary rocks of the Burntwood group interlayered with felsic metaplutonic veins and sheets (Leclair et al., 1997; Figure 1). However, the discovery of several VMS deposits (Watts River, Harmin, Fenton, and Talbot) in the domain has brought this interpretation into question (Simard et al., 2010a). Recent studies (Simard et al., 2010a; Bailes, 2015; Reid, 2017) suggest complex structural interleaving of Flin Flon domain arc rocks, Kiseynew domain Burntwood group rocks, and possibly TNB rocks within the East Kiseynew domain. Felsic and mafic gneisses associated with the VMS deposits are interpreted to consist of arc-derived felsic rocks, and contaminated to uncontaminated E-MORB and N-MORB mafic rocks suggesting a possible rifted arc to back-arc environment (Simard et al., 2010a; Bailes, 2015). Samarium–neodymium isotope chemistry for mafic and intermediate gneisses yield initial $\epsilon_{Nd(1.88 Ga)}$ values ranging from +3.0 to +3.7 and values of +3.0 to +3.4 for felsic gneiss, indicating little to no involvement of continental crust (Simard et al., 2010a, b).

Geology of the Tower deposit

The Tower deposit occurs along the eastern margin of the sub-Phanerozoic TNB (Figure 1). The Precambrian rocks are overlain by 70–170 m of Paleozoic limestone and sandstone

(Beaudry, 2007). Falconbridge geologists described the mineralization as being hosted in a thick package of Pipe formation pelitic and siliceous sedimentary rocks intruded by altered ultramafic rocks (Assessment Files 73953, 73950), consistent with the compilation map of Macek et al. (2006), which suggests that the Tower property may be underlain by Archean and Ospwagan group rocks (Figure 4). Approaching the mineralization from the hangingwall, the sequence consists of magnetite-bearing silicate-facies iron formation, turbidite, and then a thick sequence of pelitic sedimentary rocks intruded by an altered ultramafic sill (Beaudry, 2007). The mineralization is hosted in the pelitic sedimentary rocks in proximity to the ultramafic body.

Conversely, work conducted by Rockcliff Resources determined the Tower property to be underlain by dominantly volcanic and ultramafic rocks with subordinate sedimentary rocks (Assessment File 63G13256). The volcanic rocks are dark green and fine to medium grained, contain possible pillow selvages, and have sharp contacts with adjacent units. The ultramafic rocks are described as peridotite, as well as dark green to black, fine- to coarse-grained rocks variably enriched in amphibole, garnet and biotite. In contrast to the Falconbridge work, the mineralization of the T1 zone was interpreted to occur within the ultramafic rocks, in proximity to Pipe formation sedimentary rocks that consist of grey metapelite containing fine-grained garnet and muscovite.

The mineralization of the T1 zone has a strike of approximately 013° with a dip of 75–85° to the east (Assessment File 73953). The mineralization transects the regional foliation and is characterized by rounded to subangular, millimetre- to centimetre-scale fragments of wallrock within a matrix of semi-solid to solid sulphide (Assessment Files 73953, 63G13256, 63G14375), which is interpreted to be mobilized from the source and forming the matrix of a fault breccia. Mineralization of the T2 zone is interpreted to be in situ, within pervasively altered volcanic rocks approximately 200 m east of the T1 zone (Rockcliff Resources Inc., 2012; Assessment File 63G13256).

The Cu- and Zn-rich nature of the mineralization is unusual for the TNB, as are the low concentrations of Ni and platinum-group elements (Beaudry, 2007). The mineralization is more akin to VMS deposits west of the TNB in the sub-Phanerozoic Flin Flon belt (Simard et al., 2010a), and has been interpreted as a Besshi-type VMS system (Beaudry, 2007; Couëslan, 2017).

Stratigraphy of the Tower deposit

Methodology

Five drillholes were selected for re-examination. Drillholes TP-10-003 and TP-10-004 were both collared in the structural footwall and drilled toward the east, across strike through the T1 zone, and into the hangingwall (Figure 4). Drillholes TP-12-027, TP-12-032 and TP-12-033 were collared in the structural hangingwall and drilled toward the west, across strike through the T1 zone, and into the footwall. Drillholes TP-10-004 and TP-12-032 were collared roughly across strike from each other, allowing for the construction of a continuous section from the footwall into the hangingwall of the deposit. The core from each drillhole was laid out in its entirety, allowing for the entire

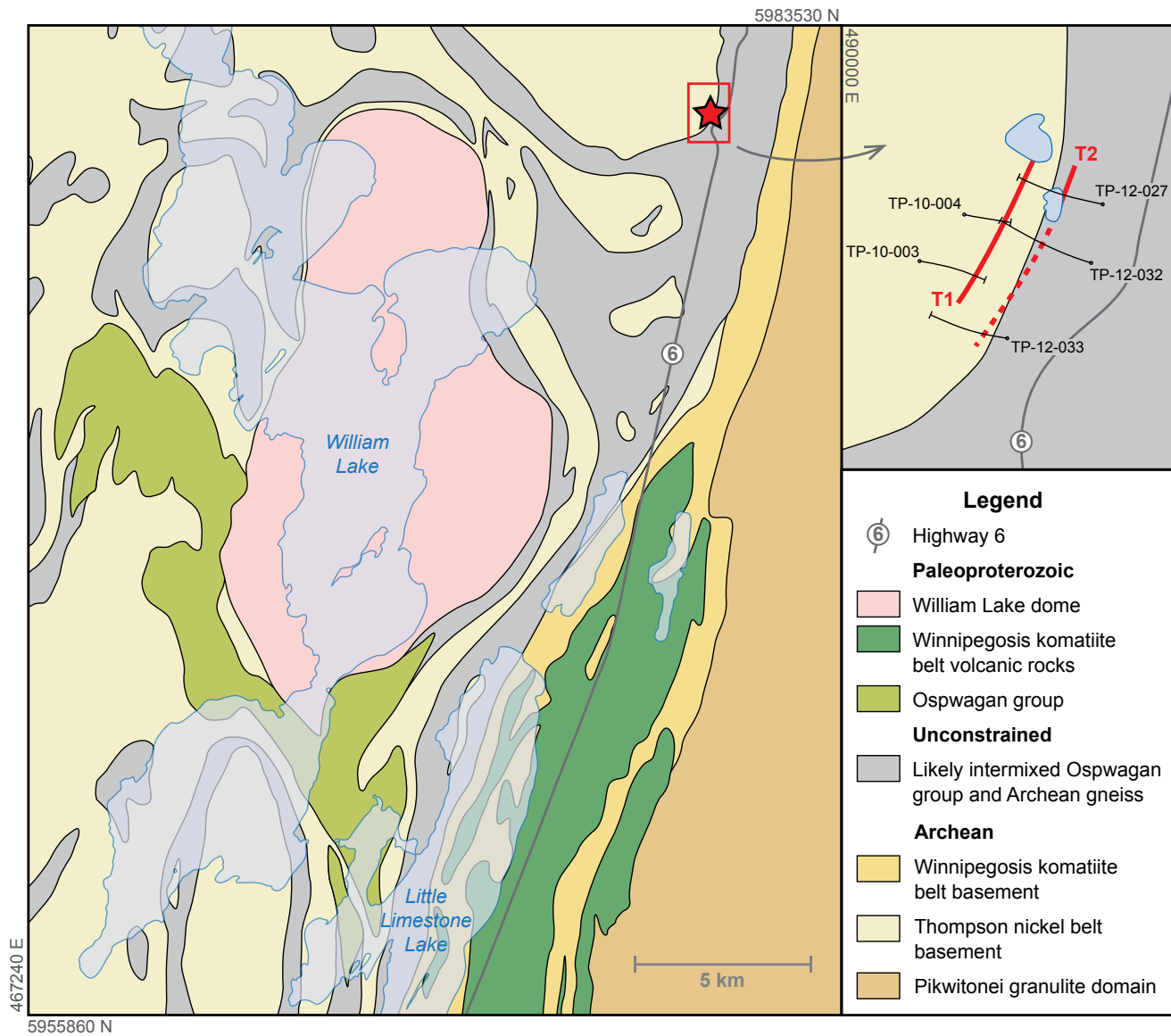


Figure 4: Simplified geology of the William Lake area (modified from Macek et al., 2006). The inset shows the locations of the five examined drillholes and the approximate trace of the T1 and T2 mineralized zones projected to surface. The dashed portion of the T2 zone indicates the possible extension of this horizon along strike.

sequence to be viewed and separated into petrographically distinct intervals. Core logs are provided in Data Repository Item DRI2018004 (Couëslan, 2018)¹.

The following stratigraphic description is from the structural footwall in the west to the hangingwall on the east side of the Tower deposit (Figure 5). The widths of stratigraphic units are reported as approximate true width, while thicknesses of potentially discordant intrusive units are reported as the length of the core intercept. Because of intense deformation, stratigraphic units commonly pinch and swell, and significant variations should be expected along strike. The stratigraphy presented below is idealized and based only on the five examined

drillholes. All units were metamorphosed to amphibolite-facies conditions, and typically have moderate to strong foliations that parallel the stratigraphic layering. Although all rocks described in this report are metamorphosed, the ‘meta-’ prefix has been omitted from rock names for brevity.

The main focus of this study is the rocks that host the Tower deposit; however, the mineralization of the T1 and T2 zones is discussed here briefly in relation to the stratigraphy. For more information regarding mineralization and resource estimates, the reader is referred to Assessment Files 63G1148 and 63G13256, and Caracle Creek International Consulting Inc. (2013).

¹ MGS Data Repository Item DRI2018004 containing the data or other information sources used to compile this report is available to download free of charge at <http://www.gov.mb.ca/iem/info/library/downloads/index.html>, or on request from minesinfo@gov.mb.ca, or from the Resource Centre, Manitoba Growth, Enterprise and Trade, 360–1195 Ellice Avenue, Winnipeg, Manitoba, R3G 3P2, Canada.

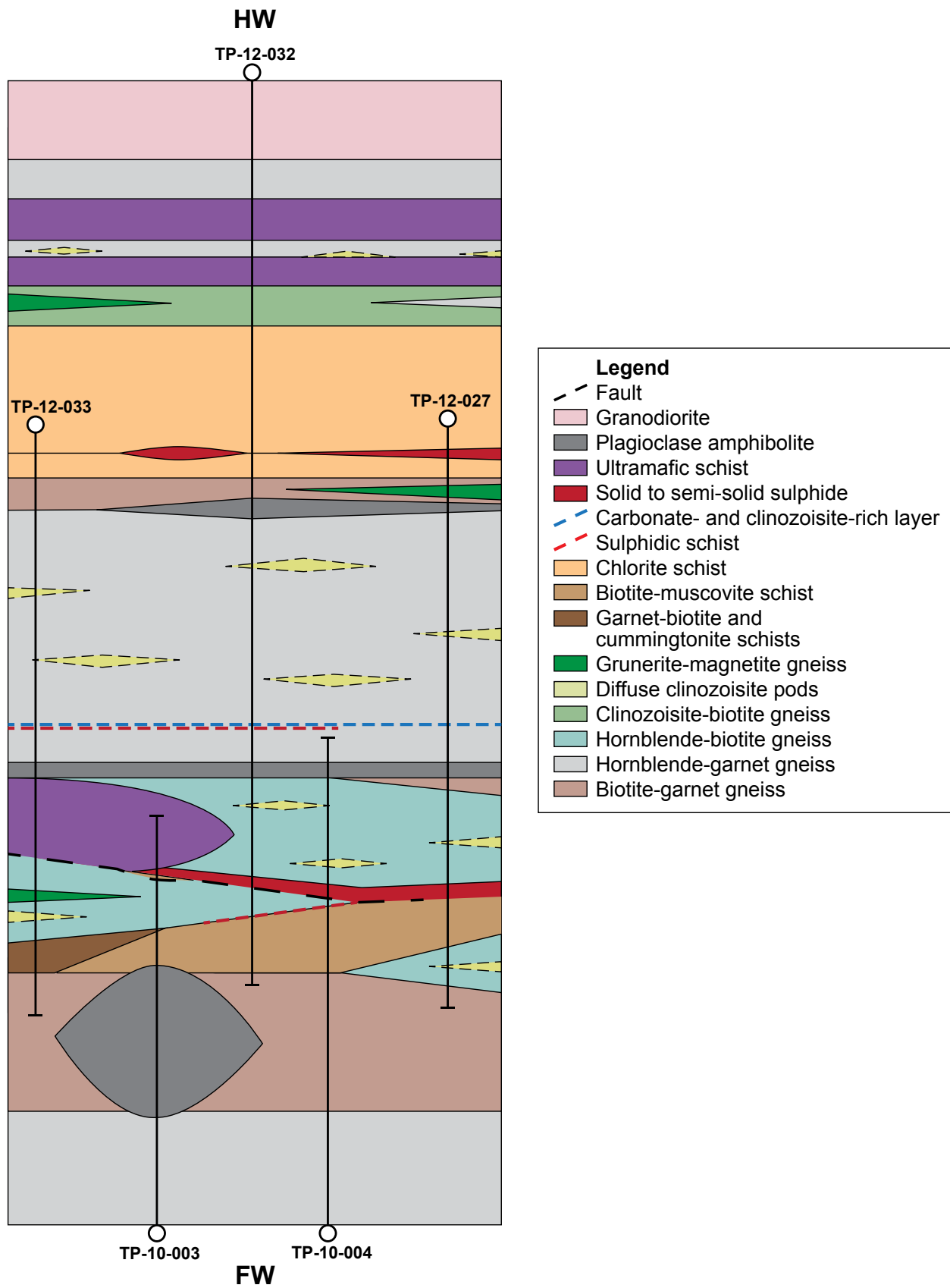


Figure 5: Schematic petrostratigraphic section of the Tower deposit from structural footwall to hangingwall. The approximate intersections of each drillhole are indicated with TP-10-003 and TP-10-004 collared in the structural footwall, and TP-12-027, TP-12-032, and TP-12-033 collared in the structural hangingwall.

Footwall to the T1 zone mineralization

The lowermost unit intersected in the footwall consists of grey-green, medium-grained and laminated to layered, hornblende-garnet gneiss (Figure 6a). The gneiss is locally biotite bearing and typically contains <25 % mafic minerals. It forms a package at least 22 m thick with intercalations, <20 cm thick, of more mafic gneiss (up to 50% mafic minerals).

Overlying the hornblende-garnet gneiss is a grey, fine- to coarse-grained, diffusely layered biotite-garnet gneiss, 4.5–11 m thick (Figure 6b). Garnet and biotite typically make up less than 15% of the rock, which can also contain minor magnetite, ilmenite, and hornblende, and trace amounts of anthophyllite. Plagioclase and quartz make up the remainder of the gneiss and occur in variable proportions. Sparse sulphidic horizons, and occur in variable proportions.

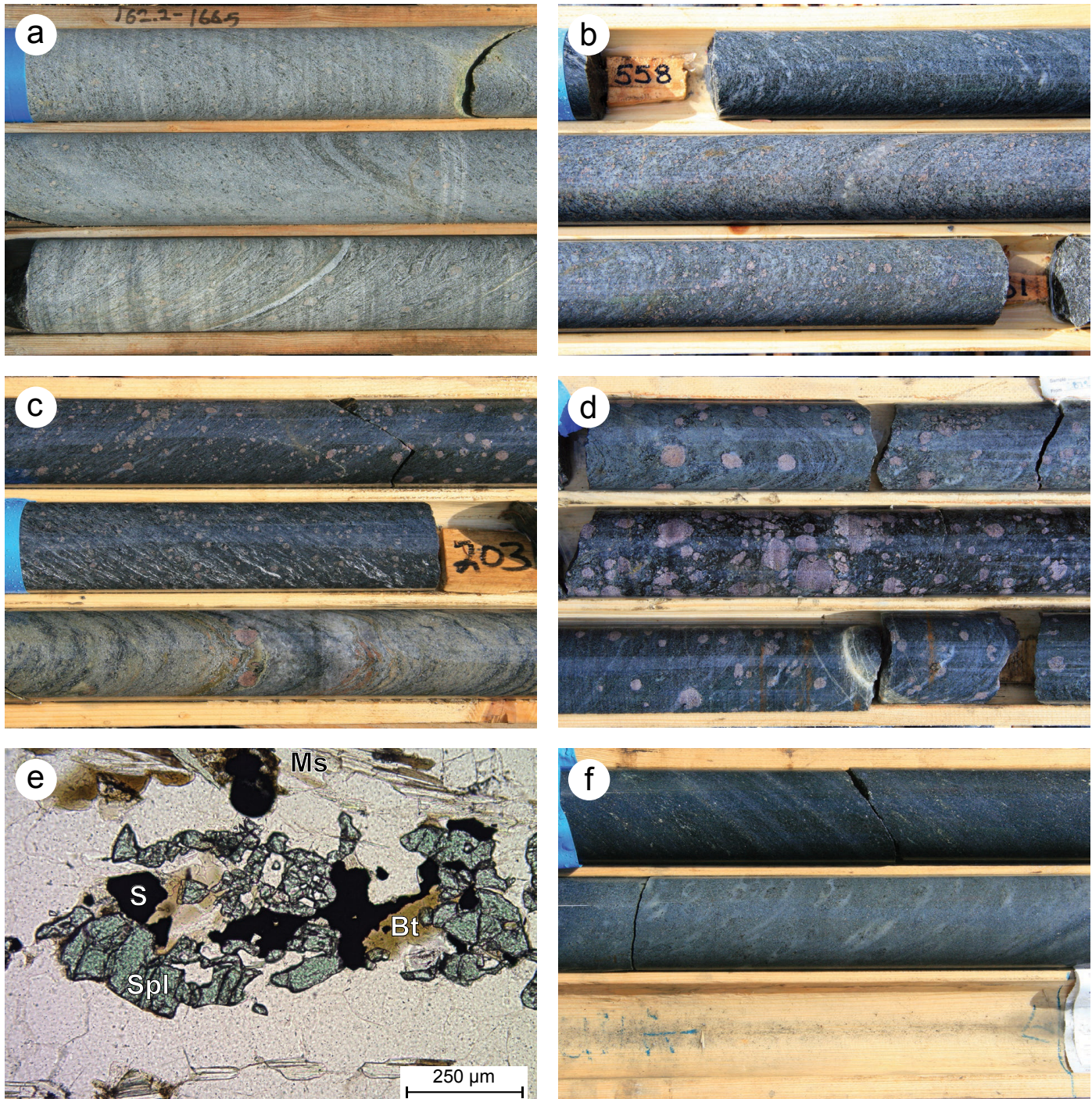


Figure 6: Drillcore and thin section images of units in the footwall to the Tower deposit: **a)** hornblende-garnet gneiss (TP-10-004, 162.2 m); **b)** biotite-garnet gneiss (TP-12-033, 558 m); **c)** biotite-muscovite schist (TP-10-004, 201.3 m), bottom row is strongly retrogressed to chlorite and sericite; **d)** garnet-biotite schist (middle row) interlayered with cummingtonite schist (top and bottom rows; TP-12-033, 518.9 m); **e)** photomicrograph in plane-polarized light of spinel spatially associated with sulphide in biotite-muscovite schist (108-17-T07); **f)** hornblende-biotite gneiss (top row) and grunerite-magnetite gneiss (middle row; TP-10-004, 210 m). Drillcore is NQ (diameter = 4.76 cm). Abbreviations: Bt, biotite; Ms, muscovite; S, sulphide; Spl, spinel.

<25 cm thick, are present. The biotite-garnet gneiss locally grades into layers where garnet becomes sparse, and hornblende becomes the dominant mafic mineral over biotite. Towards the north (drillhole TP-12-027), this hornblende-biotite gneiss becomes the dominant rock type upsection.

Upsection from the biotite-garnet gneiss and hornblende-biotite gneiss is a grey-brown, medium- to coarse-grained and diffusely layered biotite-muscovite schist (Figure 6c). The schist can be 4–120 m thick, and is garnet and locally staurolite bearing. Clinozoisite is rarely present. In drillholes TP-10-003 and TP-12-032, the schist becomes less micaceous up-section with an increase in quartz and feldspar content, while in TP-10-004 muscovite disappears and local staurolite-rich layers <5 mm thick and garnet-rich layers <5 cm thick appear. The disappearance of muscovite could indicate the depletion of potassium relative to aluminum and iron. A possible K-depleted interval is also present at the same stratigraphic level in drillhole TP-12-033, where garnet-biotite schist is interlayered with cumingtonite schist (Figure 6d). The K-depleted schist can contain minor chlorite and up to 3% chalcopyrite and 3% magnetite. The biotite-muscovite schist locally becomes increasingly sulphidic in the uppermost part of the section where it grades into a 1.0–2.3 m thick biotite-rich sulphidic schist corresponding to mineralization of the T1 zone. Green spinel was identified in thin section from a sulphidic portion of the biotite-muscovite schist (Figure 6e).

In drillhole TP-10-004 a thin layer (1.5 m thick) of grunerite-magnetite gneiss (Figure 6f) occurs between the sulphidic schist and the T1 mineralization. The grunerite-magnetite gneiss is greenish grey, medium grained, homogeneous to mottled, and strongly magnetic. It is siliceous and grunerite, magnetite, sulphide, hornblende, and biotite bearing. Magnetite forms discrete, equant porphyroblasts. The grunerite-magnetite gneiss contains local layers of the overlying, laminated hornblende-biotite gneiss.

The T1 zone mineralization

The nature of the T1 zone mineralization varies along strike from solid sulphide to sulphidic schist with foliation-parallel sulphide stringers. The sulphidic schist is typically biotite rich and contains up to 12% net-textured sulphide (Figure 7a). The solid sulphide occurs as the matrix to a breccia that contains rounded fragments of ultramafic amphibolite and rounded to angular fragments of white quartz <7 cm across (Figure 7b). The fragments are unsorted and matrix supported with rotated fabrics. The contacts of the breccia are locally marked by a seam of siliceous mylonite <5 mm thick. Local foliation-parallel stringers of chalcopyrite are present in the core up to 2 m away from the sulphide breccia. The T1 zone appears to be slightly discordant to the stratigraphy. In the northernmost intersection (TP-12-027), the T1 zone occurs immediately above the biotite-muscovite schist, whereas the mineralization in the southernmost intersection (TP-10-003) occurs within the laminated hornblende-biotite gneiss, approximately 96 m above the upper contact of the biotite-muscovite schist. The close association of the siliceous mylonite, the discordant nature of the mineralization, and its occurrence as a sulphide breccia has led to the interpretation that the sulphide was mobilized from its source,

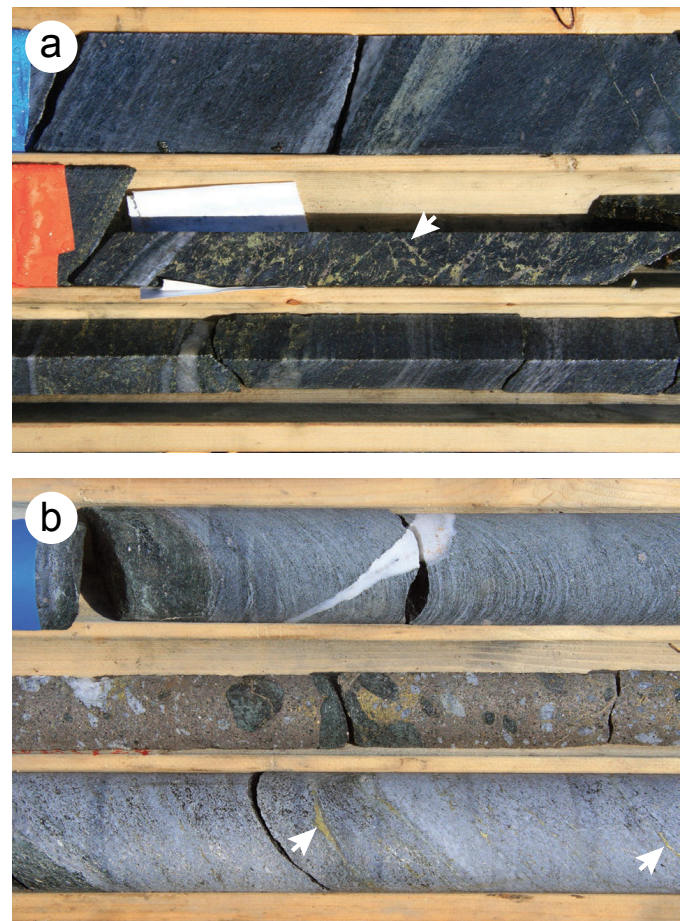


Figure 7: Drillcore images from the T1 mineralized zone of the Tower deposit: **a**) sulphidic schist of the T1 zone with stringers of chalcopyrite and pyrrhotite (middle row, arrow indicates cross-cutting veinlet of sulphide; TP-12-027, 438.4 m); **b**) solid sulphide with fragments of ultramafic amphibolite and white quartz (middle row); foliation-parallel stringers of chalcopyrite are visible in the immediate footwall (arrows, bottom row; TP-12-032, 565.7 m). Drillcore is NQ (diameter = 4.76 cm).

forming a fault breccia (Assessment File 63G13256). Assuming a similar structural history as the rest of the TNB, the brittle-ductile nature of the structure suggests it likely belongs to the later D₃–D₄ phase of deformation.

Stratigraphy between the T1 and T2 zones

The mineralization of the T1 zone is overlain by an 8.9–38 m thick sequence of laminated hornblende-biotite gneiss (Figure 8a). The rock is grey-green, medium grained and weakly magnetic in places. It is typically laminated, but local zones can have diffuse bands <20 cm thick. Sparse layers can contain up to 7% garnet. Minor sulphide can be present. Clinozoisite occurs in diffuse layers or pods <10 cm thick, which vary from layered to mottled.

In drillhole TP-12-027, the laminated hornblende-biotite gneiss is overlain by a thin layer (3 m) of biotite-garnet gneiss similar to that described in the footwall to the T1 zone. Elsewhere, the laminated hornblende-biotite gneiss is overlain by a thick (120–175 m) sequence of hornblende-garnet gneiss with diffuse pods of clinozoisite, and layers of biotite-garnet gneiss

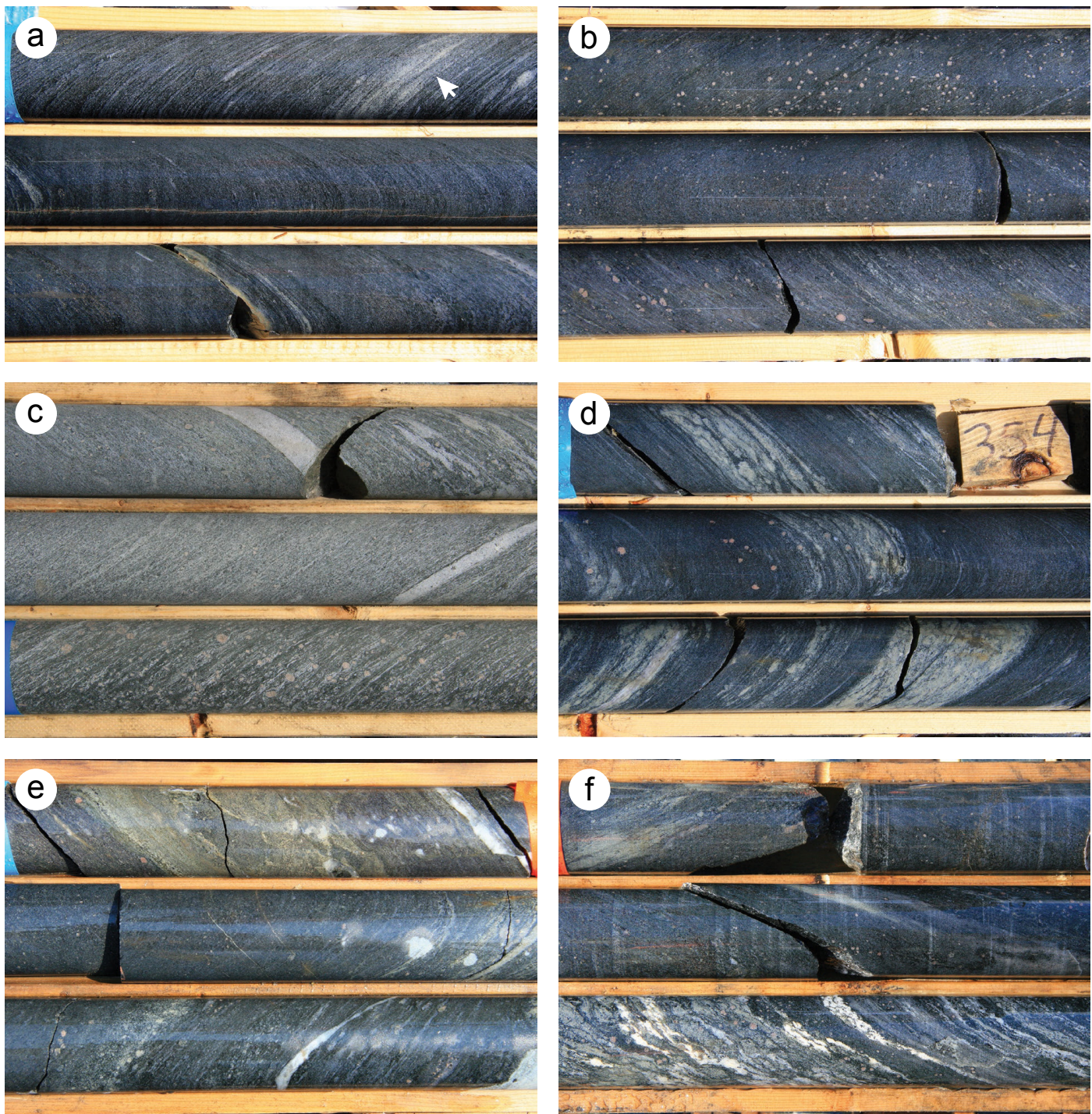


Figure 8: Drillcore images of units between the T1 and T2 mineralized zones: **a)** laminated hornblende-biotite gneiss with diffuse clinzoisite pod (arrow; TP-10-004, 227.1 m); **b)** hornblende-garnet gneiss (TP-12-027, 238.2 m); **c)** mafic-enriched hornblende-garnet gneiss with stringy quartz laminations (bottom row; TP-10-004, 274.5 m); **d)** clinzoisite-rich pods in hornblende-garnet gneiss (TP-12-027, 353.9 m); **e)** sulphidic layer (top row) in hornblende-garnet gneiss (TP-12-032, 425.5 m); **f)** interlayered carbonate- and clinzoisite-rich layers (bottom row) hosted in hornblende-garnet gneiss (TP-12-033, 350.5 m). Drillcore is NQ (diameter = 4.76 cm).

(Figure 8b). The hornblende-garnet gneiss is typically grey to green-grey, medium to coarse grained, nonmagnetic and laminated to crudely layered on a scale <3 m. In addition to garnet and hornblende, the gneiss contains variable amounts of biotite and clinzoisite. Mafic minerals generally make up <30% of the rock; however, local mafic-enriched layers (<2.5 m) may contain up to 50%. The mafic-enriched layers locally contain stringy quartz laminations (Figure 8c). The clinzoisite-rich

pods or layers are light green-grey, <20 cm thick, vary from mottled to layered, and can contain minor carbonate and garnet (Figure 8d). The biotite-garnet gneiss occurs as bands <40 cm thick and is similar to that described in the footwall to the T1 zone. A thin (25–85 cm) sulphidic layer is locally present in the lower portions of the hornblende-garnet gneiss package (Figure 8e). The sulphidic layer is brown-grey, fine to medium grained and weakly to moderately magnetic. The composition varies

from a pyrrhotite- and biotite-rich siliceous rock to a biotite- and hornblende-bearing, clinozoisite- and pyrrhotite-rich rock. Laminations and thin layers (<1 cm) of carbonate appear to form a local marker horizon at the Tower property (Figure 8f). These layers commonly occur in clusters within the hornblende-garnet gneiss, just above the previously mentioned sulphidic horizon. The carbonate layers are commonly interlayered with clinozoisite-rich and locally garnet-bearing calcsilicate.

The hornblende-garnet gneiss sequence is overlain by a 10–34 m thick package of biotite-garnet gneiss (Figure 9a). The gneiss is brown-grey, medium grained and moderately magnetic in places. Hornblende is typically present in variable proportions and chlorite and magnetite are present in minor amounts. The biotite-garnet gneiss contains local clinozoisite-enriched layers. Local layers of grunerite-magnetite gneiss, <1 m thick, can be present. The gneiss is strongly magnetic and garnet

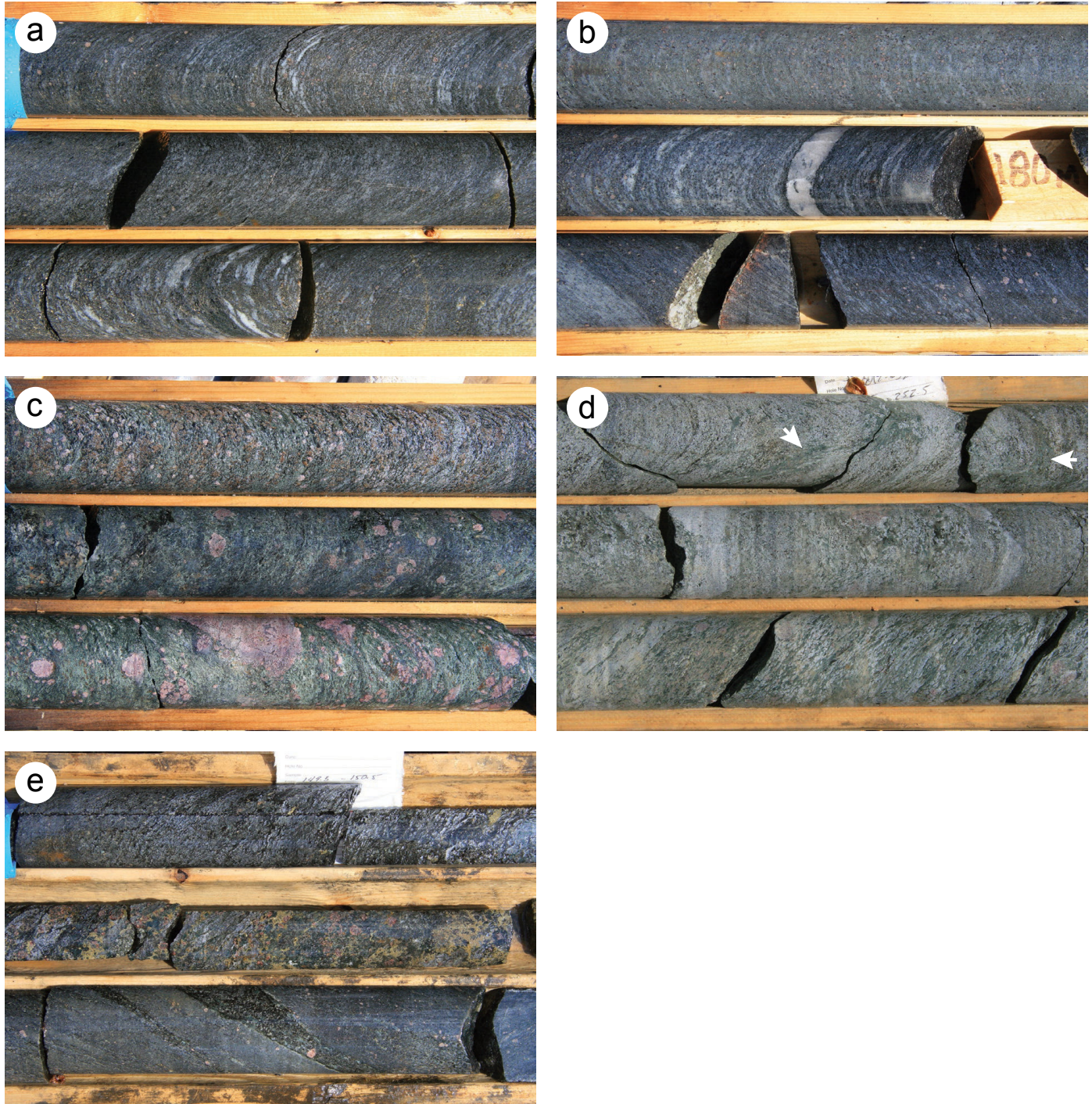


Figure 9: Drillcore images from the T2 mineralized zone and its footwall: **a)** biotite-garnet gneiss (TP-12-027, 161.2 m); **b)** grunerite-magnetite gneiss (top row) hosted in biotite-garnet gneiss (middle and bottom rows; TP-12-027, 178.4 m); **c)** garnet-bearing and staurolite-rich chlorite schist (top row) grading into garnet-rich chlorite schist (bottom row; TP-12-032, 285.9 m); **d)** chlorite-rich veins in clinozoisite-biotite gneiss (arrows, top row) overlying chlorite schist (middle and bottom rows; TP-12-032, 251.4 m); **e)** chlorite schist with pods of semi-solid chalcopyrite mineralization from the T2 zone (middle row; TP-12-033, 149.3 m). Drillcore is NQ (diameter = 4.76 cm).

bearing with minor biotite and hornblende. The magnetite occurs as discrete equant grains (Figure 9b). The biotite-garnet gneiss grades over 1–4 m into the overlying chlorite schist.

The chlorite schist is the uppermost unit in drillholes TP-12-027 and TP-12-033. Drillhole TP-12-032 intersected the entire interval of schist, which is approximately 42 m thick. It is dark green to purplish green to brown, coarse grained, crudely banded on a scale of <50 cm, variably magnetic and compositionally heterogeneous (Figure 9c). The schist is typically quartz and chlorite rich with variable amounts of garnet, staurolite, magnetite, ilmenite and biotite, and minor sulphide±carbonate, hornblende and muscovite. Garnet porphyroblasts up to 10 cm across locally form up to 70% of the rock. Quartz occurs as discrete laminations, layers and pods <10 cm thick. A sulphidic horizon up to 4 m thick occurs near the base of the unit, and represents the mineralization of the T2 zone. The contact between the chlorite schist and overlying clinozoisite-biotite gneiss is gradational over approximately 1 m (Figure 9d), with abundant chlorite veins up to 3 cm thick present at the contact and decreasing in abundance and thickness to form sparse chlorite veins <5 mm thick.

The T2 zone mineralization

Mineralization of the T2 zone occurs as disseminated sulphide blebs <1 cm across, and as stringers and pods of semi-solid sulphide <5 cm across within the chlorite schist (Figure 9e). The stringers and pods typically have diffuse margins, parallel the foliation and appear to be concentrated toward the bottom of the chlorite schist unit. Of the selected drillholes, the core from TP-12-027 was the only one previously described to contain T2 zone mineralization (Assessment File 63G13256); however, sulphide mineralization was also observed at the same stratigraphic level in TP-12-033, and weak Cu mineralization is present in TP-12-032. This suggests that, although the T2 zone may pinch and swell, it appears to form a continuous horizon toward the bottom of the chlorite schist across the Tower property, suggesting that it may be stratiform and in situ.

Hangingwall to the Tower deposit

The units above the chlorite schist are described only from drillhole TP-12-032, and their continuity along strike is not known. The chlorite schist is overlain by a 9 m thick sequence of clinozoisite-biotite gneiss with intercalations of grunerite-magnetite gneiss, <1 m thick. The clinozoisite-biotite gneiss is light grey, fine grained and weakly magnetic in places. It is diffusely banded at a scale of <5 cm and grades into the grunerite-magnetite gneiss. The clinozoisite-biotite gneiss grades upward into the overlying hornblende-garnet gneiss.

The hornblende-garnet gneiss is similar to that described in the footwall to the T1 zone and forms a sequence at least 29 m thick. In addition to hornblende and garnet, the gneiss contains varying amounts of biotite and clinozoisite. The gneiss locally grades to more mafic compositions with up to 60% mafic minerals dominated by hornblende with minor garnet, biotite, and sulphide (Figure 10a). The more mafic layers are <2 m thick and locally contain stringy quartz laminations. The hornblende-garnet gneiss is locally interlayered with clinozoisite-rich rock

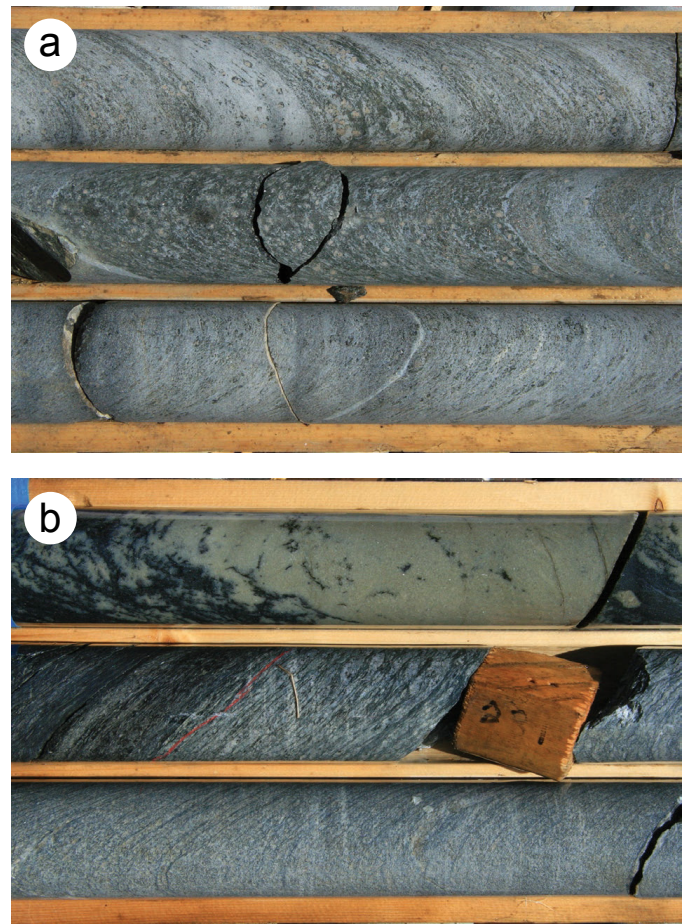


Figure 10: Drillcore images from the hangingwall of the Tower deposit: **a)** hornblende-garnet gneiss with mafic enriched layer (middle row; TP-12-032, 195.2 m); **b)** clinozoisite-rich rock hosted by hornblende-garnet gneiss (top row), the middle and bottom rows consist of ultramafic schist (TP-12-032, 226 m). Drillcore is NQ (diameter = 4.76 cm).

<40 cm thick (Figure 10b). The clinozoisite-rich rock is light greenish yellow, fine grained and locally magnetic. It is diffusely layered to massive and contains minor biotite and carbonate. The upper contact of the hornblende-garnet gneiss is defined by a granodiorite intrusion.

Comments on the Tower stratigraphy

More mafic portions of the hornblende-garnet gneiss are similar in appearance to silicate-facies iron formation, with the local stringy quartz reminiscent of chert laminations. The biotite-garnet gneiss is similar to a semipelitic rock, whereas the biotite-muscovite schist is characterized by mineral assemblages typical of metapelites. The mineral assemblages of the grunerite-magnetite gneiss are typical for lean silicate-facies iron formations; however, the relatively homogeneous texture of this unit is unusual for iron formation. The clinozoisite-rich layers and pods are similar to metasedimentary calcisilicate. Overall, many portions of the Tower stratigraphy could be interpreted as metasedimentary rock based on mineral assemblages and textures (cf. Couëslan, 2017); however, this is not the favoured interpretation based on lithogeochemistry (see Discussion section).

Intrusions

Several rock units intercepted in the Tower deposit drill-core are interpreted to be metamorphosed intrusions. Ultramafic schist occurs at various stratigraphic levels above the T1 mineralization (Figure 11a) with intersections ranging from 10–100 m long. The ultramafic schist is pale grey-green, medium to coarse grained and weakly to strongly magnetic.

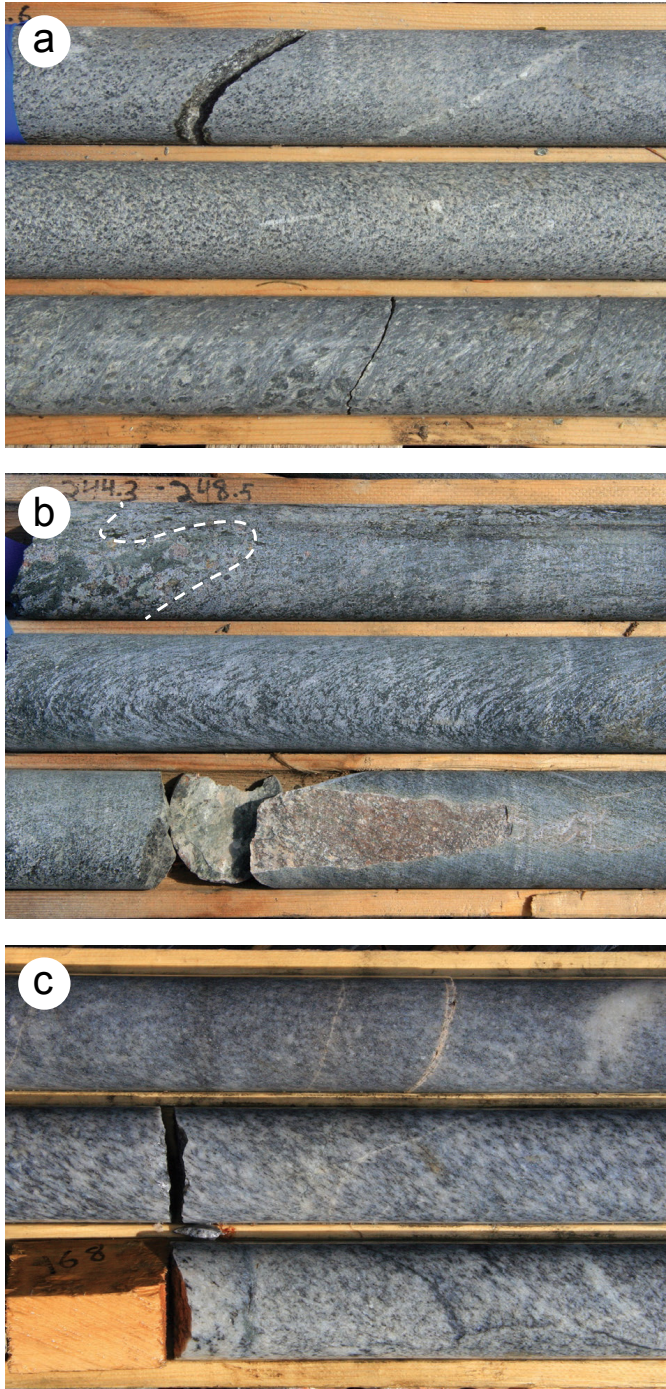


Figure 11: Drillcore images of intrusive phases at the Tower deposit: **a)** ultramafic schist interpreted as metamorphosed and altered peridotite (TP-10-003, 566.45 m); **b)** plagioclase amphibolite interpreted as metamorphosed gabbro, the gabbro contains a xenolith of sulphide-bearing chlorite schist (dashed outline, TP-10-003; 244.3 m); **c)** foliated to strongly foliated granodiorite (TP-12-032, 167.6 m). Drillcore is NQ (diameter = 4.76 cm).

It typically consists of varying amounts of talc, anthophyllite, chlorite, carbonate and serpentine, with minor magnetite and carbonate. The ultramafic schist commonly grades into ultramafic amphibolite at the margins. Because this is interpreted to be a VMS environment, it is possible that the ultramafic schist could represent zones of intense talc alteration of the Tower stratigraphy; however, the favoured interpretation is that these rocks represent altered intrusions of peridotite. Under this scenario the ultramafic amphibolite at the schist contacts could represent pyroxenitic envelopes to the peridotite intrusions. This interpretation is also supported by elevated Ni (up to 2000 ppm) reported in assays conducted by Falconbridge Ltd. on similar rocks (drill log BK00-318, Assessment File 73953). Alternatively, it is possible the ultramafic schist could represent altered ultramafic komatiite flows.

Bands of plagioclase amphibolite were intersected in all drillholes and occur at all stratigraphic levels. The amphibolite is dark green-grey, medium to coarse grained, relatively homogeneous and nonmagnetic. In addition to hornblende and plagioclase, the amphibolites contain quartz, minor biotite, and rarely garnet. Although generally <6 m long, an intersection of amphibolite in drillcore TP-10-003 is approximately 113 m long. This long intersection has possible boninitic affinity (sample 108-17-T01; see Interpretation of the Tower stratigraphy) and contains what appears to be a xenolith of sulphide-bearing chlorite schist (Figure 11b). Because of the relatively homogeneous character of these rocks the plagioclase amphibolite is interpreted as metamorphosed diabase and gabbro dikes. Although not favoured, an alternative interpretation could be that the plagioclase amphibolite represents massive mafic flows. Not all intervals contain sufficient hornblende to meet the definition of an amphibolite (>50% amphibole); however, the nomenclature is retained to differentiate these rocks from the more heterogeneous hornblende-bearing gneisses that make up much of the Tower stratigraphy.

Small granitoid dikes <2 m thick occur sporadically in the core. An intersection of strongly foliated to protomylonitic granodiorite >73 m long occurs directly below the Phanerozoic unconformity in hole TP-12-032 (Figure 11c). The granodiorite is biotite and muscovite bearing. The muscovite commonly occurs in radial aggregates, in symplectic intergrowth with quartz, or in close association with carbonate, suggesting much or all of the muscovite is secondary.

Litho-geochemistry and Sm-Nd isotope geochemistry

In order to establish the composition of rocks in the Tower deposit stratigraphy, a suite of 28 representative samples, including most of the principal units, was collected for litho-geochemical analysis. This includes four samples of biotite-garnet gneiss, five samples of biotite-muscovite schist, one sample each of the stratigraphically equivalent garnet-biotite and cummingtonite schists, two samples of grunerite-magnetite gneiss, three samples of laminated hornblende-biotite gneiss, two samples of hornblende-garnet gneiss, three samples of hornblende clinozoisite gneiss including one carbonate-bearing sample, four samples of chlorite schist, two samples of plagioclase amphibolite, and one sample of granodiorite. Because of

their geochemical similarities the various hornblende gneisses are described together as 'hornblende gneiss'. In addition, Sm-Nd isotope geochemistry was obtained for two samples of biotite-muscovite schist, two samples of hornblende gneiss, one sample of plagioclase amphibolite, and one sample of granodiorite. Results of the lithochemical and Sm-Nd isotope analyses are provided in DRI2018004 (Couëslan, 2018), and summarized in Tables 1 and 2, respectively.

Sampling and analytical methods

Representative samples were collected from most of the principal units for geochemical analysis. Approximately 30 cm long samples of representative material were selected from the drillcore. The core was sawn length-wise with one half of the core returned to the core box and the other half being retained for geochemical analysis, thin section, and archive. Samples were crushed to <5 mm at the Midland Sample and Core Library using a steel jaw-crusher. Pulps were produced in a steel swing mill and were homogenized by rolling and then splitting to approximately 55 g of analytical material. One internal standard and two blind duplicates were inserted along with the 27 samples submitted for analysis.

Samples were analyzed at Activation Laboratories Ltd. (Ancaster, Ontario) using the '4Litho' analytical package, which employs a lithium metaborate/tetraborate fusion technique, followed by nitric-acid digestion and analysis by inductively coupled plasma-emission spectrometry (ICP-ES) for the major elements and selected trace elements (Ba, Be, Sc, Sr, V, Y, Zr), and inductively coupled plasma-mass spectrometry (ICP-MS) for the remainder of the trace elements and rare-earth elements. In addition, most samples were analyzed by total-digestion ICP-ES for selected trace elements (Ag, Cd, Cu, Ni, Pb, Zn) and sulphur contained within sulphides. Fluid-soluble, large-ion lithophile elements (LILE; e.g., K, Rb, Ba, Sr) were not utilized in describing the geochemistry of samples because of their potential mobility in a VMS environment. Plots utilizing trace elements are therefore restricted to the less mobile elements, including high-field-strength elements (HFSE; Ti, Hf, Zr, Nb), rare-earth elements (REE) and Th.

Select samples were submitted for Sm-Nd isotope geochemical analysis to the University of Alberta Radiogenic Isotope Facility (Edmonton, Alberta). The rock-sampling and initial-processing procedures followed were the same as those for lithochemical samples. The samples were processed and analyzed for Sm-Nd isotopes following the chromatographic and mass-spectrometry methods outlined by Unterschutz et al. (2002) and Schmidberger et al. (2007). Samarium and neodymium isotopic compositions were determined by multicollector (MC)-ICP-MS, for which an in-house Nd isotope standard was used (Schmidberger et al., 2007). Chemical processing blanks were <200 pg for Nd and Sm. The Nd data are presented relative to a $^{143}\text{Nd}/^{144}\text{Nd}$ value of 0.511850 for the La Jolla standard, and crustal residence model ages (T_{CR}) were calculated based on the model of Goldstein et al. (1984), which assumes a linear evolution of isotopic ratios in the depleted mantle, using present-day depleted-mantle values of $^{143}\text{Nd}/^{144}\text{Nd} = 0.513160$ and $^{147}\text{Sm}/^{144}\text{Nd} = 0.2141$. All initial ϵ_{Nd} values are calculated at 1.88 Ga.

Tower chemostratigraphy

The biotite-muscovite schist is characterized by alumina saturation index values (ASI, molar $\text{Al}_2\text{O}_3/\text{CaO}+\text{Na}_2\text{O}+\text{K}_2\text{O}$) of 1.1–2.6 and Mg# (molar $\text{Mg}/\text{Mg}+\text{Fe}$) values of 0.21–0.34. These values are typical for a pelite and overlap with the composition of the Ospwagan group, P2 member pelite (ASI=1.3–2.9, Mg#=0.27–0.61; Zwanzig et al., 2007; Couëslan and Pattison, 2012). The garnet-biotite and cummingtonite schists from the same stratigraphic level have similar ASI values (1.2–1.8) but higher Mg# values (0.43–0.44). The biotite-garnet gneiss is peraluminous with ASI values of 1.0–1.3 and has Mg# values of 0.19–0.31. The grunerite-magnetite gneiss has similar values (ASI=1.0, Mg#=0.24–0.29). The hornblende gneiss is metaluminous with ASI values of 0.47–0.79, and is generally more magnesian with Mg# values of 0.31–0.60. Garnet-bearing samples of hornblende gneiss generally have lower Mg# values (0.31–0.33) than garnet-free samples (Mg#=0.36–0.60). The chlorite schist is characterized by low alkali content making the rock strongly peraluminous with ASI values of 3.2–22. These ASI values are considered extremely high and could be indicative of a hydrothermally altered rock (Tinkham, 2011). The chlorite schist is also relatively magnesian in comparison to the rest of the Tower stratigraphy with Mg# values of 0.47–0.62.

Ospwagan group rocks represent a continuum between siliciclastic and chemical sedimentary end-members. Zwanzig et al. (2007) proposed the use of a $\text{SiO}_2\text{-Al}_2\text{O}_3$ diagram as a means of estimating the clastic component of Ospwagan group rocks (Figure 12a). Pure chemical sedimentary rocks (chert, oxide-, carbonate-, and sulphide-facies iron formation) plot along the y-axis of the diagram, while pure siliciclastic rocks plot along a negatively sloping array, denoted by the thick black line in Figure 12. Impure marble and marlstone of the Thompson formation form a steep positively sloping array that stretches from near the origin towards the mid-point of the siliciclastic array. Impure chert and silicate-facies iron formation of the Pipe formation plot within a broad field stretching from the y-axis towards the mid-point of the siliciclastic array, indicated by the broad arrow in Figure 12a.

The biotite-muscovite schist, biotite-garnet gneiss, and grunerite-magnetite gneiss of the Tower stratigraphy plot in a relatively tight cluster along the siliciclastic array, within the fields for Ospwagan group pelite and semipelite (Figure 12b–d). This is roughly where the schist and biotite-garnet gneiss would be expected to plot if they represent fine-grained siliciclastic rocks; however, the grunerite-magnetite gneiss, which has an assemblage similar to a lean silicate-facies iron formation, would be expected to plot within the broad field between the y-axis and the siliciclastic array. The hornblende gneiss plots towards the confluence of the marlstone and siliciclastic arrays, outside of the broad field expected for impure chert and silicate-facies iron formation (Figure 12e). The garnet-biotite and cummingtonite schists occur at the same stratigraphic level as the biotite-muscovite schist, but plot within the same compositional range as the hornblende gneiss (Figure 12b).

Whole-rock geochemical data for rocks of the Tower stratigraphy were normalized to average P2 pelite and plotted on multi-element diagrams to compare the Tower rocks with metasedimentary rocks of the Ospwagan group, as outlined in

Table 1: Lithochemical data for representative rock samples from the Tower deposit.

Sample ¹	Hornblende gneiss					Biotite-muscovite schist			Biotite-garnet gneiss		Gru-Mt Gn		Chlorite schist		Grt-Bt Sch	Cum Sch	Plag Amp		Grdr
	T05	T09	T10	T21	T24	T02	T06	T13	T14	T27	T12	T25	T16	T18	T26A	T26B	T01	T03	T15
Protolith	MV	MV	MV	MV	MV	IFV	IFV	MV	IFV	IFV	IFV	IFV	MV	MV	MV	MV	MI	MI	FI
wt%																			
SiO ₂	56.78	61.66	53.54	45.98	56.13	70.71	70.85	67.28	69.33	72.22	69.05	70.4	59.54	63.08	57.78	58.47	53.24	63.98	71.49
Al ₂ O ₃	14.83	14.01	14.14	15.65	12.75	12.03	12.16	12.51	12.63	12.67	13.33	13.08	13.99	13.54	12.59	15.18	17.17	14.04	15.38
Fe ₂ O ₃	10.57	6.78	14.98	18.3	8.04	8.65	7.56	9.98	8.49	6.55	7.57	6.84	12.31	12.21	16.8	11.6	7.83	8.67	0.99
MnO	0.11	0.124	0.223	0.274	0.172	0.146	0.116	0.232	0.145	0.136	0.128	0.057	0.044	0.057	0.23	0.202	0.092	0.088	0.011
MgO	3.72	5.19	3.74	4.09	2.3	1.52	1.03	1.53	1.61	0.79	1.53	1.09	8.27	5.87	6.42	4.76	7.58	2.43	0.23
CaO	8.24	7.24	8.51	11.81	12.18	1.05	1.72	3.15	2.17	2.12	2.63	2.43	0.19	0.27	1.53	3.07	11	5.13	1.54
Na ₂ O	2.07	2.89	2.04	1.52	2.77	2	2.22	0.96	2.93	4.69	4.65	4.92	0.1	0.06	0.97	3.48	1.95	4.61	5
K ₂ O	0.99	0.71	0.46	0.36	0.28	1.96	2.2	2.87	1.02	0.43	0.48	0.32	0.45	0.85	2.22	0.99	0.26	0.31	3.18
TiO ₂	0.894	0.542	0.87	1.06	0.742	0.491	0.396	0.489	0.651	0.556	0.664	0.598	0.932	0.833	0.774	0.939	0.331	0.714	0.111
P ₂ O ₅	0.09	0.07	0.09	0.18	0.09	0.09	0.07	0.06	0.13	0.1	0.15	0.12	0.13	0.15	0.09	0.08	0.03	0.09	0.04
LOI	0.69	0.84	0.6	1.37	4.75	0.48	0.56	0.83	0.04	0.09	0.25	0.21	4.43	2.2	0.4	0.27	1.01	0.42	0.67
Total	98.99	100.1	99.19	100.6	100.2	99.13	98.87	99.9	99.15	100.3	100.4	100.1	100.4	99.12	99.81	99.02	100.5	100.5	98.65
S	0.037	0.008	0.107	0.367	0.242	0.072	0.078	0.089	0.034	0.009	0.053	0.039	0.005	0.012	0.025	0.015	0.011	0.004	
Mg#	0.41	0.60	0.33	0.31	0.36	0.26	0.21	0.23	0.27	0.19	0.29	0.24	0.57	0.49	0.43	0.45	0.66	0.36	0.32
ASI	0.76	0.75	0.73	0.64	0.47	1.64	1.33	1.20	1.28	1.05	1.03	1.02	14.03	8.97	1.86	1.23	0.73	0.81	1.06
(ppm)																			
Sc	31	29	37	43	22	11	15	26	16	12	16	16	27	23	28	29	33	23	< 1
V	297	172	314	400	179	9	18	161	25	12	17	39	269	211	259	279	171	276	9
Ba	161	96	111	20	50	395	252	178	193	161	19	31	146	369	398	184	27	53	1811
Sr	206	100	43	142	67	42	35	49	88	167	100	55	4	9	17	67	166	185	1136
Y	13	18	18	21	17	18	26	16	25	21	29	22	13	17	14	23	7	14	1
Zr	67	85	68	87	82	112	134	83	121	121	154	127	78	94	64	73	36	89	69
Cr	20	150	<20	<20	<20	< 20	< 20	80	< 20	< 20	< 20	< 20	< 20	< 20	40	30	20	280	< 20
Co	30	24	35	39	36	5	7	16	9	6	10	8	36	31	38	28	29	18	< 1
Ni	20	68	16	15	26	2	3	32	3	1	3	3	15	31	27	20	117	16	< 20
Cu	221	36	81	253	225	521	51	34	240	70	127	41	2	5	137	83	58	6	< 10
Zn	75	75	129	118	371	163	69	102	42	66	86	51	29	28	124	99	27	33	30
Ga	19	14	17	20	13	13	16	13	15	14	15	13	16	18	16	17	14	15	20
Rb	17	19	4	2	< 2	31	38	42	15	7	4	2	7	10	39	18	< 2	< 2	59
Nb	3	4	3	4	4	4	5	3	5	5	6	4	3	4	3	3	1	4	2
La	4.9	6.1	5.1	6.7	9	9.5	11.9	5.9	13.6	11.9	12.5	10.8	6.6	7.4	4	5.2	3.1	7.9	7.8
Ce	11.5	13.9	12.3	15.5	19.5	20.2	26.4	13.2	28.8	25.7	28.3	25	15.7	18.2	9.3	11.9	6.6	19	14.8
Pr	1.57	1.92	1.63	2.1	2.47	2.48	3.41	1.75	3.57	3.17	3.69	3.14	2.12	2.46	1.26	1.65	0.87	2.38	1.59
Nd	7	8.7	7.4	9.7	10.6	10.5	15.1	8.4	15.1	13.8	16.3	13.9	9.8	11.4	6.1	7.3	4.1	10.1	5.8
Sm	2.2	2.6	2.1	2.6	2.6	2.7	4	2.2	3.9	3.5	4.2	3.6	2.8	3.1	1.9	2.1	1.2	2.4	1
Eu	0.74	0.76	0.8	1.06	0.88	0.68	1.19	0.71	0.95	0.92	1.14	0.97	0.33	0.4	0.48	0.68	0.42	0.74	0.28
Gd	2.7	3.2	2.7	3.4	3.1	3.1	4.5	2.7	4.5	3.8	4.9	4.4	3.2	3.7	2.6	3.4	1.4	2.7	0.6
Tb	0.5	0.5	0.5	0.6	0.5	0.5	0.7	0.5	0.7	0.6	0.8	0.7	0.5	0.6	0.4	0.7	0.2	0.4	< 0.1
Dy	3	3.5	3.3	3.9	3.3	3.2	4.6	3	4.6	3.8	5.1	4.2	2.8	3.8	2.8	4.5	1.5	2.7	0.2
Ho	0.6	0.7	0.7	0.9	0.7	0.7	0.9	0.6	0.9	0.8	1.1	0.9	0.5	0.8	0.6	0.9	0.3	0.6	< 0.1
Er	1.7	2.2	2.1	2.5	2	1.9	2.8	1.8	2.7	2.2	3.2	2.5	1.6	2.1	1.7	2.5	0.9	1.6	< 0.1
Tm	0.26	0.33	0.32	0.39	0.29	0.27	0.4	0.27	0.39	0.33	0.49	0.34	0.24	0.32	0.24	0.35	0.13	0.24	< 0.05
Yb	1.7	2.2	2.2	2.5	1.9	1.9	2.8	1.7	2.6	2.2	3.2	2.2	1.7	2	1.5	2.3	0.8	1.6	< 0.1
Lu	0.26	0.34	0.35	0.39	0.29	0.31	0.43	0.27	0.42	0.35	0.49	0.33	0.27	0.3	0.24	0.36	0.12	0.26	< 0.01
Hf	1.8	2.3	1.6	2.1	2.1	2.6	3.6	2	3.4	2.9	4	3.2	2	2.4	1.7	1.9	0.9	2.4	2
Ta	0.2	0.3	0.2	0.3	0.3	0.4	0.4	0.2	0.4	0.4	0.5	0.4	0.3	0.2	0.2	< 0.1	0.3	0.1	
Th	0.7	1	0.7	0.9	1.2	2.9	2.4	0.9	2.7	3.2	2.3	2.1	0.8	1.1	0.5	0.7	0.6	2	2.4
U	0.3	0.6	0.3	0.3	1	1.1	1.1	0.4	1.2	1.2	0.9	0.7	0.3	0.4	0.3	0.3	0.3	1.1	2.5
Zr/Ti	80.0	38.2	76.7	73.0	54.2	26.3	17.7	35.3	32.2	27.5	25.8	28.2	71.6	53.1	72.5	77.1	55.1	48.1	9.6
Al ₂ O ₃ /TiO ₂	16.6	25.8	16.3	14.8	17.2	24.5	30.7	25.6	19.4	22.8	20.1	21.9	15.0	16.3	16.3	16.2	51.9	19.7	138.6
(La/Yb) _N	1.96	1.88	1.57	1.82	3.22	3.40	2.89	2.36	3.55	3.67	2.65	3.33	2.64	2.51	1.81	1.54	2.63	3.35	N/A
Eu/Eu*	0.92	0.80	1.02	1.09	0.94	0.71	0.85	0.89	0.69	0.76	0.76	0.74	0.33	0.36	0.66	0.77	0.99	0.88	1.02
(Th/Nb) _{PM}	2.04	2.19	2.04	1.97	2.63	6.34	4.20	2.63	4.73	5.60	3.35	4.59	2.33	2.41	1.46	2.04	5.25	4.38	10.50
(V/Sc) _{PM}	1.89	1.17	1.68	1.84	1.61	0.16	0.24	1.22	0.31	0.20	0.21	0.48	1.97	1.81	1.83	1.90	1.02	2.37	N/A

¹ The '108-17' prefix has been omitted from the sample numbers in this table.

Abbreviations: Amp, amphibolite; Bt, biotite; Cum, cummingtonite; FI, felsic intrusive rock; IFV, intermediate/felsic volcanic rock; Gn, gneiss; Grdr, granodiorite; Grt, garnet; Gru, grunerite; MI, mafic intrusive rock; Mt, magnetite; MV, mafic volcanic rock; Plag, plagioclase; Sch, schist.

Table 2: Sm-Nd isotopic data for select rock samples from the Tower deposit.

Sample number	Rock type	Sm (ppm)	Nd (ppm)	$^{147}\text{Sm}/^{144}\text{Nd}^{(1)}$	$^{143}\text{Nd}/^{144}\text{Nd}^{(2)}$	$\epsilon_{\text{Nd}}^{(3)}$ (1.88 Ga)	$T_{\text{CR}}^{(4)}$ (Ga)
108-17-T01	Plagioclase amphibolite	1.07	3.96	0.1631	0.510264 (10)	1.2	N/A
108-17-T02	Biotite-muscovite schist	2.68	10.78	0.1506	0.510210 (10)	0.1	N/A
108-17-T06	Biotite-muscovite schist	3.66	14.20	0.1556	0.510297 (11)	1.8	N/A
108-17-T09	Hornblende gneiss, laminated	2.36	8.48	0.1682	0.510368 (8)	3.2	N/A
108-17-T10	Hornblende garnet gneiss	2.14	7.56	0.1714	0.510294 (11)	1.8	N/A
108-17-T15	Granodiorite	0.98	5.70	0.1038	0.510278 (10)	1.4	2.21

⁽¹⁾ Estimated error is better than 0.5%

⁽²⁾ Presented relative to $^{143}\text{Nd}/^{144}\text{Nd} = 0.511850$ for the La Jolla standard; numbers in parentheses are the 2σ uncertainties $\times 10^{-6}$

⁽³⁾ ϵ_{Nd} values at 1.88 Ga calculated using present-day chondritic ratios of $^{143}\text{Nd}/^{144}\text{Nd} = 0.512638$ and $^{147}\text{Sm}/^{144}\text{Nd} = 0.1967$

⁽⁴⁾ Crustal residence Nd model ages (T_{CR}) calculated according to the linear model of Goldstein et al. (1984)

Zwanzig et al. (2007). Normalized profiles of the biotite-muscovite schist are typically characterized by a positive slope for light rare-earth elements (LREE) and large-ion lithophile elements (LILE), a relatively flat heavy rare-earth element (HREE) profile, a positive anomaly at Nb, and negative anomalies at Ti, Y, and V, and are geochemically distinct from the petrographically similar Ospwagan group, P2 member pelite (Figure 13a). One sample of the schist is unique in that it is characterized by a slightly steeper positive slope for light rare-earth elements (LREE) and large-ion lithophile elements (LILE), a slight positive Ti anomaly, and no V anomaly. Profiles of the garnet-biotite and cummingtonite schists are characterized by steep positive slopes for LREE and LILE, with positive anomalies at Nb, Ti, and V. The normalized profile of the biotite-garnet gneiss is similar to the biotite-muscovite schist; however, there is no Ti anomaly (Figure 13b). The biotite-garnet gneiss is geochemically distinct from the petrographically similar siliceous sedimentary rocks of the Ospwagan group, P3 member, which has an overall profile similar to the P2 member pelite (Figure 13c). The profile of the grunerite-magnetite gneiss is similar to both the biotite-garnet gneiss and biotite-muscovite schist, with a slight negative anomaly at Ti (Figure 13d), and is distinct from Ospwagan group, Pipe formation silicate-facies iron formation. The normalized profiles of the Tower hornblende gneiss are characterised by a slightly steeper positive slope for LREE and LILE, and have positive anomalies at Nb, Ti, and V, and negative anomalies at Y (Figure 13e). The hornblende gneiss is also geochemically distinct from Pipe formation silicate-facies iron formation. The profiles of the chlorite schist and are similar to the hornblende gneiss with less prominent enrichment at Ti, and a negative anomaly at Zr (Figure 13f).

The two samples of biotite-muscovite schist yielded initial ϵ_{Nd} values of +0.1 and +1.8, while two samples of the hornblende gneiss yielded values of +1.8 and +3.2. These values are in contrast to the range of initial ϵ_{Nd} values for Ospwagan group rocks (-6.4 to -13.8, calculated at 1.88 Ga; Böhm et al., 2007). The trace-element and Sm-Nd isotope geochemistry suggests that the Tower deposit stratigraphy is unrelated to the Ospwagan group rocks of the TNB.

Intrusions

Sampling of rock types that intrude the Tower stratigraphy was limited to two samples of plagioclase amphibolite and one sample of granodiorite. The plagioclase amphibolite has ASI

and Mg# values of 0.73–0.81 and 0.36–0.66, respectively. The plagioclase amphibolite plots within the andesite + basaltic andesite field of the Zr/Ti-Nb/Y diagram of Pearce (1996), suggesting gabbroic to dioritic compositions (Figure 14a). Chondrite-normalized REE profiles of the plagioclase amphibolite are characterized by shallow negative slopes for LREE and MREE and relatively flat HREE ($[\text{La}/\text{Yb}]_{\text{N}}$ ratios of 2.6 and 3.4; Figure 14b). Primitive mantle-normalized multi-element profiles for the amphibolite have negative slopes with enrichment of Th, weak positive anomalies at Zr, and negative anomalies at Nb, Ti, and Y (Figure 14c). Plagioclase amphibolite sample 108-17-T01 yielded an initial ϵ_{Nd} value of +1.2.

The granodiorite plots as peraluminous on the alumina-saturation index diagram (Figure 15a). Its chondrite-normalized REE profile is characterized by a steep negative slope, with HREE abundances below detection limits, and without a Eu anomaly (Figure 15b). The primitive mantle-normalized multi-element profile is characterized by enrichment in Th and LREE, with a positive anomaly at Zr, and negative anomalies at Nb and Ti (Figure 15c). The granodiorite yielded an initial ϵ_{Nd} value of +1.4. The juvenile nature of the intrusion is unusual for granitoid intrusions in the TNB which typically have ϵ_{Nd} values ranging from -1.4 to -13.9 (calculated for igneous crystallization ages; Zwanzig et al., 2003; Percival et al., 2004; Percival et al., 2005).

Metamorphism

Several samples were selected for phase equilibrium modelling because of their aluminous bulk compositions and diverse mineral assemblages. Discussion will be limited to two of these samples: a sample of biotite-muscovite schist (108-17-T02), and a sample of chlorite schist (108-17-T16), which provided the best constraints of peak metamorphic temperature and pressure.

Methods

Petrographic thin sections were examined of both samples and modal abundances were calculated based on >550 point counts of each thin section (point count results available in DRI2018004; Couëslan, 2018). Observed modal abundances were later compared to the predicted modal abundances to ensure a close fit between observed and modelled mineral assemblages. Phase equilibrium diagrams were calculated

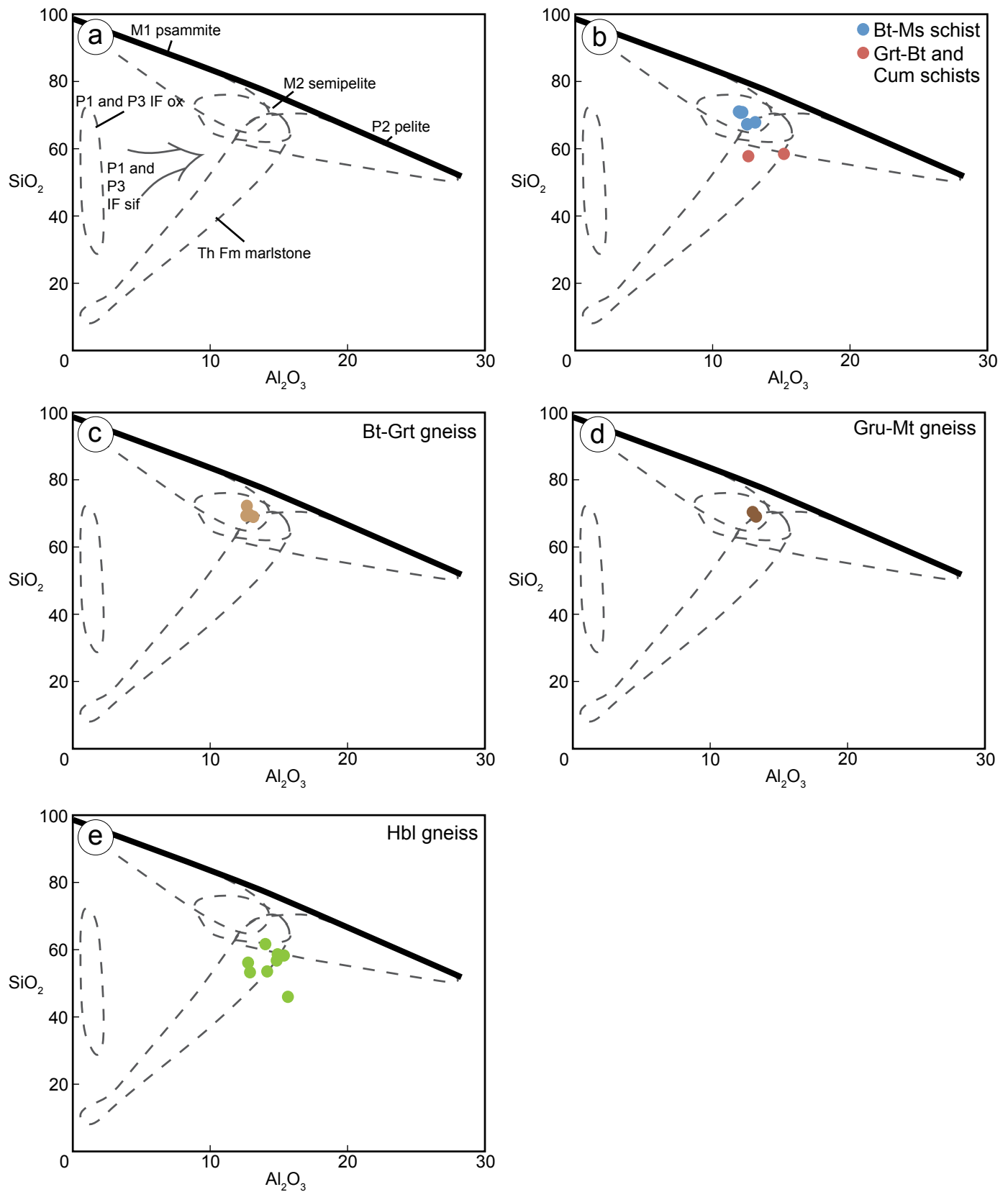


Figure 12: SiO_2 - Al_2O_3 diagrams for estimating the siliciclastic component of metasedimentary rocks (see text for details, Zwanzig et al., 2007): **a)** compositional fields for typical Oswagan group rocks (Zwanzig et al., 2007); **b–e)** rocks from the Tower stratigraphy. The hornblende gneiss includes compositions of both the hornblende-garnet and hornblende-biotite gneisses. Abbreviations: Bt, biotite; Cum, cummingtonite; Fm, formation; Grt, garnet; Gru, grunerite; Hbl, hornblende; IF sif, silicate-facies iron formation; IF ox, oxide-facies iron formation; Ms, muscovite; Mt, magnetite; Th, Thompson.

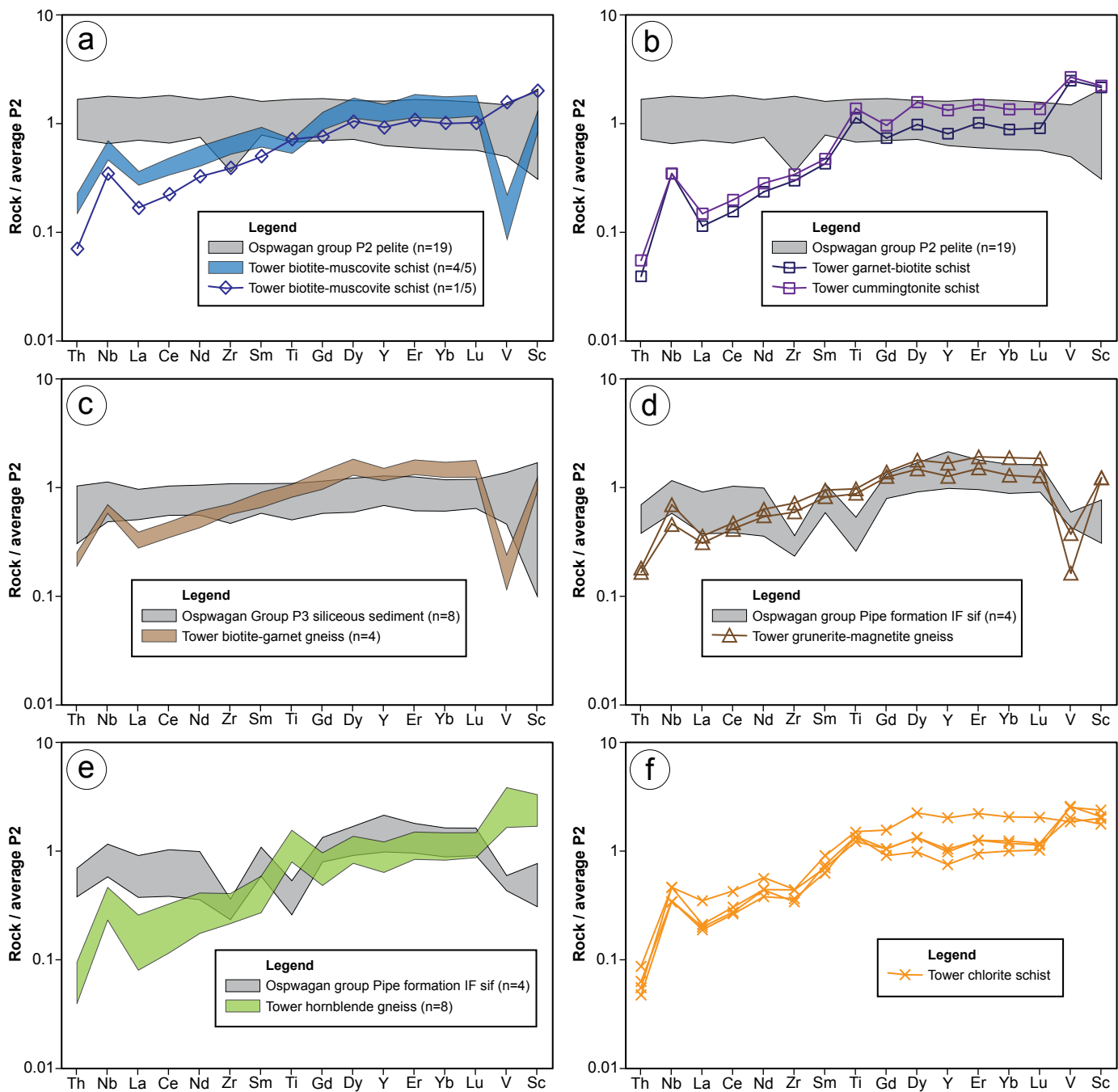


Figure 13: P2 member-normalized multi-element profiles for rocks from the Tower stratigraphy and Ospwagan group. Normalizing values are from Zwanzig et al. (2007). Reference values for Ospwagan Group rocks are from Zwanzig et al. (2007), Burnham et al. (2009), and Couëslan (2013). Abbreviation: IF sif, silicate-facies iron formation.

using the Theriak-Domino software package (de Capitani and Brown, 1987; de Capitani and Petrakakis, 2010), and using the updated ds5.5 thermodynamic dataset of Holland and Powell (1998). Activity models used in modelling are those outlined in Tinkham and Ghent (2005) and Pattison and Tinkham (2009), with the following exceptions: (i) the monoclinic amphibole model is that of Diener et al. (2007), (iii) the garnet and biotite models are those of White et al. (2007) with the addition of Mn-members that are assumed to mix ideally, and (iv) the liquid model is that of White et al. (2007) with the enthalpy of forsterite and fayalite liquid adjusted by -10 kJ/mol and -9 kJ/mol, respectively, following THERMOCALC v.3.31 data files. Samples were modelled in the chemical system MnNCK-

FMASHT (MnO-Na₂O-CaO-K₂O-FeO-MgO-Al₂O₃-SiO₂-H₂O-TiO₂) and projected from pyrrhotite and apatite. The chemical system was oversaturated with a pure H₂O fluid phase below the solidus. Above the solidus the H₂O content of each model is restricted to the amount of H₂O contained in the solid phases at 7 kbar and <0.5°C below the solidus. The H₂O content in the system at the temperature of melting is therefore at the point of saturation (White et al., 2001).

Mineral assemblages

Biotite-muscovite schist sample 108-17-T02 is medium grained with an assemblage of quartz-plagioclase-biotite-garnet-

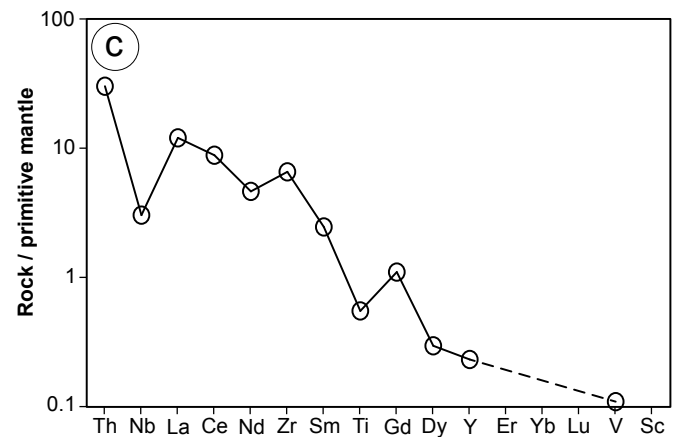
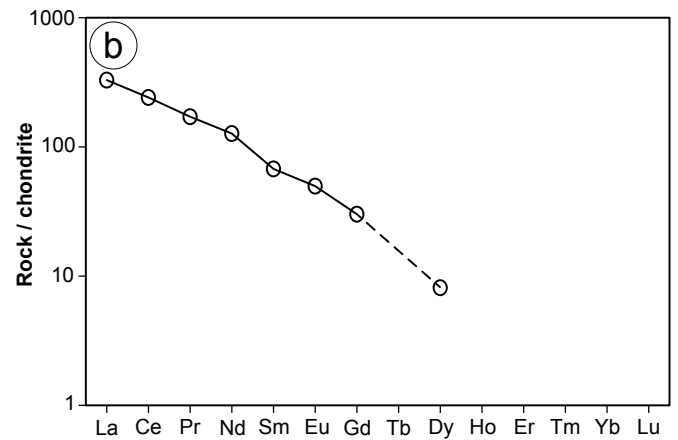
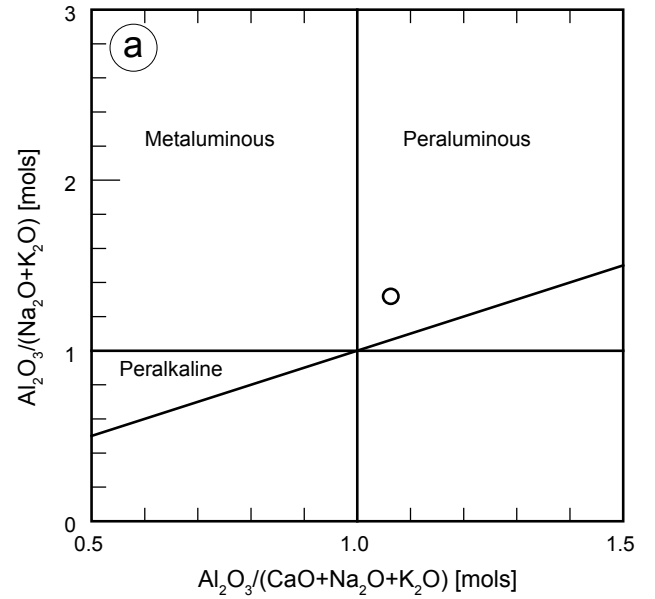
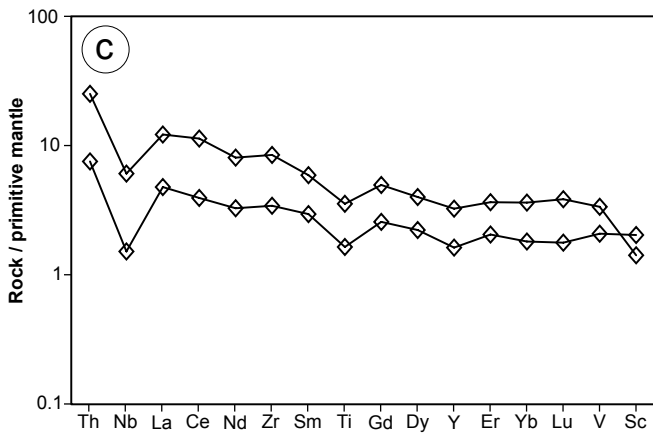
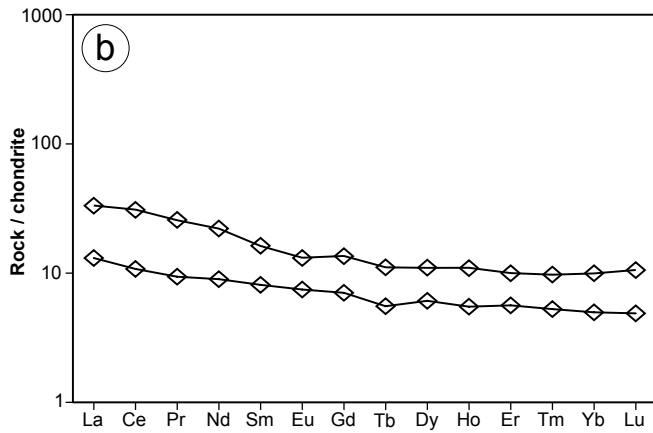
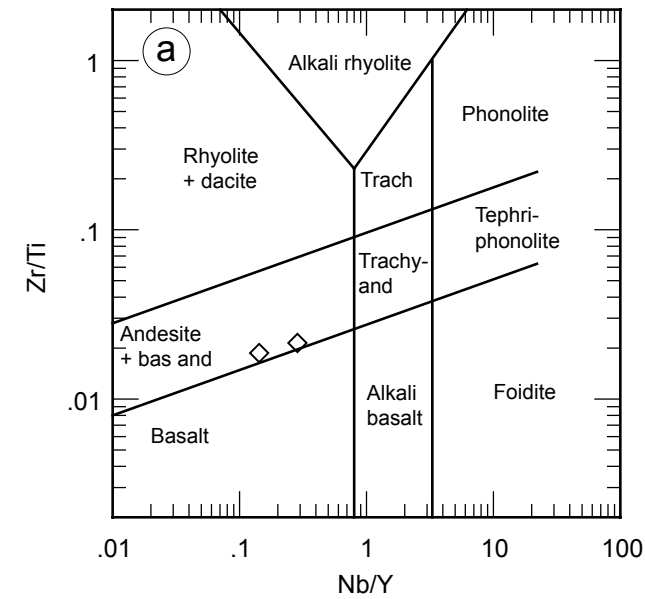


Figure 14: Geochemical diagrams for the plagioclase amphibolite: **a)** Zr/Ti-Nb/Y diagram from Pearce (1996); **b)** chondrite-normalized REE profiles; **c)** primitive mantle-normalized multi-element profiles. Normalizing values for chondrite and primitive mantle are from McDonough and Sun (1995). Abbreviations: and, andesite; bas, basaltic; Trach, trachyte.

Figure 15: Geochemical diagrams for the granodiorite: **a)** alumina saturation-index diagram of Maniar and Piccoli (1989); **b)** chondrite-normalized REE profile; **c)** primitive mantle-normalized multi-element profile. Normalizing values for chondrite and primitive mantle are from McDonough and Sun (1995).

muscovite-staurolite-ilmenite. Apatite, zircon, monazite, and chlorite occur as accessory phases. The garnet occurs as coarse poikiloblasts with rare chlorite replacement along fractures. Subidiomorphic porphyroblasts of staurolite are spatially associated with garnet. The staurolite locally appears to be partially overprinted by muscovite. Alignment of biotite and muscovite define the main foliation. Biotite is locally cross-cut and replaced by chlorite (Figure 16a). The cross-cutting and replacement textures of the chlorite suggest that it is a later retrogressive phase, and not part of the peak metamorphic assemblage. The partial replacement of staurolite by muscovite is also evidence for a weak retrograde overprint of the schist. The mineral assemblage quartz-plagioclase-biotite-garnet-muscovite-staurolite-ilmenite is typical for a pelitic schist of the middle amphibolite-facies.

Chlorite schist sample 108-17-T16 is medium grained with an assemblage of quartz-chlorite-staurolite-biotite-ilmenite. Apatite, monazite, and rutile occur as accessory minerals. The

chlorite is intergrown with biotite and defines the dominant foliation. The biotite forms local, discrete booklets in sharp contact with the chlorite (Figure 16b). Subidiomorphic to idiomorphic staurolite porphyroblasts are strongly associated with the chlorite and also exhibit sharp contacts. The sharp contacts between the chlorite, biotite, and staurolite suggest that the chlorite is part of the peak metamorphic mineral assemblage and not a retrograde phase.

Phase equilibrium modelling

The phase diagram section for biotite-muscovite schist sample 108-17-T02 provides fairly well constrained temperature and pressure conditions for the observed mineral assemblage quartz-plagioclase-biotite-garnet-muscovite-staurolite-ilmenite. The equilibrium assemblage containing muscovite-garnet-biotite-staurolite defines a field in pressure-temperature space of about 3.8–5.2 kbar and 560–625°C (Figure 17a).

The observed mineral assemblage of quartz-chlorite-staurolite-biotite-ilmenite with the addition of plagioclase provides well constrained temperature conditions for chlorite schist sample 108-17-T16. The observed assemblage plus plagioclase suggests metamorphic conditions of approximately 570–610°C and >4.3 kbar (Figure 17b). Although no plagioclase was observed in the thin section, the model predicts approximately 1.5 modal % plagioclase in the rock. The discrepancy between predicted plagioclase and no observed plagioclase in the assemblage could be an artifact of inhomogeneous distribution of plagioclase within the sample used for geochemical analysis, or misidentification of minor plagioclase in the otherwise quartz-rich groundmass. Alternatively, the presence of undetected or microscopic carbonate veins within the sample used for geochemical analysis could also result in the prediction of anomalous plagioclase. A better estimate for the metamorphic conditions at the Tower deposit can be made by overlapping the observed mineral assemblage fields from the two phase diagram sections (Figure 17b). The resulting pressure-temperature region of overlap is 4.3–5.1 kbar and 570–610°C.

Discussion

Comparison with rocks of the Pikwitonei granulite domain

The position of the Tower deposit along the eastern margin of the TNB (Figure 1), along with previous reports of garnet-bearing ultramafic rocks, raises the possibility of PGD rocks as host to the Tower deposit. However, relogging of drillcore has failed to identify garnet-bearing ultramafic rocks in the Tower stratigraphy. Peak metamorphic grades are estimated to be significantly lower at the Tower deposit (4.3–5.1 kbar, 570–610°C) than in portions of the PGD adjacent to the TNB (8–9 kbar and >950°C; Guevara et al., 2018). Pikwitonei granulite domain rocks at Partridge Crop Lake, along the TNB-PGD boundary, were retrogressed to middle amphibolite-facies mineral assemblages during the Trans-Hudson orogeny (Couëslan, 2014); however, even when tectonically reworked these rocks have retained relic migmatitic textures. No evidence for anataxis was observed in any of the rocks from the Tower deposit. The

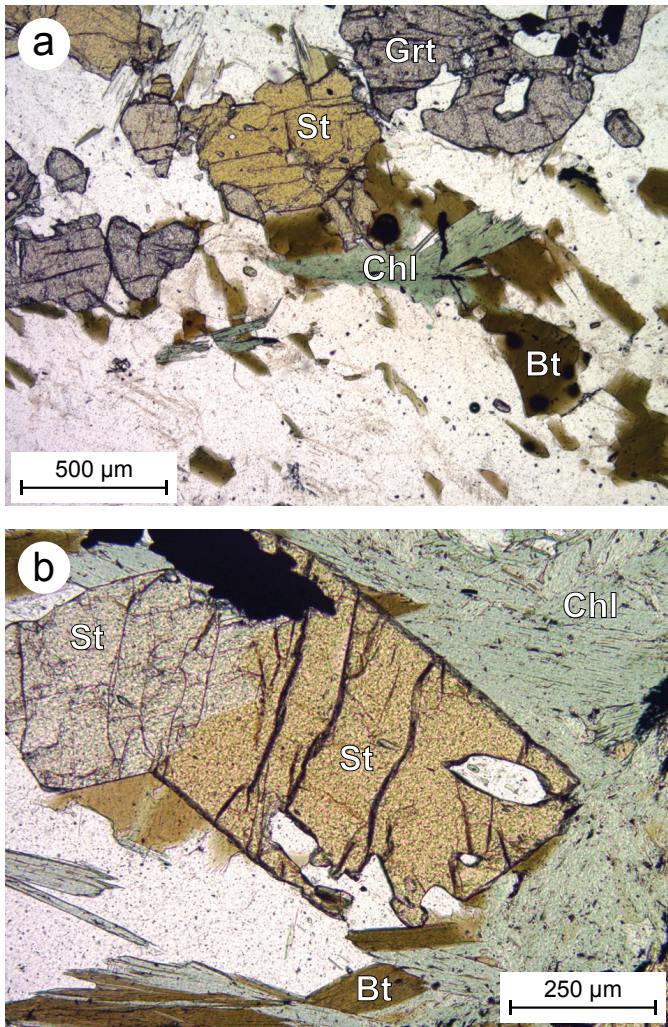


Figure 16: Photomicrographs in plane-polarized light of Tower stratigraphy rocks: **a)** retrograde chlorite overprinting biotite in biotite-muscovite schist sample 108-17-T02; **b)** prograde assemblage including chlorite, biotite, and staurolite in chlorite schist sample 108-17-T16. Abbreviations: Bt, biotite; Chl, chlorite; Grt, garnet; St, staurolite.

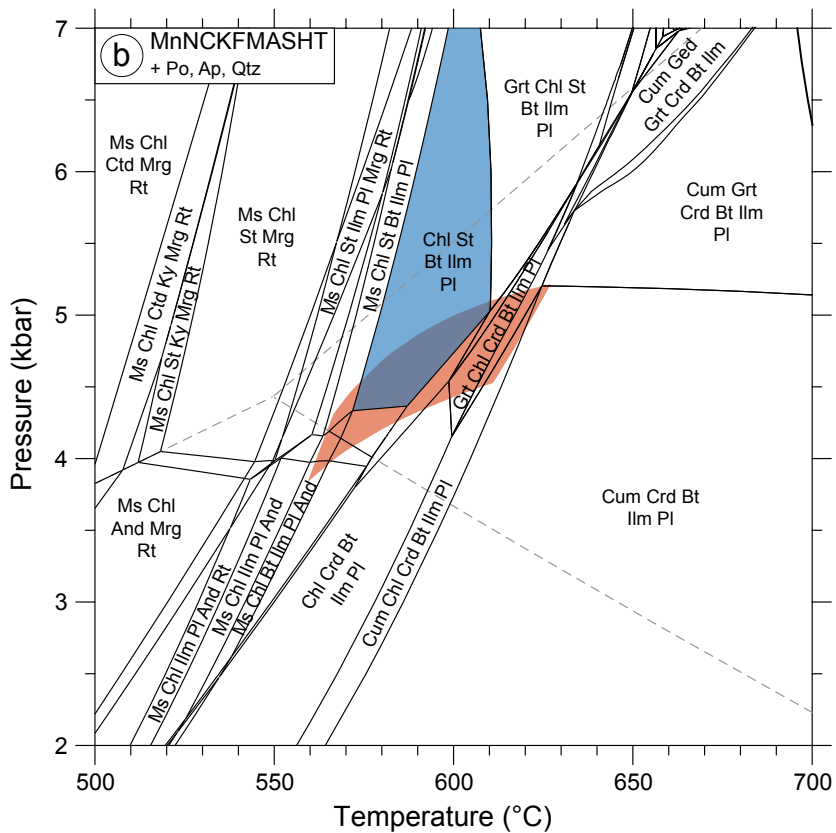
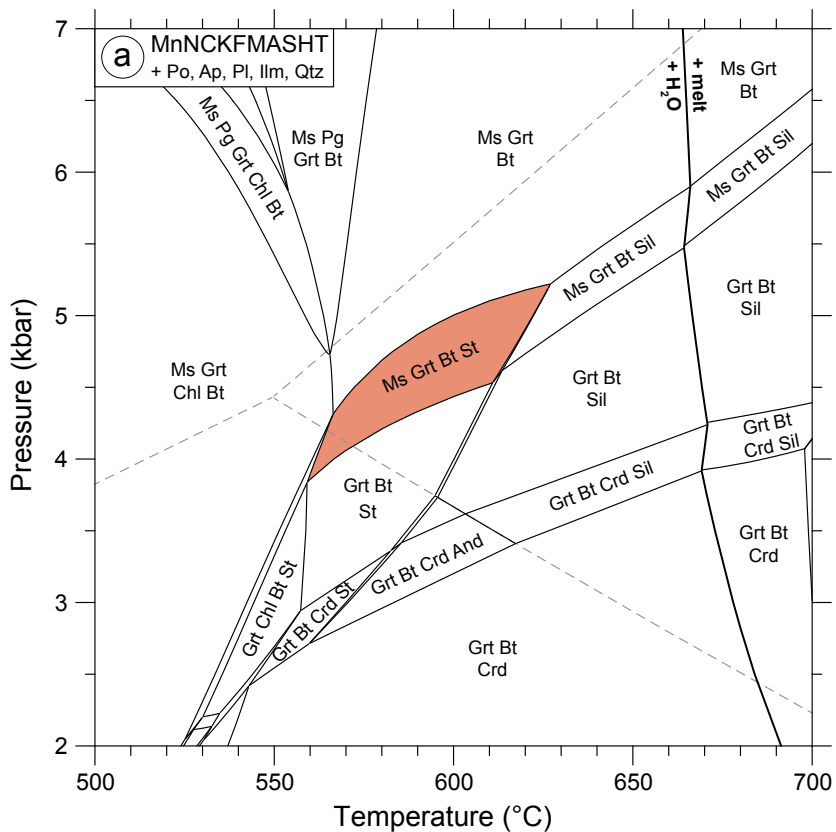


Figure 17: Phase diagram sections in MnNCKFMASHT for: **a)** biotite-muscovite schist sample 108-17-T02; **b)** chlorite schist sample 108-17-T16. Coloured fields indicate the observed mineral assemblages in each sample. The dashed grey lines indicate the aluminosilicate stability-fields in the system Al_2O_3 - SiO_2 - H_2O , as defined by Holland and Powell (1998) based on Pattison (1992). Abbreviations: And, andalusite; Ap, apatite; Bt, biotite; Chl, chlorite; Crd, cordierite; Ctd, chloritoid; Cum, cummingtonite; Ged, gedrite; Grt, garnet; Ilm, ilmenite; Ky, kyanite; Mrg, margarite; Ms, muscovite; Pg, paragonite; Pl, plagioclase; Po, pyrrhotite; Qtz, quartz; Rt, rutile; Sil, sillimanite; St, staurolite.

only possible evidence for higher-grade metamorphism in the Tower stratigraphy rocks is the occurrence of quartz + spinel in the mineral assemblage of biotite-muscovite schist sample 108-17-T07 (Figure 6e). Quartz + spinel assemblages are generally considered indicative of granulite-facies metamorphism (Spear, 1995; Pattison et al., 2003; Kelsey, 2008). The spinel bearing sample (108-17-T07) contains relatively elevated concentrations of Zn (1070 ppm) and S (1.38 wt %), and the spinel occurs in close spatial association with sulphide (Figure 6e). Zaleski et al. (1991) documented the presence of gahnite (Zn-spinel) in Zn-bearing muscovite schists at the Linda deposit, Snow Lake, where temperatures during peak metamorphism were estimated to be about 550°C. The gahnite is interpreted to form through desulphidation reactions involving sphalerite. Quartz-spinel assemblages are therefore not indicative of granulite-facies metamorphic conditions in Zn- and S-bearing rocks.

In addition to contrast in metamorphic grade, there is also a contrast in the Sm-Nd isotope geochemistry between rocks of the Tower deposit and the Pikwitonei domain. Initial ϵ_{Nd} values for supracrustal and granitoid rocks from the Pikwitonei domain typically range from -26.1 to -9.5 (calculated at 1.88 Ga; Couëslan, unpublished data, 2013–2017) in contrast to the range of ϵ_{Nd} values from +0.1 to +3.2 for the Tower deposit rocks. The evidence suggests it is unlikely that the rocks of the Tower deposit are derived from the adjacent PGD.

Stratigraphic comparison with the Ospwagan group rocks

The Tower deposit stratigraphy bears a striking resemblance to the Pipe formation of the Ospwagan group (Couëslan, 2017). In the footwall to the T1 mineralization, the biotite-garnet gneiss has a mineral assemblage similar to the lower, more siliceous portions of the Pipe formation P2 member, exposed at the Pipe II mine near Thompson (Macek and Bleeker, 1989; Bleeker, 1990). The P2 member generally becomes aluminous towards the top forming a garnet- and locally staurolite- and aluminosilicate-bearing mica schist, which is compositionally and texturally similar to the biotite-muscovite schist of the Tower stratigraphy. The position of the sulphidic schist and T1 mineralization directly above the biotite-muscovite schist is similar to the P2 member sulphide-facies iron formation that overlies the P2 member pelite. The wide variety of garnet-, biotite-, and hornblende-bearing gneisses above the T1 mineralization share many similarities with the wide variety of impure cherts, silicate-facies iron formations, and calcareous rocks of the P3 member. However, the litho-geochemistry and Sm-Nd isotope geochemistry of the Tower stratigraphy rocks do not agree with a correlation to Ospwagan group rocks.

Geochemical comparisons

The marked difference between the trace-element profiles of the Tower stratigraphy rocks and petrographically similar units from the Ospwagan group, suggest that they are unrelated (Figure 13). Although it is possible for elements considered to be immobile in most environments to become mobile in the hydrothermal fluid-rich environment of VMS systems (Ludden et al., 1982; MacLean, 1988; Gemmill and Fulton, 2001; Genna et al., 2014; Duuring et al., 2016), it is unlikely that these rocks

represent chemically modified Ospwagan group stratigraphy. If the alteration was intense enough to overprint the trace-element profiles of the units, it would likely overprint the major-element bulk composition, and therefore mineral assemblages, such that the Ospwagan group stratigraphy would no longer be recognizable.

The biotite-muscovite schist and biotite-garnet gneiss plot close to expected on the Al_2O_3 - SiO_2 diagram of Zwanzig et al. (2007; Figure 12) for pelitic and semipelitic rocks of the Ospwagan group. However, both the grunerite-magnetite and hornblende gneisses plot outside of the expected field for impure chert and silicate-facies iron formation. It is curious that the biotite-muscovite schist, biotite-garnet gneiss, and grunerite-magnetite gneiss plot in a tight cluster, even though they have distinct mineral assemblages. It is also curious that these three petrographically distinct units have very similar immobile trace-element profiles, with the exception of a single schist sample (108-17-T13) which has a profile similar to the hornblende gneiss (Figure 13a). This may suggest that the metamorphic mineral assemblages of the various units, and therefore also the major-element bulk composition, are no longer indicative of the protolith.

A diagram for differentiating metasedimentary from meta-igneous rocks was devised by Winchester et al. (1980) using relatively immobile elements. The diagram plots Ni, which should be elevated in mafic igneous rocks and the fine-grained and heavy mineral component of clastic sedimentary rocks, against Zr/TiO_2 , which should be elevated in clastic sedimentary and felsic igneous rocks. These elements are considered to be relatively immobile, even in VMS systems. Archival geochemical data for meta-igneous and metasedimentary rocks ($n=647$) were plotted in order to test the Zr/TiO_2 -Ni diagram of Winchester et al. (1980; Figure 18a). The vast majority of analyses plotted within the sedimentary field defined by Winchester et al. (1980). However, the rocks of igneous protolith and the rocks of sedimentary protolith do appear to have distinct distributions in Zr/TiO_2 -Ni space. Adjusting the position of the curve along the y-axis by an order of magnitude (solid curve) appears to form a much better fit to the dataset, effectively separating the majority of meta-igneous and metasedimentary rocks. The archival dataset did highlight several limitations of the diagram. The diagram is unable to resolve felsic igneous rocks from psammitic sedimentary rocks. Both rock types tend to plot in the igneous field, along the y-axis with elevated Zr/TiO_2 values (typically >100). Primitive alkaline rocks commonly plot within the metasedimentary rock field because they contain elevated Ni and Zr. In general, igneous rocks of intermediate composition were more likely to be misclassified than felsic or mafic compositions.

Given these limitations, rocks of the Tower stratigraphy were plotted along with petrographically similar rocks from the Ospwagan group on the modified diagram of Winchester et al. (1980; Figure 18b). The biotite-muscovite schist and biotite-garnet gneiss generally plot in a cluster along the y-axis with relatively elevated Zr/TiO_2 values (>100). The petrographically similar P2 member pelite typically plots well within the sedimentary rock field. One sample of biotite-muscovite schist (108-17-T13) plots within the sedimentary rock field and over-

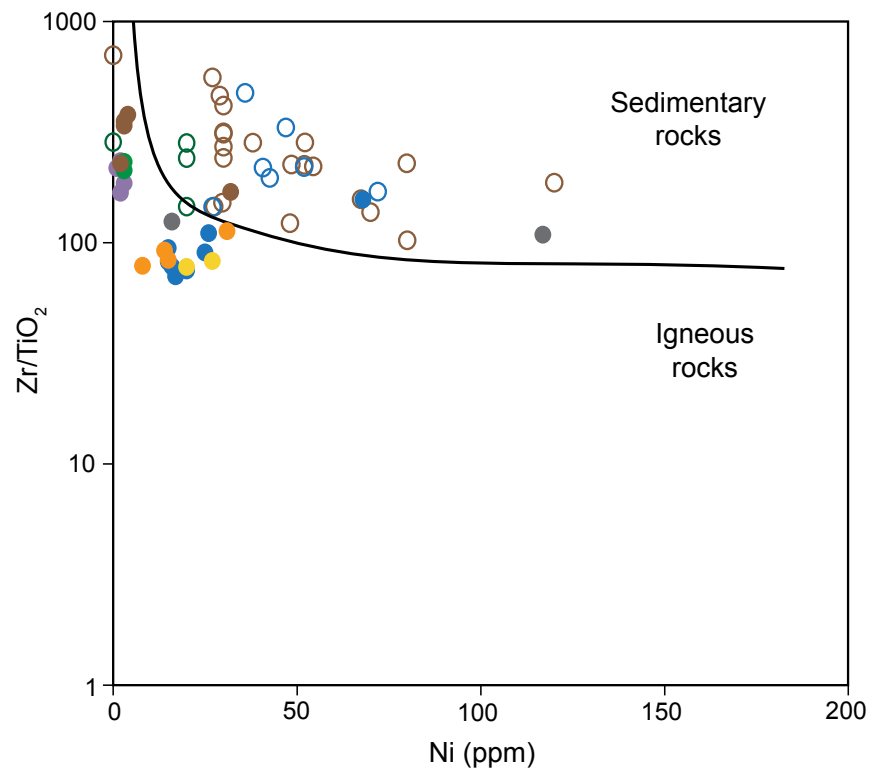
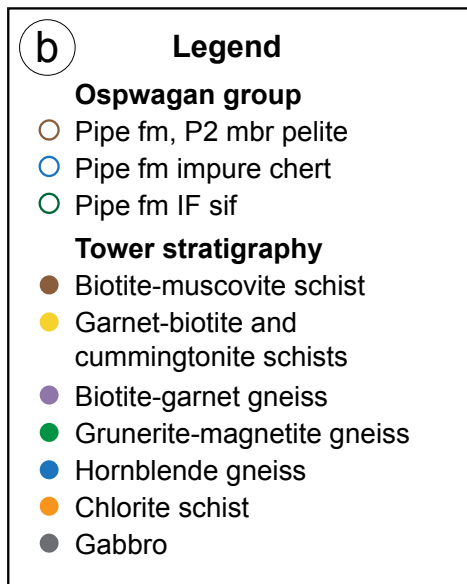
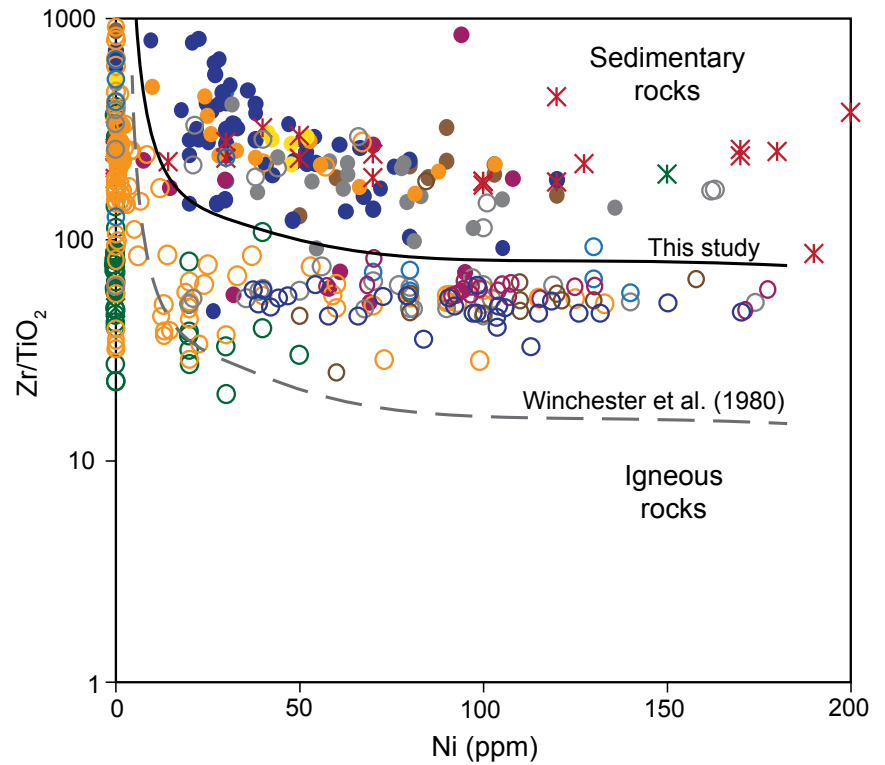


Figure 18: Zr/TiO_2 -Ni diagram adapted from Winchester et al. (1980) for discriminating metasedimentary and meta-igneous rocks (see text for details): **a)** tested using archival data ($n=647$); **b)** comparing Tower deposit and Ospwagan group rocks. Data from Bailes and Percival (2005), Gilbert and Bailes (2005), Zwanzig (2005), Simard and Creaser (2007), Zwanzig et al. (2007), Anderson (2008), Burnham et al. (2009), Heaman et al. (2009), Gagné (2011), Gagné (2012), Anderson (2013), Couëslan (2013), Couëslan (2016), Waterton et al. (2017), Couëslan (unpublished), Anderson (unpublished). Abbreviations: fm, formation; IF sif, silicate-facies iron formation; mbr, member.

laps with P2 pelite compositions. This sample also plots closer to the cluster of data points defined by the hornblende gneiss, garnet-biotite and cummingtonite schists, and chlorite schist with which, as previously mentioned, it also shares a similar trace-element profile. The grunerite-magnetite gneiss also plots in a cluster along the y-axis with the biotite-muscovite schist and biotite-garnet gneiss. Petrographically similar silicate-facies iron formation of the Pipe formation typically plot within the sedimentary rock field of the diagram, but there is some compositional overlap. The hornblende gneiss forms a cluster of points within the igneous rock field, with a single outlier in the sedimentary rock field. Samples of the petrographically similar Pipe formation impure chert plot within the sedimentary rock field, overlying the compositional range of the P2 member pelite. The two samples of plagioclase amphibolite plot on either side of the igneous-sedimentary rock boundary.

The majority of Tower stratigraphy rocks plot within the igneous rock field of the modified Zr/TiO₂-Ni diagram. The biotite-muscovite schist, biotite-garnet gneiss, and grunerite-magnetite gneiss cluster in the portion of the diagram typically reserved for felsic igneous and psammitic rocks, of which they bear little resemblance. The hornblende gneiss, garnet-biotite and cummingtonite schists, and chlorite schist typically plot within the portion of the diagram populated by intermediate and mafic igneous rocks. This suggests that the Tower stratigraphy rocks could be derived from igneous rocks subjected to varying degrees of hydrothermal alteration. Alteration indices were therefore calculated for the Tower rocks using the NORMAT approach of Piché and Jébrak (2004; Table 3; DRI2018004; Couëslan, 2018). The technique uses a normative mineral approach to calculate the overall intensity of alteration (IFRAIS), as well as specific normative-mineral alteration

Table 3: Normative mineral alteration indices calculated for Tower deposit rocks using the NORMAT method (Piché and Jébrak, 2004).

Sample	Unit	IFRAIS ¹	IPARA ²	ISER ³	ICHLO ⁴	IPYRO ⁵	IPAF ⁶
108-17-T01	Plagioclase amphibolite	100	0	0	0	0	N/A
108-17-T03	Plagioclase amphibolite	100	0	0	0	0	N/A
108-17-T05	Hornblende-biotite gneiss	99.356	0.49	0.154	0	0	N/A
108-17-T08	Hornblende-biotite gneiss, laminated	98.909	0.962	0.129	0	0	N/A
108-17-T09	Hornblende gneiss, laminated	100	0	0	0	0	N/A
108-17-T10	Hornblende-garnet gneiss	100	0	0	0	0	N/A
108-17-T20	Hornblende-clinozoisite gneiss	96.573	3.085	0.342	0	0	N/A
108-17-T21	Hornblende-garnet gneiss	100	0	0	0	0	N/A
108-17-T23	Clinozoisite-hornblende gneiss	100	0	0	0	0	N/A
108-17-T24	Hornblende gneiss, carbonate-bearing	100	0	0	0	0	13.805
108-17-T02	Biotite-muscovite schist	42.977	34.668	22.355	0	0	N/A
108-17-T06	Biotite-muscovite schist	63.771	21.93	14.299	0	0	N/A
108-17-T07	Biotite-muscovite schist	6.264	8.424	85.312	0	0	N/A
108-17-T13	Biotite-muscovite schist	65.556	11.609	22.835	0	0	N/A
108-17-T22	Biotite-muscovite schist	78.348	10.338	11.314	0	0	N/A
108-17-T04	Biotite-garnet gneiss	62.897	32.718	4.384	0	0	N/A
108-17-T14	Biotite-garnet gneiss	61.723	31.143	7.134	0	0	N/A
108-17-T19	Biotite-garnet gneiss	78.749	15.161	6.09	0	0	N/A
108-17-T27	Biotite-garnet gneiss	84.859	14.279	0.861	0	0	N/A
108-17-T12	Grunerite-magnetite schist	84.433	14.577	0.99	0	0	N/A
108-17-T25	Grunerite-magnetite schist	86.961	12.504	0.535	0	0	N/A
108-17-T26A	Garnet-biotite schist	17.551	32.902	49.547	0	0	N/A
108-17-T26B	Cummingtonite schist	64.1240	30.22	5.657	0	0	N/A
108-17-T11	Chlorite schist, carbonate-bearing	5.859	1.855	15.87	75.752	0.663	17.514999
108-17-T16	Chlorite schist	0	2.594	7.68	83.963	5.763	N/A
108-17-T17	Chlorite schist	0	0.545	2.15	85.377	11.928	N/A
108-17-T18	Chlorite schist	0	1.661	15.48	72.638	10.221	N/A

¹ Index of alkali-element depletion; lower numbers indicate increase intensity of depletion

² Index of paragonitization; higher numbers indicate increasing intensity

³ Index of sericitization; higher numbers indicate increasing intensity

⁴ Index of chloritization; higher numbers indicate increasing intensity

⁵ Index of pyrophyllitization; higher numbers indicate increasing intensity

⁶ Index of carbonatization; higher numbers indicate increasing intensity; samples with measured LOI < normative LOI = N/A

indices for paragonite (IPARA), sericite (ISER), chlorite (ICHLO), pyrophyllite (IPYRO), and carbonatization (IPAF). The carbonatization indices is estimated by comparing the measured LOI with the normative LOI values. Because the rocks contain amphibolite-facies mineral assemblages, and the normative calculations are for greenschist-facies assemblages, the IPAF values are likely an underestimate. All plagioclase amphibolite and hornblende gneiss samples yielded IFRAIS values >95, indicating relatively fresh, unaltered protolith; however, one of the samples (108-17-T24) is carbonate-bearing and yields an IPAF value of 14, indicating it was subjected to carbonatization. The biotite-muscovite schist is characterized by a wide range of IFRAIS values from 6.2 to 78, suggesting moderate to intense alteration. The alteration is calculated to be dominantly sericite (ISER=11–85) and paragonite (IPARA=8.4–35). The biotite-garnet gneiss yields IFRAIS values of 62–85, indicating moderate alteration. The alteration is projected to be dominantly paragonite (IPARA=14–33) with lesser sericite (ISER=0.86–7.1). The grunerite-magnetite gneiss is moderately to weakly altered with IFRAIS values of 84 and 87, dominated by paragonite alteration (IPARA=13–15). The garnet-biotite and cummingtonite schists yield IFRAIS values of 17–64, indicating relatively intense alteration, which is dominated by paragonite (IPARA=30–33) and locally sericite alteration (ISER=5.7–50). The most intensely altered unit of the Tower stratigraphy is the chlorite schist which yielded IFRAIS values of 0–5.9. The alteration is calculated to be dominantly chlorite (ICHLO=73–85) with lesser sericite (ISER=2.1–16) and pyrophyllite (IPYRO=0.66–12). One chlorite schist sample (108-17-T11) is carbonate-bearing and yielded a carbonatization indices (IPAF) of 18.

Because the hornblende gneiss (excepting 108-17-T24) and plagioclase amphibolite are predicted to be relatively unaltered the samples were plotted on the total alkali-silica diagram of Le Maitre (2002). The hornblende gneiss samples plot with compositions ranging from basalt to andesite, whereas the two amphibolite samples plot as basaltic andesite (108-17-T01) and dacite (108-17-T03; Figure 19a). Conversely, all but one sample of the hornblende gneiss cluster in the basalt field on the Zr/Ti-Nb/Y diagram of Pearce (1996) and both samples of amphibolite plot in the andesite + basaltic andesite field (Figure 19b). The discrepancy between the diagrams of Le Maitre (2002) and Pearce (1996) could indicate silicification, which is not quantified by the NORMAT technique. This would explain the stringing of data along the SiO₂ axis of Le Maitre (2002) for samples with otherwise similar trace-element compositions. This could also explain the stringy quartz laminations observed in some samples of the hornblende gneiss. What could be interpreted as stringy chert laminations in iron formation, may represent discrete veinlets (or attenuated veins) of quartz. Although unsuitable for plotting on the total alkali-silica diagram, the remaining Tower stratigraphy samples were plotted on the Zr/Ti-Nb/Y diagram of Pearce (1996; Figure 19b). The biotite-muscovite schist plots within the andesite + basaltic andesite field. Three samples cluster near the boundary with felsic rocks, and one sample (108-17-T13) plots close to the hornblende gneiss sample. The biotite-garnet and grunerite-magnetite gneisses plot as a tight cluster near the center of the andesite + basaltic andesite field. The chlorite schist, and garnet-biotite and cummingtonite

schists plot within the basalt field, overlapping the composition of the hornblende gneiss.

Chondrite-normalized REE profiles for the biotite-muscovite schist, biotite-garnet gneiss, and grunerite-magnetite gneiss are similar with moderate negative slopes ($[La/Yb]_N=2.7-3.7$), negative europium anomalies ($Eu/Eu^*=0.59-0.92$), and flat to slightly concave-up HREE profiles (Figure 20a). Biotite-muscovite schist sample 108-17-T13 is less LREE-enriched ($[La/Yb]_N=2.4$) with only a slight europium anomaly ($Eu/Eu^*=0.88$). Chondrite-normalized REE profiles of the hornblende gneiss typically have negative slopes, but are generally less LREE-enriched ($[La/Yb]_N=1.4-2.0$, $n=7/8$), with variable europium anomalies ($Eu/Eu^*=0.80-1.11$), and flat to slightly concave-up HREE profiles (Figure 20c). The anomalous biotite-muscovite schist sample (108-17-T13) falls within the compositional range of the hornblende gneiss. The carbonatized hornblende gneiss sample (108-17-T24) is characterized by a steeper REE profile ($[La/Yb]_N=3.2$), which could indicate mobilization of REE by a CO₂-rich hydrothermal fluid (Ludden et al., 1982; Hollings and Wyman, 2005). The chlorite schist is characterized by negative sloping REE-profiles ($[La/Yb]_N=2.3-2.6$) with prominent negative europium anomalies ($Eu/Eu^*=0.32-0.66$; Figure 20e). The garnet-biotite and cummingtonite schists are compositionally similar to the hornblende gneiss with flatter REE-profiles ($[La/Yb]_N=1.5$ and 1.8) but with negative europium anomalies ($Eu/Eu^*=0.65$ and 0.77 ; Figure 20g). The plagioclase amphibolite is characterized by steeper chondrite-normalized REE profiles ($[La/Yb]_N=2.6$ and 3.4 ; Figure 20i) than the hornblende gneiss.

Primitive mantle-normalized multi-element profiles of the biotite-muscovite schist, biotite-garnet gneiss, and grunerite-magnetite gneiss are similar with prominent negative anomalies at Nb, Ti, and V, slight negative anomalies at Y, and slight positive anomalies at Zr (Figure 20b). Schist sample 108-17-T13 is overall less enriched than the other schist and gneiss samples, with a significantly more subdued anomaly at V. Multi-element profiles of the hornblende gneiss are characterized by negative anomalies at Nb, Ti, and Y, and a slight positive anomaly at Zr (Figure 20d). The chlorite schist, and garnet-biotite and cummingtonite schists are characterized by multi-element profiles broadly similar to the hornblende gneiss (Figure 20f, h). The strong similarities between the REE- and multi-element profiles of the biotite-muscovite schist (excluding 108-17-T13), biotite-garnet gneiss, and grunerite-magnetite gneiss are suggestive of a common protolith, which is supported by similar compositions on the Zr/Ti-Nb/Y diagram of Pearce (1996), and clustering of data on the Zr/TiO₂-Ni diagram of Winchester et al. (1980). The similarities between the REE- and multi-element profiles of the hornblende gneiss, chlorite schist, garnet-biotite and cummingtonite schists, and biotite-muscovite schist sample 108-17-T13, are also indicative of a common protolith, which is again supported by the clustering of data in the diagrams of Pearce (1996) and Winchester et al. (1980). Multi-element profiles of the plagioclase amphibolite are characterized by greater Th enrichment and stronger negative anomalies at Nb and Ti than the hornblende gneiss (Figure 20j). However, negative anomalies at Nb, Ti, and Y, and a positive anomaly at Zr, may be consistent with a similar source for both the plagioclase amphibolite and hornblende gneiss.

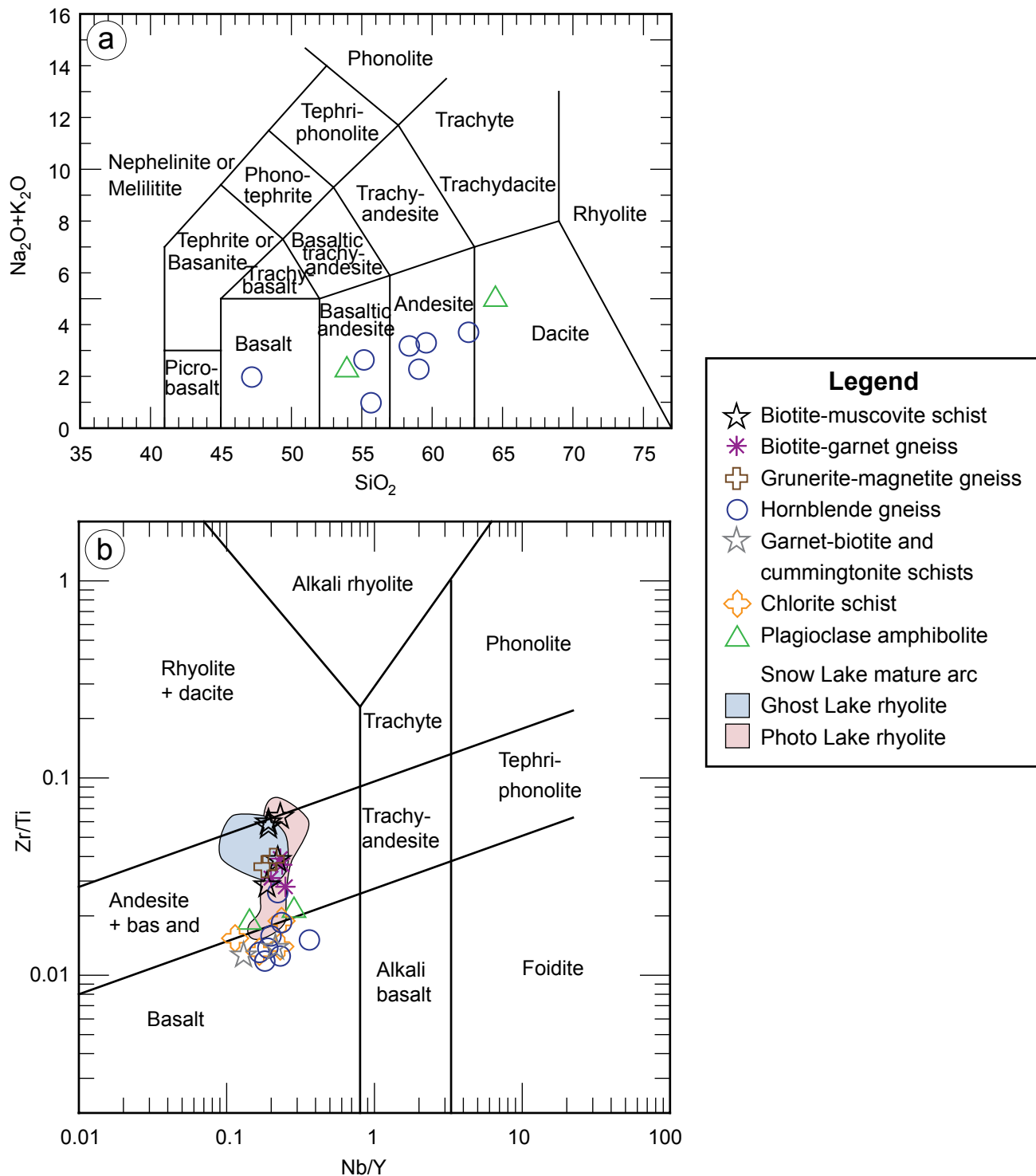


Figure 19: Discrimination diagrams showing the compositions of Tower stratigraphy rocks: **a)** total alkali-silica (TAS) diagram of Le Maitre (2002); **b)** Zr/Ti-Nb/Y diagram of Pearce (1996). Data for the Ghost Lake and Photo Lake rhyolites of the Snow Lake belt are from Bailes and Galley (2001). Abbreviations: and, andesite; bas, basaltic.

Comparison with East Kisseynew deposits

The widespread occurrence of VMS deposits in the sub-Phanerozoic Flin Flon and East Kisseynew domains has led to the suggestion that the Tower deposit could represent an inlier of juvenile THO rocks along the Superior craton margin. Therefore, a comparison is made between the mafic rocks of the Tower deposit, represented by the least altered hornblende

gneiss, and mafic rocks associated with VMS deposits of the East Kisseynew domain. The closest of these to the Tower zone is the Talbot deposit, located roughly 32 km across strike to the northwest (Figure 1). Mafic rocks from the Talbot deposit are characterized by flat chondrite-normalized REE profiles and primitive mantle-normalized multi-element profiles typical of N-MORB-affinity rocks (Figure 21a, b). Conversely, mafic

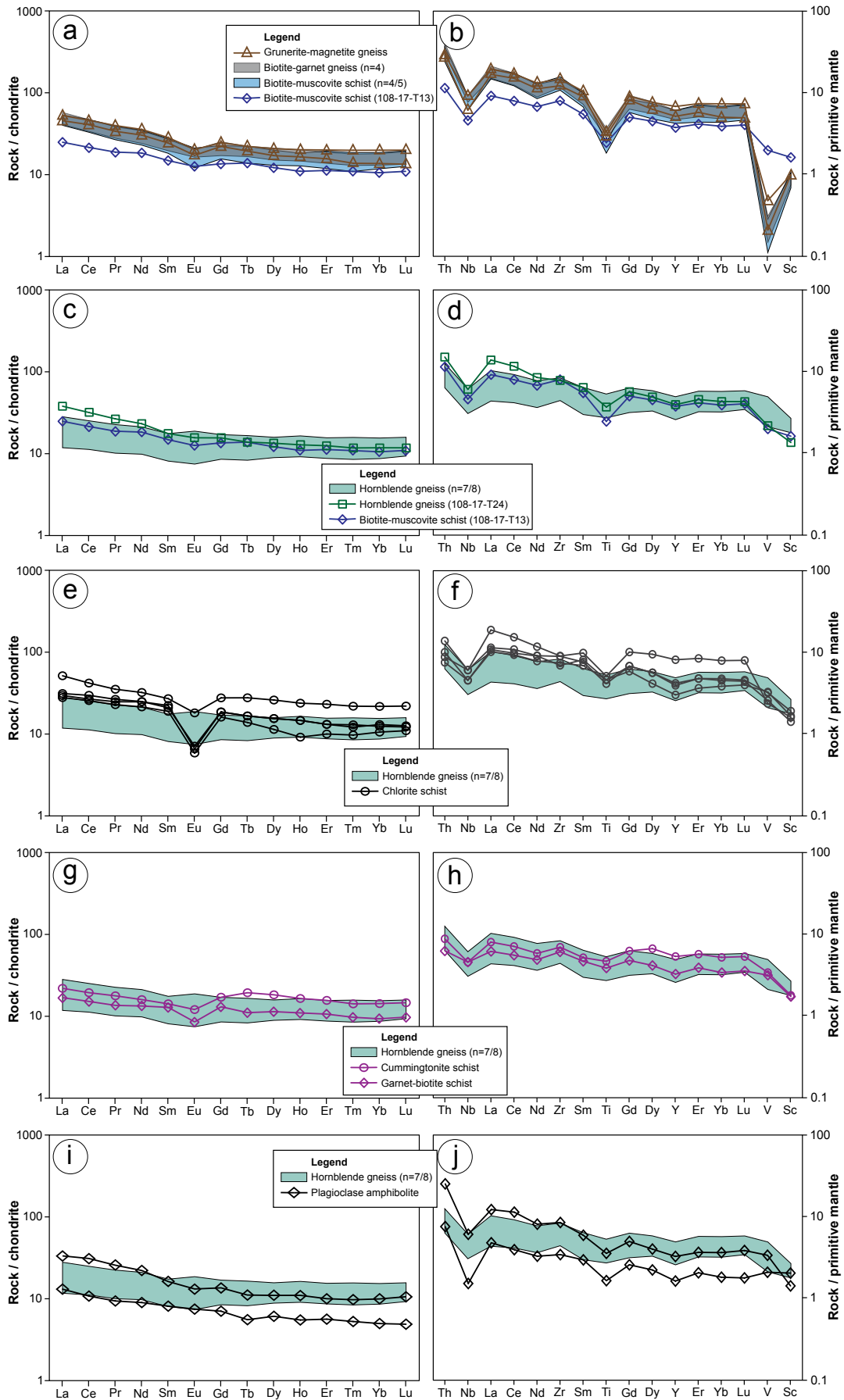


Figure 20: Chondrite-normalized REE profiles (left column) and primitive mantle-normalized multi-element profiles (right column) for Tower stratigraphy rocks. Normalizing values for chondrite and primitive mantle are from McDonough and Sun (1995).

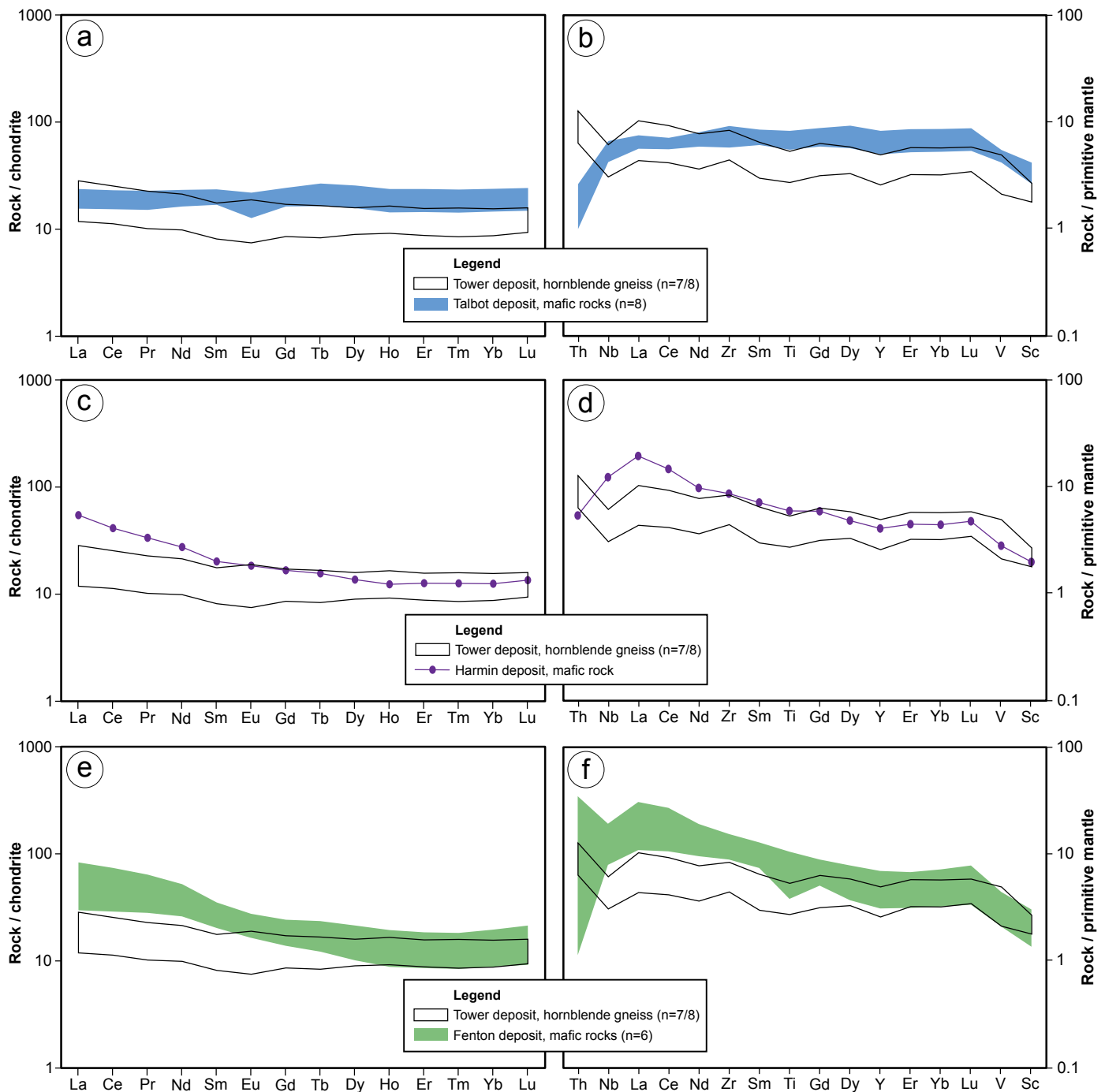


Figure 21: Chondrite-normalized REE profiles (left column) and primitive mantle-normalized multi-element profiles (right column) of mafic rocks associated with East Kiseynew domain VMS deposits, and least-altered hornblende gneiss of the Tower stratigraphy. East Kiseynew domain data is from Simard et al. (2010b). Normalizing values for chondrite and primitive mantle are from McDonough and Sun (1995).

rocks from the Harmin and Fenton deposits are more enriched with E-MORB-like REE and multi-element profiles (Figure 21c–f). The profiles of the East Kiseynew domain rocks show little to no evidence for Archean crustal contamination, which is supported by juvenile initial ϵ_{Nd} values of +3.3 and +3.7 (at 1.88 Ga) for mafic rocks from Fenton and Talbot, respectively (Simard et al., 2010a, b). This contrasts with the somewhat lower ϵ_{Nd} values of the Tower deposit hornblende gneiss and plagioclase amphibolite (+1.2 to +3.2) which are characterized

by REE and trace-element profiles suggestive of arc-affinity rocks.

Primitive mantle-normalized multi-element profiles of intermediate and felsic rocks associated with the East Kiseynew domain VMS deposits can also be compared with the biotite-garnet and grunerite-magnetite gneisses of the Tower deposit (Figure 22). Profiles of intermediate rocks from the Talbot, Harmin, and Fenton deposits are typically more enriched in LREE, Nb, and Zr. The profile of intermediate rocks from

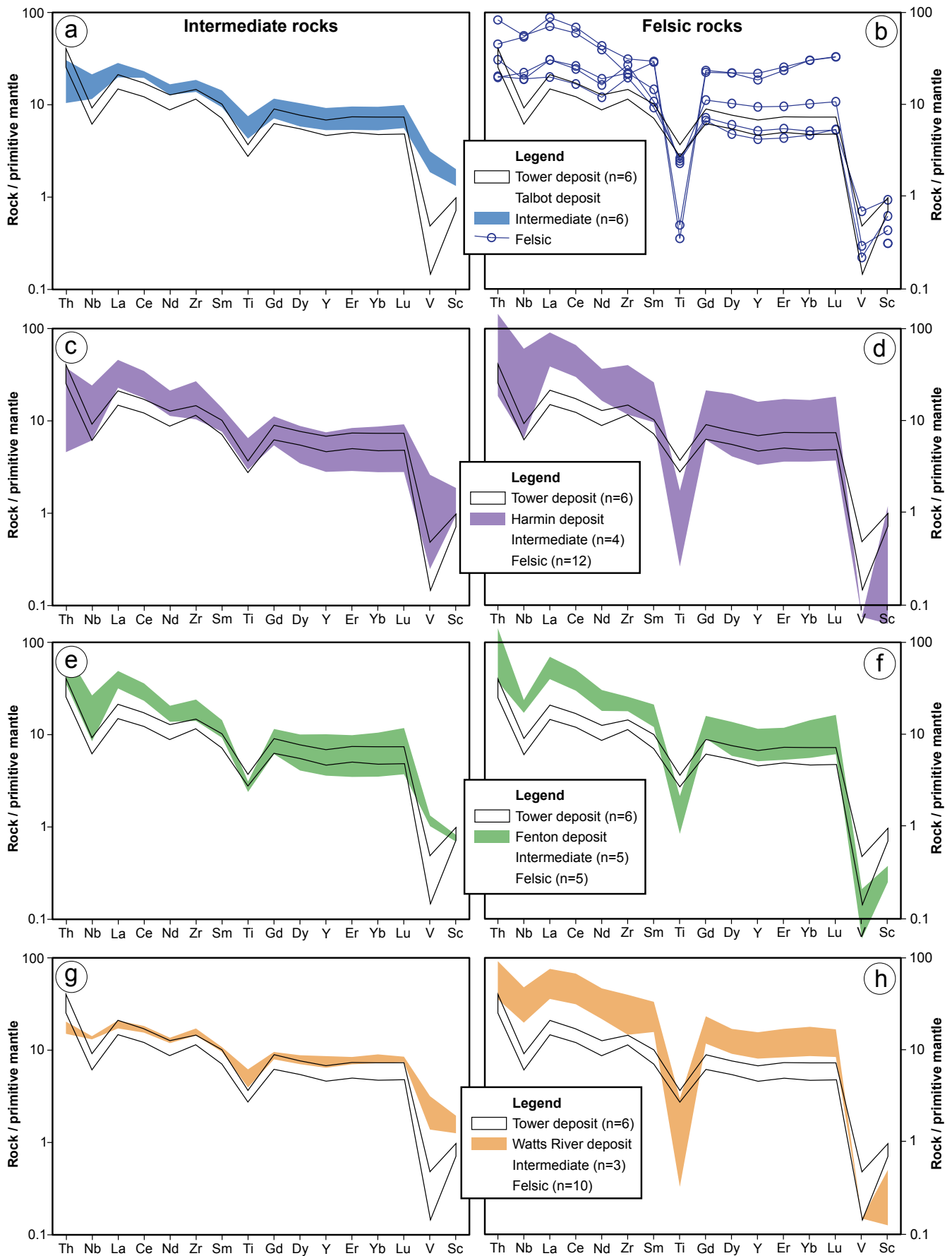


Figure 22: Primitive mantle-normalized multi-element profiles of intermediate (left column) and felsic rocks (right column) associated with East Kiseynew domain VMS deposits, and the grunerite-magnetite and biotite-garnet gneisses of the Tower stratigraphy. East Kiseynew domain data is from Simard et al. (2010b). Normalizing values for primitive mantle are from McDonough and Sun (1995).

Watts River is less enriched in Th, but more enriched in Nb, and Ti. Negative anomalies at V are generally not present in the intermediate rocks, which are also more enriched in Sc than the rocks from the Tower deposit. Felsic rocks associated with the East Kisseynew domain deposits are typically more enriched than the Tower deposit rocks, with less pronounced negative anomalies at Nb, and more pronounced negative anomalies at Ti. Negative anomalies at V are typically more pronounced than for Tower deposit rocks. Initial ϵ_{Nd} values for intermediate and felsic rocks from the East Kisseynew deposits range from +3.0 to +3.5 (calculated at ca. 1.88 Ga) indicating little to no interaction with evolved crust (Simard et al., 2010a, b). These values are higher than that yielded by the two samples of biotite-muscovite schist ($\epsilon_{Nd} = +0.1$ and +1.8) from the Tower deposit. Overall, the REE- and multi-element profiles, and Sm-Nd isotope geochemistry of the Tower deposit rocks differ significantly from rocks associated with VMS deposits in East Kisseynew domain, and suggest that the rocks were derived from different sources.

Although not diagnostic, the absence of negative V anomalies in the intermediate Kisseynew domain rocks could suggest that the biotite-muscovite schist, biotite-garnet gneiss, and grunerite-magnetite gneiss of the Tower deposit represent felsic rocks rather than intermediate rocks as suggested by the Zr/Ti-Nb/Y diagram of Pearce (1996). Felsic volcanic rocks from the Snow Lake belt commonly plot within the andesite field of the Zr/Ti-Nb/Y diagram (Figure 19; e.g. Ghost Lake rhyolite, Photo Lake rhyolite), a function of their generally low Zr contents (Stern et al., 1995; Bailes, 1997). A felsic precursor for the biotite-muscovite schist, biotite-garnet gneiss, and grunerite-magnetite gneiss is also supported by the clustering of these samples along the y-axis of the Zr/TiO₂-Ni diagram of Winchester et al. (1980), which is typical of felsic volcanic and psammitic rocks. Demonstrating a felsic precursor for these units would imply a bimodal volcanic sequence for the Tower stratigraphy.

Interpretation of the Tower stratigraphy

The rocks of the Tower deposit appear to represent a mafic-dominated volcanic sequence, with intercalations of intermediate to possibly felsic volcanic rocks, variably altered by VMS-related hydrothermal systems (Figure 23). Least altered mafic rocks are represented by the hornblende gneiss. All intermediate/felsic rocks appear to be altered to some degree with the biotite-garnet gneiss and grunerite-magnetite gneiss representing the least affected rocks. Two zones of intense hydrothermal alteration are present in the Tower stratigraphy. A zone of intense sericite-paragonite alteration is associated with the T1 mineralization and represented by the biotite-muscovite schist, and garnet-biotite and cummingtonite schists. This zone of alteration appears to have affected dominantly intermediate/felsic rocks; however, mafic rocks were also affected (samples 108-17-T13 and 108-17-T26A and B). A zone of intense chlorite alteration is associated with the T2 mineralization and is represented by the chlorite schist. This zone appears to consist largely of mafic precursor, although the chlorite alteration grades into intermediate/felsic rocks in the footwall and hangingwall to this zone. A narrow zone of carbonate altered mafic

rocks is present between the T1 and T2 mineralized zones and is represented by thin carbonate-bearing horizons in the hornblende gneiss. The stratigraphy has been intruded by ultramafic and mafic magmas now represented by ultramafic schist and plagioclase amphibolite, respectively. In drillcore TP-10-003, one band of plagioclase amphibolite occurs within the biotite-muscovite schist, while another appears to contain a xenolith of chlorite altered rock. This suggests at least some of the mafic intrusions post-date the VMS-related hydrothermal systems. A granodiorite intrusion is present in the structural hangingwall to the T2 zone, and is characterized by relatively steep REE and multi-element profiles (Figure 15), making it geochemically distinct from the rest of the Tower stratigraphy (Figure 20). This suggests that it is likely petrogenetically unrelated to the stratigraphy it intrudes.

It remains uncertain if the Tower stratigraphy is upright or overturned. Intense hydrothermal alteration typically occurs in the immediate footwall to VMS mineralization. In the case of the Tower deposit, the T1 zone occurs structurally above a zone of intense sericite-paragonite alteration, suggesting the stratigraphy remains upright; however, the T2 zone occurs near the structural base of a zone of intense chlorite alteration suggesting overturned stratigraphy. Evidence suggests that the T1 zone may represent structurally remobilized sulphide, as such, it may not be a reliable indicator of the stratigraphic younging direction. In addition, the sericite-paragonite alteration affects both mafic and felsic protolith suggesting the zone of alteration may be discordant to stratigraphy. The T2 zone appears to be in situ and stratiform suggesting it may be a more reliable indicator of the younging direction. Assuming that the stratigraphy is overturned, the continuation of intense chlorite alteration above the T2 zone could represent proximal hangingwall alteration. Although this is currently the favoured interpretation, the T2 zone could alternatively be interpreted as a zone of stratiform sub-seafloor hydrothermal replacement (Couëslan, 2017), which would leave the question of younging direction unresolved. An ultramafic intrusion intersected by drillcore TP-12-033 grades from ultramafic schist in the direction of the hangingwall, to ultramafic amphibolite in the direction of the footwall. This apparent gradation from altered peridotite to pyroxenite may corroborate an overturned stratigraphy; however, it could also be the result of variable alteration of an ultramafic body. This scenario could be further complicated if the ultramafic intrusion post-dates significant folding and/or is discordant to the stratigraphy. Additional insight into the younging direction may be found by examining the geochemical zonation of the ultramafic intrusions and looking for evidence of fractionation trends; however, this is contingent on the ultramafic bodies being conformable to the stratigraphy at the time of intrusion.

The mafic volcanic rocks and mafic intrusions have normalized trace-element profiles characteristic of arc affinity rocks (Figure 20). Least altered samples of mafic rocks typically plot as arc basalt with tholeiitic affinity transitional to calc-alkaline-affinity (Figure 24a-c). One mafic intrusion sample (108-17-T01; Figure 24d) displays boninitic affinity, which is supported by its relatively high Mg# (0.66), Ni (117 ppm), Cr (280 ppm), and Al₂O₃/TiO₂ (52), and low TiO₂ (0.33 wt%). Boninites are interpreted as high temperature melts derived from refractory

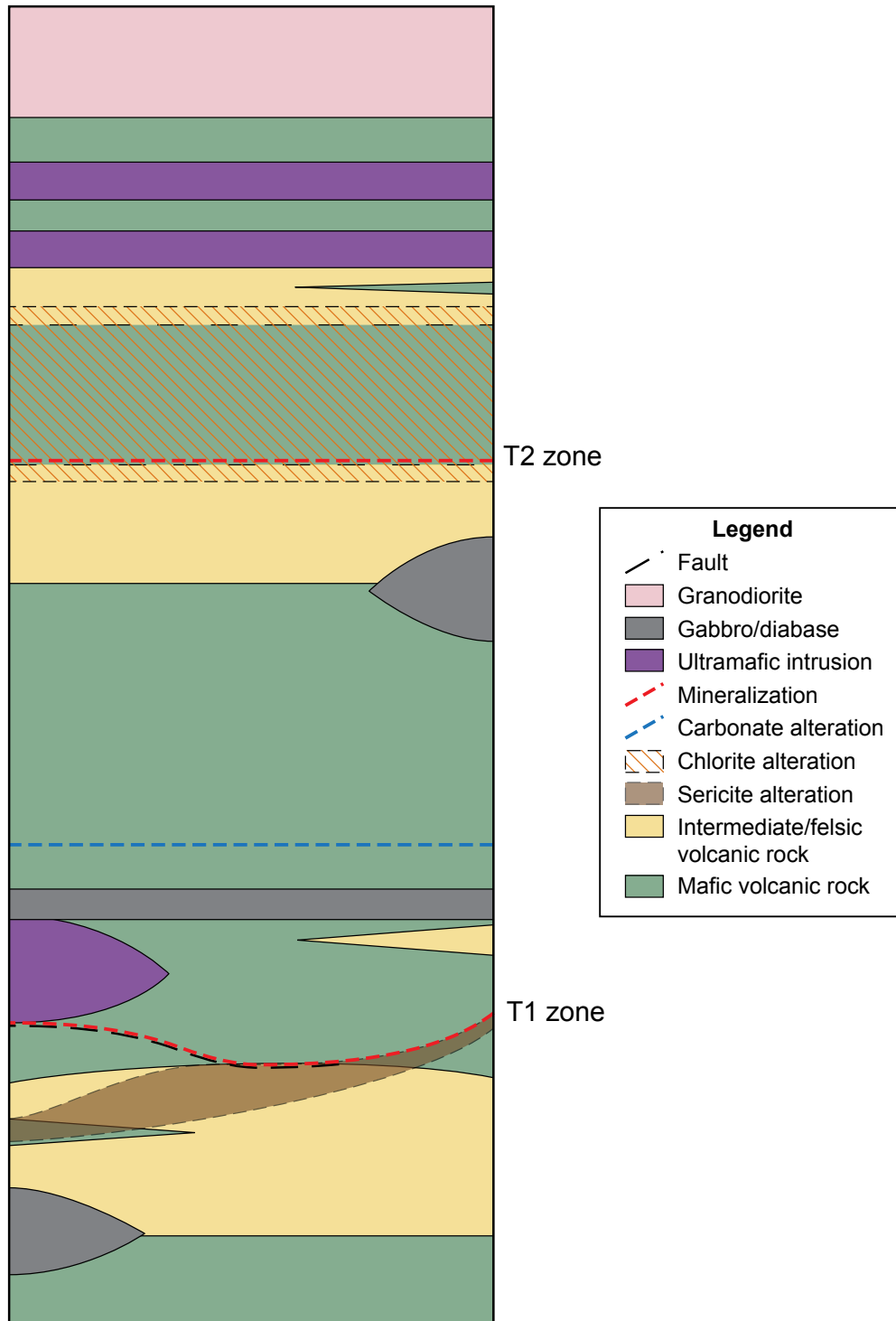


Figure 23: Schematic protolithostratigraphic section of the Tower stratigraphy from the structural footwall (bottom) to the structural hangingwall (top).

mantle, and are typically associated with arc-rifting (Piercey, 2010). The intermediate/felsic volcanic rocks of the Tower stratigraphy are also characterised by arc-like normalized trace-element profiles. Three samples of biotite-muscovite schist plot close to rhyolite + dacite boundary on the Zr/Ti-Nb/Y diagram (Figure 19) and likely represent felsic volcanic rocks. They plot within the volcanic-arc granite and syn-collisional granite field of the Nb-Y diagram, forming a cluster of points distinct from the hangingwall granodiorite (Figure 25a). The felsic volcanic

rocks are transitional between the potentially ore-bearing FII and FIIIa rhyolite fields in $(La/Yb)_N$ - $(Yb)_N$, Zr/Y-Y, and Th/Yb- $(Yb)_N$ diagrams (Figure 25b-d). The hangingwall granodiorite plots off the scale of these diagrams, along the y-axis, closest to the barren FI rhyolite fields. The FII and FIIIa rhyolites are interpreted to be high temperature melts formed by shallow-level, partial melting of mafic crust in extensional environments, such as a rifted arc setting (Piercey, 2011). Although the relative timing and geochemical affinity for the ultramafic

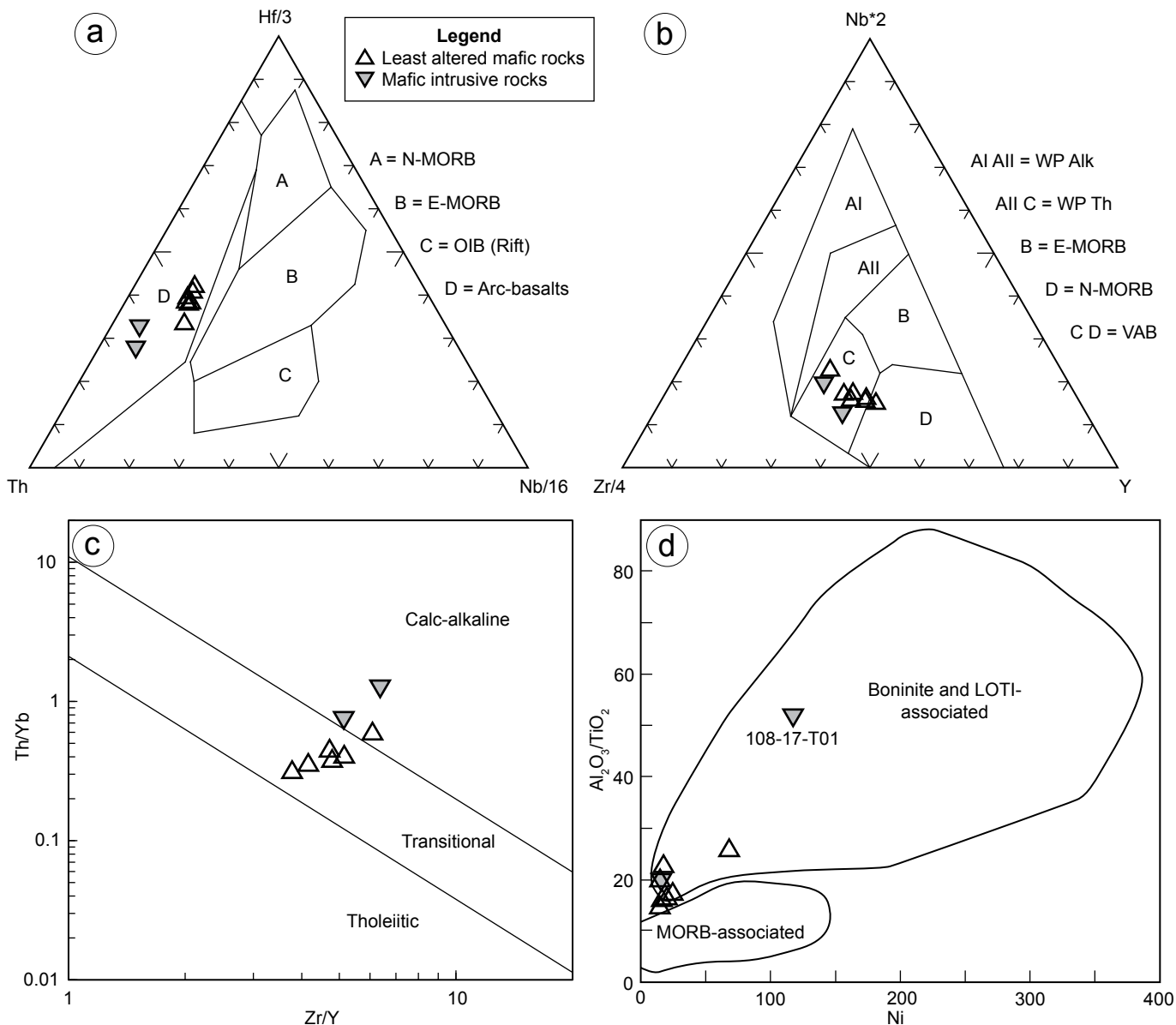


Figure 24: Discrimination diagrams for the least altered mafic rocks of the Tower deposit: **a)** Th-Hf/3-Nb/16 of Wood et al. (1979); **b)** Zr/4-Nb*2-Y of Meschede (1986); **c)** Th/Yb-Zr/Y of Ross and Bédard (2009); **d)** Al₂O₃/TiO₂-Ni of Piercey (2010). Abbreviations: E-MORB, enriched mid-ocean-ridge basalt; LOTI, low-titanium tholeiitic basalt; MORB, mid-ocean-ridge basalt; N-MORB, normal mid-ocean-ridge basalt; OIB, ocean-island basalt; VAB, volcanic-arc basalt; WP Alk, within-plate alkali basalt; WP Th, within-plate tholeiitic basalt.

rocks is unknown, they could be additional evidence for extension and high-temperature magmatism.

The initial ϵ_{Nd} values for the Tower stratigraphy range from +0.1 to +3.2 which suggests variable contamination by an evolved crustal component. Crustal contamination could also result in elevated Th and LREE of a tholeiitic magma, leading to the transitional character of the mafic rocks between tholeiite- and calcalkaline-affinity. This may suggest the presence of Archean crust in the basement to the volcanic arc. Tholeiitic mafic magmatism is widespread in the adjacent Winnipegosis komatiite belt (WKB), the northern extension of which is situated approximately 2 km to the east, across strike, and rocks from the WKB have yielded overlapping initial ϵ_{Nd} values (+1.0 to +7.8). However, the tholeiitic magmatism is distinctly MORB-like in chemistry (Lin et al., 1998; Burnham et

al., 2009; Ciborowski et al., 2017) and no intermediate/felsic or arc magmatism has been recognized in the WKB. There is also a disparity in metamorphic grade with the rocks of the northern WKB interpreted to be of the sub-greenschist to greenschist facies, and rocks of the Tower stratigraphy interpreted to be of the middle amphibolite-facies.

The mafic-dominated nature of the Tower stratigraphy, arc tholeiite- to calcalkaline affinity mafic rocks, presence of boninitic rocks, and Sm-Nd isotope geochemistry are suggestive of a juvenile environment (Piercey, 2010), making it unlikely that the arc was formed during intracratonic rifting along the Superior craton margin. It is more likely that the Tower stratigraphy formed in an island-arc environment on a cratonic fragment at an unknown distance from the Superior craton margin within the Manikewan ocean basin (Corrigan et

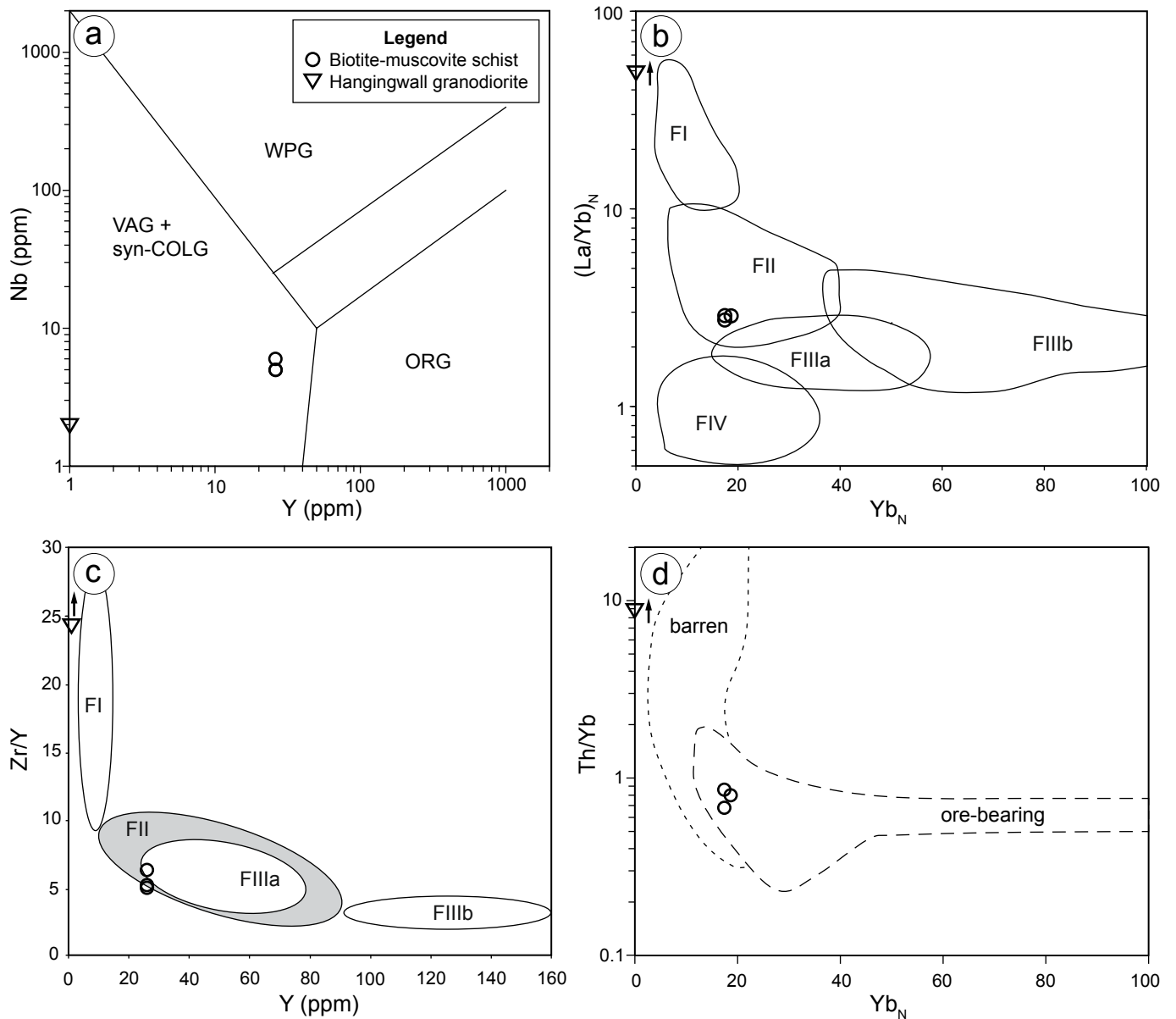


Figure 25: Discrimination diagrams for the hangingwall granodiorite and biotite-muscovite schist samples 108-17-T06, 108-17-T07, and 108-17-T22: **a)** Nb-Y diagram of Pearce et al. (1984); **b)** $(La/Yb)_N$ - Yb_N diagram of Harte et al. (2004; modified after Leshner et al., 1986); **c)** Zr/Y-Y diagram of Leshner et al. (1986); **d)** Th/Yb- Yb_N of Bailes and Galley (1999; modified after Barrie et al., 1993). Abbreviations: syn-COLG, syncollisional granite; ORG, ocean-ridge granite; VAG, volcanic-arc granite; WPG, within-plate granite.

al., 2009). A similar setting has been proposed for the mature arc sequence of the Snow Lake arc assemblage, which contains lithochemically and isotopically similar mafic volcanic rocks (Snell Lake basalt, initial ϵ_{Nd} -0.3 to +2.5) and felsic volcanic rocks (Ghost Lake rhyolite, initial ϵ_{Nd} +3.4; Stern et al., 1995; Bailes and Galley, 1999). The mature arc of the Snow Lake assemblage is also host to the Cu-Zn-Au Photo Lake VMS deposit (Bailes 1997; Bailes and Galley, 1999). However, boninite is not present in the mature arc sequence of the Snow Lake assemblage (although it is present in the older primitive arc sequence); and the felsic volcanic rocks of the mature sequence are more isotopically juvenile than the associated mafic volcanic rocks, a trend not observed in the mafic and intermediate/felsic volcanic rocks of Tower stratigraphy. If the Tower stratigraphy represents a portion of an island arc, its current position along the eastern margin of the TNB is enigmatic.

The present day margin of the Superior craton is interpreted to subcrop approximately 30 km west across strike. This requires that the Tower deposit rocks were thrust onto the Superior craton margin during the Trans-Hudson orogeny and preserved as a klippe. Ultramafic rocks in the Flin Flon domain occur almost exclusively within layered gabbro complexes with the possible exception of the Namew Lake pyroxenite in the sub-Phanerozoic Clearwater Lake domain (Ayres and Young, 1989; Syme and Whalen, 2012; Gagné and Anderson, 2014; Menard et al., 1996; Leclair et al., 1997); however, peridotite and pyroxenite intrusions are relatively common in the TNB and WKB along the Superior boundary zone (Bleeker, 1990; Hulbert et al., 1994; Lin et al., 1998; Macek et al., 2006; Ciborowski et al., 2017; Scoates et al., 2017; Waterton et al., 2017). This may suggest that the Tower stratigraphy rocks were already emplaced on the Superior craton margin prior to ultramafic magmatism

in the TNB (ca. 1883 Ma) or the WKB (ca. 1870 Ma). More detailed work on the ultramafic rocks would be required before this could be confirmed.

Economic considerations

The evidence suggests that the Tower deposit is associated with bimodal, mafic-dominated arc magmatism. The presence of felsic rocks with FII–FIIIa rhyolite-type geochemistry and local boninitic intrusions suggests a rifted arc setting. Volcanogenic massive-sulphide deposits form in areas of high heat flow, typically related to upwelling mafic magmas in extensional environments (Franklin et al., 2005; Galley et al., 2007; Piercey, 2011). The thinned crust and pooled mafic magmas provide the necessary heat to drive the hydrothermal circulation required to scavenge, transport and deposit base metals, while extensional structures provide the permeability required for recharge and discharge of hydrothermal fluids (Piercey, 2011).

Volcanogenic massive-sulphide deposits typically occur in clusters, around calderas or along linear rifts (Galley et al., 2007). Hence, there may be potential for additional deposits along strike. A horizon of biotite-muscovite schist, previously misidentified as metapelite, is now interpreted as a zone of intense sericite-paragonite alteration. This zone is spatially associated with the structurally remobilized mineralization of the T1 zone, and could potentially represent an alteration zone related to the mineralization. A heterogeneous horizon of chlorite schist with varying amounts of staurolite, biotite, and garnet is interpreted as a zone of intense chlorite alteration. The zone of chlorite alteration is host to the mineralization of the T2 zone, which appears to pinch and swell near the structural base of the altered zone. The recognition of two styles of intense alteration associated with VMS mineralization could be used as local exploration vectors.

The Tower stratigraphy is likely preserved in a klippe, or erosional remnant of juvenile crust that was thrust onto the margin of the Superior craton during the Trans-Hudson orogeny. The lateral extent of the klippe is unknown. Burntwood group rocks were thrust onto the Superior craton margin and incorporated into km-scale domal structures in the northwestern TNB (Figure 2, Macek et al., 2006; Böhm et al., 2007). Although the crustal slices of Burntwood group can be narrow (~100 m) they can be laterally continuous over 10s of km. The rocks that host the Tower deposit could potentially be continuous over a similar scale. Rocks of the Tower stratigraphy are easily mistaken for metasedimentary rocks (Beaudry, 2007; Couëslan, 2017). It is possible that similar rocks have been intersected and misidentified elsewhere. Anomalous Cu and Zn encountered in drillholes on the adjacent William Lake property (Beaudry, 2007), suggests that crustal slices of juvenile rocks with VMS potential may be more widespread than is currently recognized along the sub-Phanerozoic portion of the Superior margin.

Although the Tower stratigraphy is not related to the Oswagan group of the TNB, the presence of ultramafic bodies intruded into stratigraphy with sulphidic horizons indicates a notional potential for magmatic Ni-Cu deposits. The Namew Lake Ni-Cu deposit in the sub-Phanerozoic, Clearwater Lake domain (~60 km south of Flin Flon) is characterized by elevated concentrations of Cu, Zn, and Pb, which may have resulted

from partial assimilation of volcanogenic Cu-Zn-Pb sulphides (Menard et al., 1996) by ultramafic magma. No evidence for Ni-Cu mineralization has been observed to date at the Tower deposit; however, potential could exist along strike.

Acknowledgments

The author thanks N. Clark, M. Stocking and S. Walker for providing enthusiastic field assistance; N. Brandon and E. Anderson for logistical support. Thanks to A. Bailes, S. Gagné, K. Reid, and J. Macek for helpful discussions during the drafting of this manuscript. S. Anderson and S. Gagné provided helpful and constructive comments on earlier drafts of this manuscript. This project was made possible by Akuna Minerals Inc. and Rockcliff Metals Corp., who provided access to the Tower property drillcore. Thanks go to M. Lapierre for looking after our needs at the Rockcliff core-storage facility and for cutting samples.

References

- Anderson, S.D. 2008: Lithochemical database, Sm-Nd isotopic data and U-Pb geochronological data for the Rice Lake area, Rice Lake greenstone belt, southeastern Manitoba (parts of NTS 52L13, 52M4); Manitoba Science, Technology, Energy and Mines, Manitoba Geological Survey, Data Repository Item DRI2008002, Microsoft® Excel® file.
- Anderson, S.D. 2013: Lithochemical database, Sm-Nd isotopic data and U-Pb geochronological data for the eastern Rice Lake greenstone belt, southeastern Manitoba (parts of NTS 52L11, 14); Manitoba Mineral Resources, Manitoba Geological Survey, Data Repository Item DRI2013002, Microsoft® Excel® file.
- Ayres, L.D. and Young, J. 1989: Characterization of mafic-ultramafic intrusive rocks in the Flin Flon–Snow Lake area, Manitoba; *in* Investigations by the Geological Survey of Canada in Manitoba and Saskatchewan during the 1984–1989 Mineral Development Agreements, A.G. Galley (ed.), Geological Survey of Canada, Open File 2133, p. 64–68.
- Bailes, A.H. 1997: Geochemistry of Paleoproterozoic volcanic rocks in the Photo Lake area, Flin Flon belt (part of NTS 63K16); *in* Report of Activities 1997, Manitoba Energy and Mines, Minerals Division, Geological Services, p. 61–72.
- Bailes, A.H. 2015: Geological setting of the Watts River base metal massive sulphide deposit; HudBay Minerals Inc., unpublished internal geological report, 70 p.
- Bailes, A.H. and Galley, A.G. 1999: Evolution of the Paleoproterozoic Snow Lake arc assemblage and geodynamic setting for associated volcanic-hosted massive sulphide deposits, Flin Flon belt, Manitoba, Canada; Canadian Journal of Earth Sciences, v. 36: p. 1789–1805.
- Bailes, A.H. and Galley, A.G. 2001: Geochemistry and tectonic setting of volcanic and intrusive rocks in the VMS-hosting Snow Lake area assemblage, Flin Flon Belt, Manitoba: a preliminary release of the geochemical data set; Manitoba Industry, Trade and Mines, Manitoba Geological Survey, Open File OF2001-6, 1 CD-ROM.
- Bailes, A.H. and Percival, J.A. 2005: Lithochemical and lithological data, Sm-Nd isotopic data and geochronological data for the Black Island area, Lake Winnipeg, Manitoba (parts of NTS 62P1, 7 and 8) and the Rice Lake greenstone belt (parts of NTS 62P, 52M and 52L); Manitoba Industry, Economic Development and Mines, Manitoba Geological Survey, Data Repository Item 2005004, Microsoft® Excel® file.

- Barrie, C.T., Ludden, J.N. and Green, T.H. 1993: Geochemistry of volcanic rocks associated with Cu-Zn and Ni-Cu deposits in the Abitibi Subprovince; *Economic Geology*, v. 88, p. 1341–1358.
- Beaudry, C. 2007: Technical report on the William Lake property, Grand Rapids, Manitoba, Canada; NI 43-101 report prepared for Pure Nickel Inc., 133 p., URL <http://www.purenickel.com/i/pdf/wl_43101_techreport.pdf> [August 2017].
- Bleeker, W. 1990: Evolution of the Thompson Nickel Belt and its nickel deposits, Manitoba, Canada; Ph.D. thesis, University of New Brunswick, Fredericton, New Brunswick, 400 p.
- Bleeker, W. and Hamilton, M.A. 2001: New SHRIMP U-Pb ages for the Ospwagan group: implications for the SE margin of the Trans-Hudson orogen; Geological Association of Canada–Mineralogical Association of Canada 2001 Joint Annual Meeting, St. John's, Newfoundland, May 27–30, 2001, Abstracts, v. 26, p. 15.
- Böhm, C.O. 2005a: Bedrock geology of northern and central Winterring Lake, Manitoba (parts of NTS 63P5 and 12); *in* Report of Activities 2005, Manitoba Industry, Economic Development and Mines, Manitoba Geological Survey, p. 32–39.
- Böhm, C. 2005b: Bedrock geology of northern and central Winterring Lake, Manitoba; Manitoba Industry, Economic Development and Mines, Manitoba Geological Survey, Manitoba Mining and Minerals Convention 2012, Winnipeg, Manitoba, November 17–19, 2005, poster presentation.
- Böhm, C.O., Zwanzig, H.V. and Creaser, R.A. 2007: Sm-Nd isotopic technique as an exploration tool: delineating the northern extension of the Thompson Nickel Belt, Manitoba, Canada; *Economic Geology*, v. 102, p. 1217–1231.
- Burnham, O.M., Halden, N., Layton-Matthews, D., Leshner, C.M., Liwanag, J., Heaman, L., Hulbert, L., Machado, N., Michalak, D., Pacey, M., Peck, D.C., Potrel, A., Theyer, P., Toope, K. and Zwanzig, H. 2009: CAMIRO project 97E-02, Thompson Nickel Belt: final report, March 2002, revised and updated 2003; Manitoba Science, Technology, Energy and Mines, Manitoba Geological Survey, Open File OF2008-11, 434 p. plus appendices and GIS shape files for use with ArcInfo®.
- Caracle Creek International Consulting Inc. 2013: Independent technical report, Tower property, Grand Rapids, Manitoba; Rockcliff Resources Inc., NI 43-101 technical report, 161 p.
- Ciborowski, T.J.R., Minifie, M.J., Kerr, A.C., Ernst, R.E., Baragar, B. and Millar, I.L. 2017: A mantle plume origin for the Paleoproterozoic circum-Superior large igneous province; *Precambrian Research*, v. 294, p. 189–213.
- Corrigan, D., Pehrsson, S., Wodicka, N. and De Kemp, E. 2009: The Paleoproterozoic Trans-Hudson Orogen: a prototype of modern accretionary processes; *in* Ancient Orogens and Modern Analogues, J.B. Murphy, J.D. Keppie and A.J. Hynes (ed.), Geological Society of London, Special Publications, v. 327, p. 457–479.
- Couëslan, C.G. 2013: Metamorphic and tectonic evolution of the Paleoproterozoic Thompson nickel belt, Manitoba; Ph.D. thesis, University of Calgary, Calgary, Alberta, 264 p.
- Couëslan, C.G. 2014: Preliminary results from bedrock mapping in the Partridge Crop Lake area, eastern margin of the Thompson nickel belt, central Manitoba (parts of NTS 63P11, 12); *in* Report of Activities 2014, Manitoba Mineral Resources, Manitoba Geological Survey, p. 18–31.
- Couëslan, C.G. 2016: Whole-rock litho geochemistry, Sm-Nd isotope geochemistry, and U-Pb zircon geochronology for samples from the Paint and Phillips lakes area, Manitoba (parts of NTS 63O1, 8, 9, 63P5, 12); Manitoba Growth Enterprise and Trade, Manitoba Geological Survey, Data Repository Item DRI2016001, Microsoft® Excel® file.
- Couëslan, C.G. 2017: Evaluation of diamond-drill core from the Tower Cu-Zn-Ag-Au deposit, sub-Phanerozoic Thompson nickel belt, central Manitoba (part of NTS 63G14); *in* Report of Activities 2017, Manitoba Growth, Enterprise and Trade, Manitoba Geological Survey, p. 52–64.
- Couëslan, C.G. 2018: Whole-rock litho geochemistry, Sm-Nd isotope geochemistry, NORMAT alteration indices and normative mineral estimates, and thin section point count results for samples from the Tower Cu-Zn-Ag-Au deposit (part of NTS 63G14); Manitoba Growth Enterprise and Trade, Manitoba Geological Survey, Data Repository Item DRI2018004, Microsoft® Excel® file.
- Couëslan, C.G. and Pattison, D.R.M. 2012: Low-pressure regional amphibolite-facies to granulite-facies metamorphism of the Paleoproterozoic Thompson Nickel Belt, Manitoba; *Canadian Journal of Earth Sciences*, v. 49, p. 1117–1153.
- de Capitani, C. and Brown, T.H. 1987: The computation of chemical equilibrium in complex systems containing non-ideal solutions; *Geochimica et Cosmochimica Acta*, v. 51, p. 2639–2652.
- de Capitani, C. and Petrakakis, K. 2010: The computation of equilibrium assemblage diagrams with Theriak/Domino software; *American Mineralogist*, v. 95, p. 1006–1016.
- Diener, J.F.A., Powell, R., White, R.W. and Holland, T.J.B. 2007: A new thermodynamic model for clino- and orthoamphiboles in the system Na₂O–CaO–FeO–MgO–Al₂O₃–SiO₂–H₂O–O; *Journal of Metamorphic Geology*, v. 25, p. 631–656.
- Duuring, P., Hassan, L., Zelic, M. and Gessner, K. 2016: Geochemical and spectral footprint of metamorphosed and deformed VMS-style mineralization in the Quinns district, Yilgarn craton, Western Australia; *Economic Geology*, v. 111, p. 1411–1438.
- Franklin, J.M., Gibson, H.L., Jonasson, I.R. and Galley, A.G. 2005: Volcanogenic massive sulphide deposits; *in* Economic Geology One Hundredth Anniversary Volume 1905–2005, J.W. Hedenquist, J.F.H. Thompson, R.J. Goldfarb and J.P. Richards (ed.), Society of Economic Geologists, p. 523–560.
- Gagné, S. 2011: Whole-rock geochemistry of volcanic, volcanoclastic and intrusive rocks in the Squall–Varnson lakes area, west-central Manitoba (part of NTS 63K16); Manitoba Innovation, Energy and Mines, Manitoba Geological Survey, Data Repository Item DRI2011007, Microsoft® Excel® file.
- Gagné, S. 2012: Geological investigations in the Brunne Lake area of the Flin Flon Belt, Manitoba (part of NTS 63K11 and 63K14); Manitoba Innovation, Energy and Mines, Manitoba Geological Survey, Data Repository Item DRI2012005, Microsoft® Excel® file.
- Gagné, S. and Anderson, S.D. 2014: Update on the geology and geochemistry of the west Reed Lake area, Flin Flon greenstone belt, west-central Manitoba (part of NTS 63K10); *in* Report of Activities 2014, Manitoba Mineral Resources, Manitoba Geological Survey, p. 77–93.
- Galley, A.G., Hannington, M.D. and Jonasson, I.R. 2007: Volcanogenic massive sulphide deposits; *in* Mineral Deposits of Canada: A Synthesis of Major Deposit-Types, District Metallogeny, the Evolution of Geological Provinces, and Exploration Methods, W.D. Goodfellow (ed.), Geological Association of Canada, Mineral Deposits Division, Special Publication 5, p. 141–161.
- Gemmell, J.B. and Fulton, R. 2001: Geology, genesis, and exploration implications of the footwall and hanging-wall alteration associated with the Hellyer volcanic-hosted massive sulphide deposit, Tasmania, Australia; *Economic Geology*, v. 96, no. 5, p. 1003–1035.
- Genna, D., Gaboury, D. and Roy, G. 2014: Evolution of a volcanogenic hydrothermal system recorded by the behavior of LREE and Eu: case study of the Key tuffite at Bracemac–McLeod deposits, Matagami, Canada; *Ore Geology Reviews*, v. 63, p. 160–177.

- Gilbert, H.P., Bailes, A.H. 2005: Lithochemical and lithological data and field photographs for the southern Wekusko Lake area, Manitoba (NTS 63J12NW), Manitoba Industry, Economic Development and Mines, Manitoba Geological Survey, Data Repository Item DRI2005003, Microsoft® Excel® file.
- Goldstein, S.L., O’Nions, R.K. and Hamilton, P.J. 1984: A Sm-Nd study of atmospheric dusts and particulates from major river systems; *Earth and Planetary Science Letters*, v. 70, p. 221–236.
- Guevara, V.E., Dragovic, B., Caddick, M.J., Kylander-Clark, A.R.C. and Couëslan, C.G. 2016a: Ultrahigh temperature metamorphism of the Archean Pikwitonei granulite domain; Geological Society of America, Annual Meeting, Denver, Colorado, September 25–28, 2016, Abstracts with Programs, v. 48, paper 270-4, URL <<https://gsa.confex.com/gsa/2016AM/webprogram/Paper284904.html>> [August 2017].
- Guevara, V., MacLennan, S.A., Schoene, B., Dragovic, B., Caddick, M.J., Kylander-Clark, A.R. and Couëslan, C.G. 2016b: Quantifying the timescales of Archean UHT metamorphism through U-Pb monazite and zircon petrochronology; American Geophysical Union, Fall Meeting, San Francisco, California, December 12–16, 2016, abstract V51B-07, URL <<https://agu.confex.com/agu/fm16/meetingapp.cgi/Paper/175259>> [August 2017].
- Guevara, V.E., Dragovic, B., Caddick, M.J., Couëslan, C.G., Kylander-Clark, A.K.C., MacLennan, S.A., Schoene, B. and Baxter, E.F. 2018: Ultrahigh temperature metamorphism of Archean continental crust: insights from the petrochronology arsenal; Geological Society of America, 53rd annual northeastern section meeting, Burlington, Vermont, March 18–20, 2018, paper no. 16-1, URL <<https://gsa.confex.com/gsa/2018NE/meetingapp.cgi/Paper/310491>> [May 2018].
- Hart, T.R., Gibson, H.L. and Leshner, C.M. 2004: Trace element geochemistry and petrogenesis of felsic volcanic rocks associated with volcanogenic massive Cu-Zn-Pb sulfide deposits; *Economic Geology*, v. 99, no. 5, p. 1003–1013.
- Heaman, L.M., Peck, D. and Toope, K. 2009: Timing and geochemistry of 1.88 Ga Molson Igneous Events, Manitoba: insights into the formation of a craton-scale magmatic and metallogenic province; *Precambrian Research*, v. 172, p. 143–162. doi:10.1016/j.precamres.2009.03.015
- Heaman, L.M., Böhm, C.O., Machado, N., Krogh, T.E., Weber, W. and Corkery, M.T. 2011: The Pikwitonei Granulite Domain, Manitoba: a giant Neoproterozoic high-grade terrane in the northwest Superior Province; *Canadian Journal of Earth Sciences*, v. 48, p. 205–245.
- Holland, T.J.B. and Powell, R. 1998: An internally consistent thermodynamic data set for phases of petrological interest; *Journal of Metamorphic Geology*, v. 16, no. 3, p. 309–343.
- Hollings, P. and Wyman, D. 2005: The geochemistry of trace elements in igneous systems: principles and examples from basaltic systems; in *Rare-Element Geochemistry and Mineral Deposits*, R.L. Linnen and I.M. Samson (ed.), Geological Association of Canada, GAC Short Course Notes 17, p. 1–16.
- Hubregtse, J.J.M.W. 1980: The Archean Pikwitonei granulite domain and its position at the margin of the northwestern Superior Province (central Manitoba); Manitoba Energy and Mines, Manitoba Geological Survey, Geological Paper GP80-3, 16 p.
- Hulbert, L., Stern, R., Kyser, T.K., Pearson, J., Leshner, M. and Grinenko, L. 1994: The Winnipegosis komatiite belt central Manitoba; Manitoba Mining, Minerals, and Petroleum Convention, November 20–23, 1994, Program, p. 21.
- Kelsey, D.E. 2008: On ultrahigh-temperature crustal metamorphism; *Gondwana Research*, v. 13, p. 1–29.
- Leclair, A.D., Lucas, S.B., Broome, H.J., Viljoen, D.W. and Weber, W. 1997: Regional mapping of Precambrian basement beneath Phanerozoic cover in southeastern Trans-Hudson Orogen, Manitoba and Saskatchewan; *Canadian Journal of Earth Sciences*, v. 34, p. 618–634.
- Le Maitre, R.W. 2002: *Igneous rocks: a classification and glossary of terms*, Cambridge University Press, United Kingdom, 236 p.
- Leshner, C.M., Goodwin, A.M., Campbell, I.H. and Gorton, M.P. 1986: Trace-element geochemistry of ore-associated and barren, felsic metavolcanic rocks in the Superior Province, Canada; *Canadian Journal of Earth Sciences*, v. 23, p. 222–237.
- Lin, S., Pacey, M., Theyer, P., Lenton, P., Macek, J., Peck, D., Zwanzig, H., Burnham, M., Keays, R., Leshner, M., Ferguson, I., Halden, N., Larocque, A., Bleeker, W., Broome, J., Lucas, S., White, D., Hulbert, L., Machado, N., Heaman, L. and Ansdell, K. 1998: Thompson nickel belt project; CAMIRO Project 97-E02, Annual Report – Year 1, 77 p. + appendices.
- Ludden, J., Gélinas, L. and Trudel, P. 1982: Archean metavolcanics from the Rouyn–Noranda district, Abitibi greenstone belt, Quebec. 2. Mobility of trace elements and petrogenetic constraints; *Canadian Journal of Earth Sciences*, v. 19, no. 12, p. 2276–2287.
- Macek, J.J. and Bleeker, W. 1989: Thompson Nickel Belt project – Pipe pit mine, Setting and Ospwagan lakes; in *Report of Field Activities 1989*, Manitoba Energy and Mines, Minerals Division, p. 73–87.
- Macek, J.J., Zwanzig, H.V. and Pacey, J.M. 2006: Thompson nickel belt geological compilation map, Manitoba (parts of NTS 63G, J, O, P and 64A and B); Manitoba Science, Technology, Energy and Mines, Manitoba Geological Survey, Open File Report OF2006-33.
- MacLean, W.H. 1988: Rare earth element mobility at constant inter-REE ratios in the alteration zone at the Phelps Dodge massive sulphide deposit, Matagami, Quebec; *Mineralium Deposita*, v. 23, no. 4, p. 231–238.
- Maniar, P.D. and Piccoli, P.M. 1989: Tectonic discrimination of granitoids; *Geological Society of America Bulletin*, v. 101, no. 5, p. 635–643.
- McDonough, W.F. and Sun, S.-s. 1995: The composition of the Earth; *Chemical Geology*, v. 120, p. 223–253.
- McGregor, C.R. 2012: GIS compilation of relogged sub-Phanerozoic Precambrian exploration drillcore from the Thompson Nickel Belt, eastern Flin Flon Belt and Winnipegosis Komatiite Belt (parts of NTS 63B, 63C, 63F, 63G, 63J); Manitoba Innovation, Energy and Mines, Manitoba Geological Survey, Open File OF2011-1, 1 DVD.
- Menard, T., Leshner, C.M., Stowell, H.H., Price, D.P., Pickell, J.R., Onstott, T.C. and Hulbert, L. 1996: Geology, genesis, and metamorphic history of the Namew Lake Ni-Cu deposit, Manitoba; *Economic Geology*, v. 91, no. 8, p. 1394–1413.
- Meschede, M. 1986: A method of discriminating between different types of mid-ocean ridge basalts and continental tholeiites with the Nb-Zr-Y diagram; *Chemical Geology*, v. 56, p. 207–218.
- Mezger, K., Bohlen, S.R. and Hanson, G.N. 1990: Metamorphic history of the Archean Pikwitonei granulite domain and the Cross Lake subprovince, Superior Province, Manitoba, Canada; *Journal of Petrology*, v. 31, p. 483–517.
- NATMAP Shield Margin Project Working Group 1998: *Geology, NATMAP Shield Margin Project area, Flin Flon belt, Manitoba/Saskatchewan*; Geological Survey of Canada, Map 1968A, scale 1:100 000.
- Pattison, D.R.M. 1992: Stability of andalusite and sillimanite and the Al₂SiO₅ triple point: constraints from the Ballachulish aureole, Scotland; *Journal of Geology*, v. 100, p. 423–446.

- Pattison, D.R.M., Chacko, T., Farquhar, J. and McFarlane, C.R.M. 2003: Temperatures of granulite facies metamorphism; constraints from experimental phase equilibria and thermobarometry corrected for late Fe-Mg exchange; *Journal of Petrology*, v. 44, p. 867–900.
- Pattison, D.R.M. and Tinkham, D.K. 2009: Interplay between equilibrium and kinetics in prograde metamorphism of pelites: an example from the Nelson aureole, British Columbia; *Journal of Metamorphic Geology*, v. 27, p. 249–279.
- Pearce, J.A. 1996: A user's guide to basalt discrimination diagrams; *in* Trace-Element Geochemistry of Volcanic Rocks: Applications for Massive Sulphide Exploration, D.A. Wyman (ed.), Geological Association of Canada, Short Course Notes, v. 12, p. 79–113.
- Pearce, J.A., Harris, N.B.W. and Tindle, A.G. 1984: Trace element discrimination diagrams for the tectonic interpretation of granitic rocks; *Journal of Petrology*, v. 25, p. 956–983.
- Pearson, J. 1996: Exploration, geophysics, and geology of the Winnipegosis basin, Thompson nickel belt, Manitoba Mining and Minerals Convention, November 14–16, 1996, Program, p. 39.
- Percival, J.A., Whalen, J.B. and Rayner, N. 2004: Pikwitonei–Snow Lake, Manitoba transect (parts of NTS 63J, 63O and 63P), Trans-Hudson Orogen–Superior Margin Metalotect Project: initial geological, isotopic and SHRIMP U-Pb results; *in* Report of Activities 2004, Manitoba Industry, Economic Development and Mines, Manitoba Geological Survey, p. 120–134.
- Percival, J.A., Whalen, J.B. and Rayner, N. 2005: Pikwitonei–Snow Lake Manitoba transect (parts of NTS 63J, 63O and 63P), Trans-Hudson Orogen–Superior Margin Metalotect Project: new results and tectonic interpretations; *in* Report of Activities 2005, Manitoba Industry, Economic Development and Mines, Manitoba Geological Survey, p. 69–91.
- Piché, M. and Jébrak, M. 2004: Normative minerals and alteration indices developed for mineral exploration; *Journal of Geochemical Exploration*, v. 82, no. 1, p. 59–77.
- Piercey, S.J. 2010: An overview of petrochemistry in the regional exploration for volcanogenic massive sulphide (VMS) deposits; *Geochemistry: Exploration, Environment, Analysis*, v. 10, p. 119–136.
- Piercey, S.J. 2011: The setting, style, and role of magmatism in the formation of volcanogenic massive sulphide deposits; *Mineralium Deposita*, v. 46, p. 449–471.
- Reid, K.D. 2017: Sub-Phanerozoic basement geology of Wekusko Lake, eastern Flin Flon belt, north-central Manitoba (parts of NTS 63J5, 12, 63K8, 9): insights from drillcore observations and whole-rock geochemistry of mafic rocks; *in* Report of Activities 2017, Manitoba Growth, Enterprise and Trade, Manitoba Geological Survey, p. 65–77.
- Rockcliff Resources Inc. 2012: Rockcliff reports discovery of new copper zone at Tower: additional DPEM anomalies identified with copper potential; Rockcliff Resources Inc., news release, May 23, 2012, URL <http://www.sedar.com/search/search_en.htm> [August 2017].
- Ross, P.-S. and Bédard, J.H. 2009: Magmatic affinity of modern and ancient sub-alkaline volcanic rocks determined from trace-element discriminant diagrams; *Canadian Journal of Earth Sciences*, v. 46, p. 823–839.
- Schmidberger, S.S., Simonetti, A., Heaman, L.M., Creaser, R.A. and Whiteford, S. 2007: Lu-Hf, in-situ Sr and Pb isotope and trace element systematics for mantle eclogites from the Diavik diamond mine: evidence for Paleoproterozoic subduction beneath the Slave craton, Canada; *Earth and Planetary Science Letters*, v. 245, p. 55–68.
- Scoates, J.S., Scoates, J.R.F., Wall, C.J., Friedman, R.M. and Couëslan, C.G. 2017: Direct dating of ultramafic sills and mafic intrusions associated with Ni-sulfide mineralization in the Thompson nickel belt, Manitoba, Canada; *Economic Geology*, v. 112, p. 675–692.
- Simard, R.-L. and Creaser, R.A. 2007: Geochemical analyses of the volcanic rocks of the Schist Lake–Mandy mines area, Manitoba (NTS 63K12); Manitoba Science, Technology, Energy and Mines, Manitoba Geological Survey, Data Repository Item DRI2007001, Microsoft® Excel® file.
- Simard, R.-L., McGregor, C.R., Rayner, N. and Creaser, R.A. 2010a: New geological mapping, geochemical, Sm-Nd isotopic and U-Pb age data for the eastern sub-Phanerozoic Flin Flon belt, west-central Manitoba (parts of NTS 63J3-6, 11, 12, 14, 63K1-2, 7–10); *in* Report of Activities 2010, Manitoba Innovation, Energy and Mines, Manitoba Geological Survey, p. 69–87.
- Simard, R.-L., McGregor, C.R., Rayner, N. and Creaser, R.A. 2010b: Geochemistry, Sm-Nd isotopic and U-Pb age data for the eastern sub-Phanerozoic Flin Flon Belt, west-central Manitoba (parts of NTS 63J3-6, 11, 12, 14, 63K1-2, 7–10); Manitoba Innovation, Energy and Mines, Manitoba Geological Survey, Data Repository Item DRI2010006, Microsoft® Excel® file.
- Spear, F.S. 1995: Metamorphic phase equilibria and pressure-temperature-time paths; Mineralogical Society of America, Washington, D.C., 799 p.
- Stern, R.A., Syme, E.C., Bailes, A.H. and Lucas, S.B. 1995: Paleoproterozoic (1.90–1.86 Ga) arc volcanism in the Flin Flon belt, Trans-Hudson Orogen, Canada; *Contributions to Mineralogy and Petrology*, v. 119, p. 117–141.
- Syme, E.C. and Whalen, J.B. 2012: Geology of the Elbow Lake area, central Flin Flon Belt, Manitoba (part of NTS 63K15W); Manitoba Innovation, Energy and Mines, Manitoba Geological Survey, Geoscientific Report GR2012-1, 100 p.
- Tinkham, D.K. 2011: Distinguishing metamorphosed hydrothermally altered rocks from restite using phase equilibrium calculations, Sherridon complex, Manitoba; Geological Association of Canada–Mineralogical Association of Canada, Joint Annual Meeting, Ottawa, Ontario, May 25–27, 2011, Abstracts, v. 34, p. 218.
- Tinkham, D.K. and Ghent, E.D. 2005: Estimating P–T conditions of garnet growth with isochemical phase diagram sections and the problem of effective bulk-composition; *The Canadian Mineralogist*, v. 43, p. 35–50.
- Waterton, P., Pearson, D.G., Kjarsgaard, B., Hulbert, L., Locock, A., Parman, S. and Davis, B. 2017: Age, origin, and thermal evolution of the ultra-fresh ~1.9 Ga Winnipegosis Komatiites, Manitoba, Canada; *Lithos*, v. 268–271, p. 114–130.
- Unterschutz, J.L.E., Creaser, R.A., Erdmer, P., Thompson, R.I. and Daughtry, K.L. 2002: North American margin origin of Quesnel terrane strata in the southern Canadian Cordillera: inferences from geochemical and Nd isotopic characteristics of Triassic metasedimentary rocks; *Geological Society of America Bulletin*, v. 114, no. 4, p. 462–475.
- White, D.J., Lucas, S.B., Bleeker, W., Hajnal, Z., Lewry, J.F. and Zwanzig, H.V. 2002: Suture-zone geometry along an irregular Paleoproterozoic margin: the Superior boundary zone, Manitoba, Canada; *Geology*, v. 30, p. 735–738.
- White, R.W., Powell, R. and Holland, T.J.B. 2001: Calculation of partial melting equilibria in the system Na₂O–CaO–K₂O–FeO–MgO–Al₂O₃–SiO₂–H₂O (NCKFMASH); *Journal of Metamorphic Geology*, v. 19, no. 2, p. 139–153.
- White, R.W., Powell, R. and Holland, T.J.B. 2007: Progress relating to calculation of partial melting equilibria for metapelites; *Journal of Metamorphic Geology*, v. 25, no. 5, p. 511–527.
- Winchester, J.A., Park, R.G. and Holland, J.G. 1980: The geochemistry of Lewisian semipelitic schists from the Gairloch district, Wester Ross; *Scottish Journal of Geology*, v. 16, p. 165–179.
- Wood, D.A., Joron, J.-L. and Treul, M. 1979: A re-appraisal of the use of trace elements to classify and discriminate between magma series erupted in different tectonic settings; *Earth and Planetary Science Letters*, v. 45, no. 2, p. 326–336.

- Zaleski, E., Froese, E. and Gordon, T.M. 1991: Metamorphic petrology of Fe–Zn–Mg–Al alteration at the Linda volcanogenic massive sulfide deposit, Snow Lake, Manitoba; *Canadian Mineralogist*, v. 29, no. 4, p. 995–1017.
- Zwanzig, H.V. 2005: Geochemistry, Sm-Nd isotope data and age constraints of the Bah Lake assemblage, Thompson Nickel Belt and Kisseynew Domain margin: relation to Thompson-type ultramafic bodies and a tectonic model (NTS 63J, O and P); *in* Report of Activities 2005, Manitoba Industry, Economic Development and Mines, Manitoba Geological Survey, p. 40–53.
- Zwanzig, H.V., Böhm, C.O., Protrel, A. and Machado, N. 2003: Field relations, U-Pb zircon ages and Nd model ages of granitoid intrusions along the Thompson Nickel Belt–Kisseynew Domain boundary, Setting Lake area, Manitoba (NTS 63J15 and 63O2); *in* Report of Activities 2003, Manitoba Industry, Economic Development and Mines, Manitoba Geological Survey, p. 118–129.
- Zwanzig, H.V., Macek, J.J. and McGregor, C.R. 2007: Lithostratigraphy and geochemistry of the high-grade metasedimentary rocks in the Thompson Nickel Belt and adjacent Kisseynew Domain, Manitoba: implications for nickel exploration; *Economic Geology*, v. 102, p. 1197–1216.